



UNIVERSITÀ DEGLI STUDI DI MILANO
FACOLTÀ DI SCIENZE AGRARIE E ALIMENTARI

Department of Food, Environmental and Nutritional Sciences (DeFENS)

**Graduate School in Molecular Sciences and Plant, Food and
Environmental Biotechnology**

PhD program in Food Science, Technology and Biotechnology

XXVII cycle

**POTENTIAL USE OF GRAPHENE FOR THE GENERATION
OF BIONANOCOMPOSITE MATERIALS
FOR FOOD PACKAGING APPLICATIONS**

Scientific Field AGR\15

İLKE UYSAL ÜNALAN

Supervisor: Dr. Stefano Farris
Co-Supervisor: Prof. Luciano Piergiovanni

PhD course coordinator: Prof. Maria Grazia Fortina

December 2014

The dissertation of **İlke Uysal Ünalán** was reviewed and approved by the following:

Prof. Lamberto Duò

Committee Chair

Department of Physics

Polytechnic University of Milan, Italy

Prof. Wender Bredie

Committee Member

Department of Food Science

University of Copenhagen, Denmark

Dr. Maurizio Ruzzi

Committee Member

Department of Innovation of Biological Systems Food and Forestry

University of Tuscia, Italy

5 December 2014

*This thesis is dedicated to my parents
for their love, endless support
and encouragement.*

CONTENTS

LIST OF FIGURES	IV
LIST OF TABLES	VI
ABSTRACT	VII
RIASSUNTO	VIII
PREFACE	IX
ACKNOWLEDGEMENTS	X
1. INTRODUCTION	1
1.1. (Bio)Nanocomposites: Overview	1
1.1.1. Pullulan: structure, properties and applications	1
1.1.2. Graphene	4
1.1.2.1. Graphene: structure and properties	4
1.1.2.2. Graphene: production methods	5
1.1.2.2.1. Ultrasonication process	5
1.1.2.3. Graphene based nanocomposites	6
1.1.3. Bionacomposite coatings in food packaging	7
1.1.4. Fabrication of (bio)nanocomposites	8
1.1.4.1. Solution casting method	9
1.2. References	11
2. AIMS OF THE THESIS	15
3. TOPIC 1: Transparent pullulan/graphene oxide bionanocomposites with high oxygen barrier	16
3.1. Materials and Methods	17
3.1.1. Materials	17
3.1.2. Methods	17
3.1.2.1. Chemical synthesis of graphene oxide	17
3.1.2.2. Preparation of pullulan/GO bionanocomposite films	17
3.1.2.3. Atomic force microscopy	17
3.1.2.4. Transmission electron microscopy	18
3.1.2.5. X-ray photoelectron spectroscopy	18
3.1.2.6. X-ray diffraction	18
3.1.2.7. Thermogravimetric analysis	18
3.1.2.8. Raman spectroscopy	18
3.1.2.9. Scanning electron microscopy	18
3.1.2.10. Oxygen barrier properties	19
3.1.2.11. Tensile properties	19
3.1.2.12. Optical properties	19
3.1.2.13. Statistical analysis	19
3.2. Results and discussion	20
3.2.1. Exfoliation and dispersion of graphene oxide	20

3.2.2. Characterization and pullulan/GO nanocomposite films	25
3.2.2.1. Thermal stability	25
3.2.2.2. Oxygen barrier performance	28
3.2.2.3. Tensile properties	32
3.2.2.4. Optical properties	35
3.3. Conclusions	37
3.4. References	38
4. TOPIC 2: High performance pullulan/chitosan or pullulan/alginate blend systems with graphene oxide for food packaging applications	40
4.1. Materials and methods	41
4.1.1. Materials	41
4.1.2. Methods	41
4.1.2.1. Chemical synthesis of graphene oxide	41
4.1.2.2. Preparation of blend systems	41
4.1.2.3. Thermogravimetric analysis	41
4.1.2.4. Oxygen barrier properties	41
4.1.2.5. Tensile properties	41
4.1.2.6. Optical properties	41
4.1.2.7. Statistical analysis	41
4.2. Results and discussions	42
4.2.1. Blend systems	42
4.2.2. Thermal stability	42
4.2.3. Oxygen barrier performance	45
4.2.4. Mechanical properties	47
4.2.5. Optical properties	49
4.3. Conclusions	52
4.4. References	53
5. TOPIC 3: Pullulan/graphene oxide bionanocomposite coatings with high oxygen barrier properties	54
5.1. Materials and Methods	55
5.1.1. Materials	55
5.1.2. Methods	55
5.1.2.1. Chemical synthesis of graphene oxide	55
5.1.2.2. Preparation of bionanocomposite coatings	55
5.1.2.3. Thickness determination	56
5.1.2.4. Variable-angle spectroscopic ellipsometry	56
5.1.2.5. Transmittance measurements	57
5.1.2.6. Haze measurements	57
5.1.2.7. Friction measurements	57
5.1.2.8. Tensile testing	58
5.1.2.9. Oxygen barrier measurements	58
5.1.2.10. Water vapour barrier measurements	58
5.1.2.11. Statistical analysis	58

5.2. Results and discussion	59
5.2.1. Ellipsometry	59
5.2.2. Transmittance	60
5.2.3. Haze	61
5.2.4. Mechanical properties	63
5.2.4.1. Friction behaviors	63
5.2.4.2. Tensile properties	65
5.2.5. Barrier performance	66
5.3. Conclusions	69
5.4. References	70
6. TOPIC 4: High-concentration, stable, and water dispersible graphene through polysaccharide-assisted rapid ultrasonication	71
6.1. Materials and Methods	72
6.1.1. Materials	72
6.1.2. Methods	72
6.1.2.1. Direct exfoliation of graphite into graphene nanosheets	72
6.1.2.2. UV Spectroscopy	72
6.1.2.3. Transmission electron microscopy	73
6.1.2.4. Atomic force microscopy	73
6.1.2.5. Thermogravimetric analysis	73
6.1.2.6. Raman spectroscopy	73
6.1.2.7. X-ray photoelectron spectroscopy	73
6.2. Results and discussion	74
6.2.1. Yield and quality of the exfoliated graphene	74
6.2.2. Stability of the graphene-polysaccharides water dispersions	76
6.2.3. Adsorption of polysaccharides on the graphene surface	78
6.2.4. Morphology and thickness of graphene sheets	81
6.2.5. Raman spectroscopy	82
6.2.6. XPS analyses	84
6.2.7. Efficiency of the ultrasonication process	85
6.3. Conclusions	88
6.4. References	89
7. GLOSSARY	91
Appendix 1 Honors and awards	92
Appendix 2 Conference abstracts	95
Appendix 3 Peer-reviewed publications	100

LIST OF FIGURES

Figure 1.1.	Representive chemical structure of pullulan as repeating units of maltotriose.	2
Figure 1.2.	Graphite structure.	4
Figure 1.3.	Schematic illustration of the ultrasonication method based on the acoustic cavitation.	6
Figure 1.4.	Schematic illustration of the ‘packaging lightweighting’ concept: the use of multifunctional nanocomposite coatings makes possible avoiding multiple layers packages.	8
Figure 1.5.	Schematic representation of (a) in situ polymerization, (b) melt processing, and (c) solution casting.	9
Figure 3.1.	GO water dispersion (0.15 wt%) after 6 months.	20
Figure 3.2.	(a) $30 \times 30 \mu\text{m}^2$ AFM height image of GO nanosheets (both individual and overlapping sheets are clearly visible); (b) thickness determination of GO sheets by height profile of a $10 \times 10 \mu\text{m}^2$ AFM image; (c) TEM image of GO nanosheets.	21
Figure 3.3	FT-IR spectra of GO.	22
Figure 3.4.	(a) XPS survey spectra of graphite and GO; (b) deconvolution of the C 1s peak of GO.	23
Figure 3.5.	XRD diffractogram of (a) graphite; (b) GO powder.	24
Figure 3.6.	Raman spectra of graphite and GO.	24
Figure 3.7.	TGA and DTG curves of GO.	25
Figure 3.8.	(a) TGA traces; b) their first-order derivatives of four representative bionanocomposite films.	26
Figure 3.9.	Cross-sectional SEM images of (a) pristine pull film; (b) pull/GO film (ϕ 0.002); (c) pull/GO film (ϕ 0.01).	28
Figure 3.10.	Oxygen permeability value at 70% RH as a function of GO concentration.	29
Figure 3.11.	Oxygen permeability of bionanocomposite films. Experimental values (\square), and values predicted by Nielsen’s model (panel a, eq. 3.2 in the text) and Cussler’s models (panels b and c, eqs. 3.3a and 3.3b in the text) for different aspect ratios (\square) are depicted.	31
Figure 3.12.	Typical stress–strain curves for pristine pull and pull nanocomposite films with various contents of GO.	32
Figure 3.13.	Experimental Young modulus values of bionanocomposite films and theoretical simulation for both random orientation and unidirectional distribution of GO sheets in the pullulan matrix according to Halpin–Tsai theoretical models (eqs. 3.4a and 3.4b in the text).	34
Figure 3.14.	Image of a) pristine pullulan film and pull/GO films	36
Figure 4.1.	(a) TGA traces and (b) their first-order derivatives of pull and pull:chit blend systems.	44
Figure 4.2.	(a) TGA traces and (b) their first-order derivatives of pull and pull:alg blend systems.	45

Figure 4.3	Typical stress–strain curves for pull and pull:chit blend systems with various contents of GO.	48
Figure 4.4	Typical stress–strain curves for pull and pull:alg blend systems with various contents of GO.	49
Figure 4.5.	Images of pull blend film with or without GO 0.2 wt%	51
Figure 5.1.	Molecular structure and plastic identification code of PET.	55
Figure 5.2.	Coating preparation process (a) corona treatment; (b) automatic film applicator.	56
Figure 5.3.	Measured transmittance spectra of PET, pristine pullulan coated PET and pullulan/GO coated PET films.	60
Figure 5.4.	AFM height images ($10 \times 10 \mu\text{m}^2$) of (a) pristine pullulan coating and (b) pullulan/GO nanocomposite coating with 0.06 wt% GO content.	63
Figure 5.5.	Image of (a) uncoated PET (b) pristine pullulan coated PET and (c) GO/pullulan coated PET with 0.2 wt% of GO content.	63
Figure 5.6.	O ₂ TR evolutions at different relative humidities (%RH) as a function of GO content.	67
Figure 6.1.	Effect of initial graphite concentration (full squared), and pullulan concentration (half squared) on the yield of graphene exfoliation.	74
Figure 6.2.	TEM images of pull-G for: (a) 10 min; (b) 20 min; (c) 30 min; (d) 60 min; (e) chit-G for 30 min; (f) alg-G for 30 min.	75
Figure 6.3.	Digital images of freshly-prepared graphene in alginate, chitosan, and pullulan water dispersions after (a) 24 h; (b) 7 days; and (c) 6 months storage at room temperature.	76
Figure 6.4.	Representative image of graphene behavior in pullulan, alginate and chitosan water dispersions.	77
Figure 6.5.	TGA traces of graphite, pullulan, alginate, chitosan and pull-G, alg-G and chit-G exposed to a N ₂ atmosphere. The inset in each panel is a zoomed view of the traces within the 0–700 °C range.	79
Figure 6.6.	Absorbance unit values for different concentrations of pull-G (■), chit-G (▲), and alg-G (●) water dispersions.	80
Figure 6.7.	AFM height images ($5 \times 5 \mu\text{m}^2$) of (a) pull-G, (b) alg-G and (c) chit-G nanosheets deposited on mica substrates.	81
Figure 6.8.	(a) Raman spectra of graphite, pull-G, alg-G, and chit-G; (b) detail of the 2D Raman band.	83
Figure 6.9.	XPS survey spectra of pristine graphite powder, pull-G, alg-G, and chit-G.	84

LIST OF TABLES

Table 3.1.	Main parameters drawn from the TGA analysis of pull and pull/GO bionanocomposites.	27
Table 3.2.	GO content, GO volume fraction (ϕ), thickness (l), oxygen transmission rate (O_2TR), and oxygen permeability coefficient ($P'O_2$) of bionanocomposite films at 70% relative humidity and 23 °C.	28
Table 3.3.	Tensile properties of pristine pull and pull nanocomposite films with various contents of GO.	33
Table 3.4	Optical properties of pristine pull and pull nanocomposite films with various contents of GO.	35
Table 4.1.	Main parameters drawn from the TGA analysis of blend systems.	42
Table 4.2.	GO content, GO volume fraction (ϕ), thickness (l), oxygen transmission rate (O_2TR), and oxygen permeability coefficient ($P'O_2$) of blend systems at 70% relative humidity and 23 °C.	46
Table 4.3.	Tensile properties of pristine pull and blend systems with various contents of GO.	47
Table 4.4.	Optical properties of pristine pull and blend systems with various contents of GO.	50
Table 5.1.	Parameters n_A , n_B , t , and t_{n-u} of the top layer obtained by fitting the ellipsometry $\Psi(\lambda)$ and $\Delta(\lambda)$ experimental data.	60
Table 5.2.	Measured transmittance ($T_{mean} \pm \text{std dev}$) and simulated transmittance and reflectance ($T_{simul} \pm \text{std dev}$, $R_{simul} \pm \text{std dev}$)	61
Table 5.3.	Haze value of uncoated PET and bionanocomposite coatings.	62
Table 5.4.	Friction coefficients of uncoated PET and bionanocomposite coatings.	64
Table 5.5.	Tensile properties of uncoated PET and bionanocomposite coatings.	65
Table 5.6.	GO content (wt%, on dry basis), thickness (l), oxygen transmission rate (O_2TR) and water vapor transmission rate ($WVTR$) of uncoated PET and bionanocomposite coatings.	66
Table 6.1.	Elemental surface analysis of pristine graphite powder, pull-G, alg-G, and chit-G samples determined by XPS.	85
Table 6.2.	Direct exfoliated graphene by ultrasonication in different polymer systems.	86

ABSTRACT

The development of new packaging materials offering new functionalities, less environmental impact, and economical benefits is nowadays an urgent necessity. The advent of nanotechnology opened new possibilities toward this goal, e.g. by the generation of a new class of bionanocomposite films or coatings for “greener” packaging structures with same or even better overall performance compared to the conventional materials. This PhD thesis has been conceived as an effective and promising strategy for the development of biopolymer nanocomposites based on graphene specifically intended for food packaging applications. Within this context, the use of graphene aims to prompt new research on this unexplored inorganic filler in the food packaging sector as a potential alternative to the currently used solutions. The overall project has been divided into four parts.

In the first part, the use of pullulan to produce graphene oxide (GO)-bionanocomposites was investigated for the first time in terms of oxygen barrier, tensile, thermal, and optical properties. To get deep understanding on the physical arrangement of the newly generated biopolymer nanocomposites, both oxygen permeability and elastic modulus experimental data were compared with predictive models (Nielsen and Cussler models, and Halpin–Tsai model, respectively). These models, complemented by morphological observations, suggested that the simultaneous improvement of mechanical and oxygen barrier properties was attributed to three main effects: i) chemical affinity between GO and pullulan, which significantly enhanced the interfacial adhesion between the two phases; ii) prevalent unidirectional alignment of GO sheets in the pullulan matrix, parallel to the surface of nanocomposite films; and iii) high specific surface area and 2D geometry of GO.

The results obtained in the first part disclosed the great potential of graphene-based pullulan bionanocomposites as oxygen barrier even at high relative humidity (70% RH) values. However, high cost of pullulan may limit its applications in food packaging. Therefore, in the second part, GO-enhanced pullulan/chitosan and pullulan/alginate blend systems were prepared using the same technique used in part 1. Compared to pure pullulan films, optimized bionanocomposite blend films exhibited enhanced mechanical and thermal properties and comparable oxygen performance while keeping the haze formation within the 3% threshold and transmittance below 90% at 550 nm, which are adequate values for most applications in the food packaging sector. These optimized formulations allowed achieving a well-balanced performance/cost ratio.

The third part of the project was aimed to design bionanocoatings combining pullulan and GO to be applied on polyethylene terephthalate (PET). The rationale behind this approach lies in the fact that most examples on the use of nanosized fillers concern bulky biopolymers. Only very recently it has been proposed the use of fillers within coatings made of biopolymers to produce bionanocomposite coatings to improve the properties of a plastic substrate without jeopardizing its original attributes and optimize cost efficiency. Full exfoliation of GO platelets during preparation of the coating water dispersions was mediated by ultrasonic treatment, which turned out to be a pivotal factor in the oxygen barrier performance of the final material at 0 and 30% RH condition as well as in its stiffness, elongation, and friction properties.

The fourth and last part of the PhD project focused on the graphene production. Specifically, the capability of three different biopolymers (the positively charged polyelectrolyte chitosan, the uncharged pullulan, and the anionic polyelectrolyte alginate) was evaluated to promote the direct exfoliation of graphite into graphene sheets in an aqueous medium by means of high-intensity ultrasonication. Findings arising from this work suggest that non-ionic pullulan and cationic chitosan are more effective to exfoliate graphite into graphene under ultrasonication than anionic alginate, which was attributed to thermodynamic reasons. This approach provides an economical, solvent-free, high-yield, and industrially scalable route for new applications of graphene-based nanocomposites, e.g. in the food packaging industry.

RIASSUNTO

Potenziale impiego del grafene per lo sviluppo di materiali bionanocompositi per applicazioni nel settore dell'imballaggio alimentare

Lo sviluppo di nuovi materiali multifunzionali, a minore impatto ambientale e con benefici economici, rappresenta una impellente necessità. L'avvento delle nanotecnologie ha aperto la strada a nuove possibilità, ad esempio attraverso lo sviluppo di materiali biopolimerici nanostrutturati. Questa tesi di dottorato si propone di illustrare nuove strategie per lo sviluppo di bionanocompositi a base di grafene per specifiche applicazioni nel settore dell'imballaggio alimentare. L'uso del grafene mira ad approfondire le conoscenze circa la potenziale applicazione di tale filler inorganico come alternativa alle attuali soluzioni. Il progetto è stato suddiviso in quattro parti.

Nella prima parte è stato valutato l'uso del pullulano per la produzione di bionanocompositi a base di ossido di grafene (GO), con particolare riferimento alle proprietà di barriera all'ossigeno, proprietà meccaniche, termiche ed ottiche. I dati sperimentali di barriera all'ossigeno e quelli meccanici, inoltre, sono stati confrontati con quelli ottenuti mediante l'uso di tre modelli predittivi, ovvero Nielsen e Cussler per le barriere, Halpi-Tsai per le prove meccaniche. La modellazione ha indicato come il miglioramento delle proprietà di barriera e di quelle meccaniche fosse dovuto a tre effetti principali: i) affinità chimica tra GO e pullulano, con conseguente miglioramento delle forze di adesione all'interfaccia tra le due fasi; ii) prevalente allineamento unidirezionale del filler inorganico; iii) elevata area superficiale e bidimensionalità del GO.

I risultati ottenuti nella prima parte del progetto hanno evidenziato l'enorme potenzialità dei bionanocompositi a base di pullulano e grafene ad agire da barriera all'ossigeno anche ad elevate umidità (70% RH). Tuttavia, i costi elevati possono limitarne l'applicazione nel settore dell'imballaggio alimentare. Per tale motivo, nella seconda parte del progetto si è deciso di valutare la possibilità di utilizzare altri biopolimeri in combinazione col pullulano. Sono stati pertanto sviluppati film a base di pullulano e chitosano e pullulano e alginato. Questi films hanno evidenziato proprietà meccaniche e termiche superiori ai film di solo pullulano mantenendo le proprietà barriera. Inoltre, i valori di opacità e trasmittanza sono stati mantenuti entro i valori 'limite' del 3% e del 90% (a 550 nm) comunemente accettati per le applicazioni nell'imballaggio alimentare. Non meno importante, l'ottenimento di tali blend ha permesso una maggiore efficienza in termini di performance/costi.

La terza parte del progetto ha avuto come obiettivo lo sviluppo di sottili strati bionanocompositi a base di pullulano e GO. Tali strati sono stati depositati su polietilene tereftalato (PET), al fine di migliorarne specifiche proprietà, senza comprometterne la funzionalità. L'esfoliazione del GO è avvenuta mediante ultrasonicazione, che è risultato essere un trattamento 'chiave' al fine di ottenere specifiche proprietà di barriera e meccaniche del coating finale.

La quarta ed ultima parte del progetto si è incentrata su nuove strategie per la produzione di grafene, con particolare riferimento all'uso dell'ultrasonicazione facilitare l'esfoliazione di grafite in grafene mediata dalla presenza di polisaccaridi. I risultati ottenuti in quest'ultima fase del progetto hanno evidenziato la possibilità di ottenere grafene mediante un processo pulito, efficiente e a basso costo.

PREFACE

This dissertation is submitted for the degree of *Doctor of Philosophy* (PhD) at the Department of Food, Environmental and Nutritional Sciences (DeFENS), University of Milan. The research described herein was conducted under the supervisions of Dr. Stefano Farris and Prof. Luciano Piergiovanni from 2011 to 2014. Full PhD fellowship was awarded from the University of Milan.

I hereby declare that except where specific reference is made to the work of others, the contents of this dissertation are original and have not been submitted in whole or in part for consideration for any other degree or qualification in this, or any other university. This dissertation is my own work and contains nothing which is the outcome of work done in collaboration with others, except as specified in the text and Acknowledgements.

I carried out some part of my PhD thesis at the University of Warwick, UK, at the Nanocomposite Research Group of the Department of WMG led by Prof. Tony McNally under the supervision of Dr. Chaoying Wan from July 1st, 2013 to April 15th, 2014.

ACKNOWLEDGEMENTS

I gratefully acknowledge the financial support of University of Milan, which made it possible for me to pursue this PhD. First and foremost I wish to thank my supervisor, Dr. Stefano Farris, whose guidance and support throughout my PhD years has been invaluable to me. I wish to appreciate deeply to my co-supervisor, Prof. Luciano Piergiovanni, a kind mentor, who accepted me to work as a part of Packlab.

I especially thank Dr. Chaoying Wan in Nanocomposite Research Group, University of Warwick for having me a visiting PhD student and for getting me started on the fascinating topic of solvent-free graphene production method. I am thankful to the head of Nanocomposite Research Group, Prof. Tony McNally, for his welcoming and kind behavior, and to Dr. Vanessa Goodship for fruitful discussions that have given me new perspectives on the injection/melt molding process, and to my colleague, George Pappas for his help in Raman spectroscopy. My special thanks to senior administrative officer, Mr. Richard Moffatt for his endless help and support during my time in Warwick.

I specially thank Dr. Richard T. Olsson for his kind help in the modeling.

I would also like to thank to the assessment committee of my PhD examination, Prof. Lamberto Duò, Prof. Wender Bredie and Dr. Maurizio Ruzzi, for their valuable comments.

I am so grateful to our PhD course coordinator, Prof. Maria Grazia Fortina, for her kind help and patience.

I like to express my deep gratitude to Dr. Sara Limbo, Dr. Carlo Cazzolino, Dr. Elenora Ubaldi, Alessandro Adobati, Miriam Zanolleti, Dr. Erika Mascheroni, Riccardo Rampazzi, Dr. José Maria Fuentes-Alventosa, Derya Boyacı, Gaetano Campanella, Dr. Valeria Guazzotti, Sara Pozzo, Dr. Fei Li, Dr. Laura Introzzi, Dr. Alessandra Marti, Carlos Fuenmayor, Sriharsha Pedapati, Levent Eraydın, Tatiane Terumi, Seda Yamaç, and Paola Campion for being supportive both as colleagues and as friends. I would like to thank my dear flat mates in UK, Suzanne Wu, Raouf Bouguerra and Leopoldo Carbajal, for reminding me there are other things than work in Warwick.

I wish to express my gratitude to my parents, Nurten Uysal and İsmail Uysal and to my dear sister and brother, Ekin Uysal Uzel and İlhan Uzel, and to other members of my family for their love and great source of encouragement.

Finally, I would like to thank my husband, Bülent Ünalán. He was always there cheering me up and deeply understanding with his love.

1. INTRODUCTION

1.1. (Bio)Nanocomposites: Overview

Since the first milestone mentioned by Richard Feynman in 1959 (Feynman, 1961), the concept of nanotechnology has developed into a multidisciplinary field of fundamental and applied science and technology and has become one of the most appealing topics within the research programs of both public agencies (e.g., universities) and private companies.

The food industry seems to receive the largest benefits from nanotechnology, with potential uses already identified in virtually every segment of the sector (i.e., agriculture, food processing, food packaging, and nutrient supplements) (Duncan, 2011). Moreover, a number of the world's largest food companies are actively exploring the potential of nanomaterials for use in food applications (Chaudhry et al., 2008). Within the food industry, however, packaging applications form the largest share of the current and short-term predicted market for nano-enabled products (Cientifica, 2006), with an estimated annual growth rate of ~ 12% by 2014 (IRAP, 2009). One of the reasons for this trend is the consumers' willingness to embrace nanotechnology in "out-of-food" applications more than direct addition of nanoparticles directly into the food (Siegrist et al., 2007; Siegrist et al., 2008). This is also why most nanotechnology applications for food and beverages are lagging behind applications for food packaging, which are already becoming a commercial reality (Chaudhry et al., 2010).

One of the most successful applications of the nanotechnology in the field of packaging concerns the development of "nanocomposites" (Lagaron et al., 2005). In polymer science, while the term "composites" generally refers to mixtures of polymers with inorganic or organic additives having micron-length scale and certain geometries (fibers, flakes, spheres, and particulates), the use of nano-length-scale fillers (at least one dimension $\leq 100\text{nm}$) can be more specifically referred to as "nanocomposites" (Sanguansri & Augustin, 2006). Nanocomposites represent a radical alternative to-conventional polymer composites, because if properly manipulated, they can offer extra benefits such as low density, transparency, good flow, better surface properties, and recyclability even at very low filler contents (generally lower than 5 wt%) (Sinha Ray & Okamoto, 2003; Sorrentino et al., 2007).

A new subclass of nanocomposite materials has recently stemmed from the increasing endeavor to replace oil-based polymers with polymers partially or totally obtained from renewable resources. The term "bionanocomposites" refers to those materials in which the polymer matrix carrying the nano-sized fillers is a biopolymer (e.g., polysaccharides and proteins) or by a polymer of natural origin obtained by synthetic (e.g. poly-lactic acid, PLA) or biotechnological (pullulan, poly-hydroxyalkanoates-PHA) routes (Uysal Unalan et al., 2014). Among the biopolymers pullulan is have attracted much attention over recent years due to its peculiar characteristics.

1.1.1. Pullulan: structure, properties and applications

This non-ionic exopolysaccharide is obtained from the fermentation medium of the fungus-like yeast *Aureobasidium pullulans* (originally called *Pullularia pullulans*) under limiting conditions (e.g., nitrogen), with media composition and culture conditions highly affecting the final yield (Leathers, 2002). The production of pullulan by *A. pullulans* was first discovered by Bauer in 1938 (Bauer, 1938), although isolation and characterization of pullulan were described by Bernier 20 years later (Bernier, 1958). The basic structure of pullulan was first provided by Wallenfels,

Bender, Keilich, and Bechtler, who also coined the name “pullulan” (Bender et al., 1959; Wallenfells et al., 1961). Large-scale production of pullulan was started in 1976 by Hayashibara Company Limited (Okayama, Japan); pullulan films from the same company appeared on the market in 1982 (Tsujisaka & Mitsuhashi, 1993).

The chemical formula of pullulan has been suggested to be $(C_6H_{10}O_5)_n$ (Singh & Saini, 2008). Its chemical structure can be viewed as a maltotriose trimer given by the succession of α -(1 \rightarrow 6)-linked (1 \rightarrow 4)- α -D-triglucosides (Gibbs & Seviour, 1996; Leathers, 2003) (Figure 1.1). This peculiar structure is also reflected in the lack of crystalline regions within the polymer: pullulan has a completely amorphous organization, as experimentally confirmed by recent studies (Kristo & Biliaderis, 2007; Fuentes-Alventosa et al., 2013).

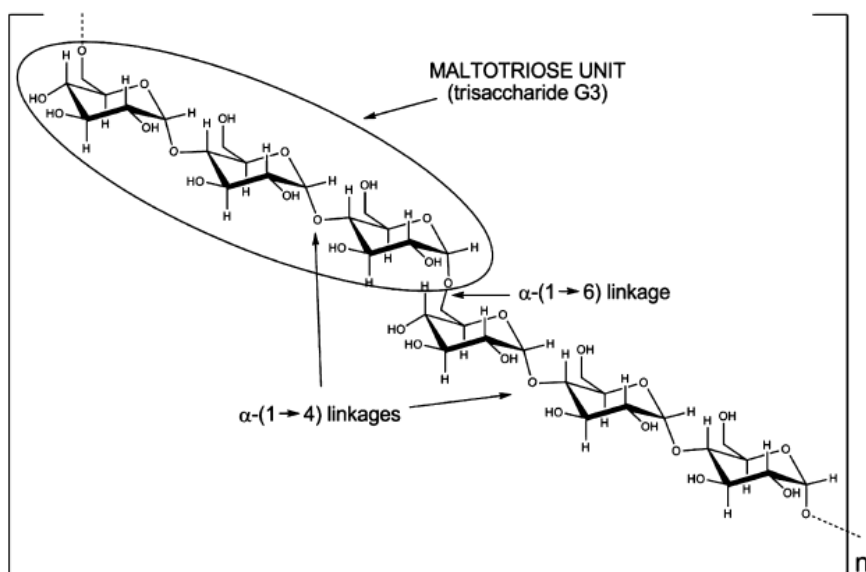


Figure 1.1. Representative chemical structure of pullulan as repeating units of maltotriose (Source Farris et al., 2014).

Early attempts to employ pullulan in the food packaging industry lagged behind the established use as a food additive (e.g., thickening agent, binder, stabilizer), the first works dating back to the beginning of the '90s. At that time, it was understood that great benefits would have arisen from certain peculiar properties of pullulan, such as its high water solubility and the barrier property against oxygen and carbon dioxide. At the beginning, water-soluble edible films of pullulan were proposed as edible pouches for premeasured portions that could be gradually dissolved in water or in hot food (Labell, 1991).

In very recent studies, pullulan nanocomposite films and coating have been investigated in terms of their oxygen, mechanical and thermal performance (Trovatti et al., 2012; Introzzi et al., 2012, Cozzolino et al., 2014).

Although it has many fascinating properties, pullulan has not been as adequately exploited as it deserves. The main reason for such commercial underdevelopment is its high price. Pullulan cost ranges between 25 and 30 US\$/kg, which is much higher than most biopolymers of both polysaccharides and protein origin. The high cost of pullulan is mainly linked to its production (Farris et al., 2014).

The use of inorganic nano-sized particles as fillers in the preparation of polymer/inorganic nanocomposites has attracted increasing interest in recent years, owing to their unique properties that find numerous applications in many industrial fields. As shown in Chart 1.1, a first arbitrary classification of inorganic fillers, primarily based on chemical composition and crystal structure, is between silicate and non-silicate minerals. Both families include several classes and many groups that, in turn, comprise different mineral species potentially suitable to produce nanocomposites. Among inorganic fillers, due to the promising properties of graphene more recently it has become more interest to develop graphene based nanocomposites for wide range applications (Uysal Unalan et al., 2014).

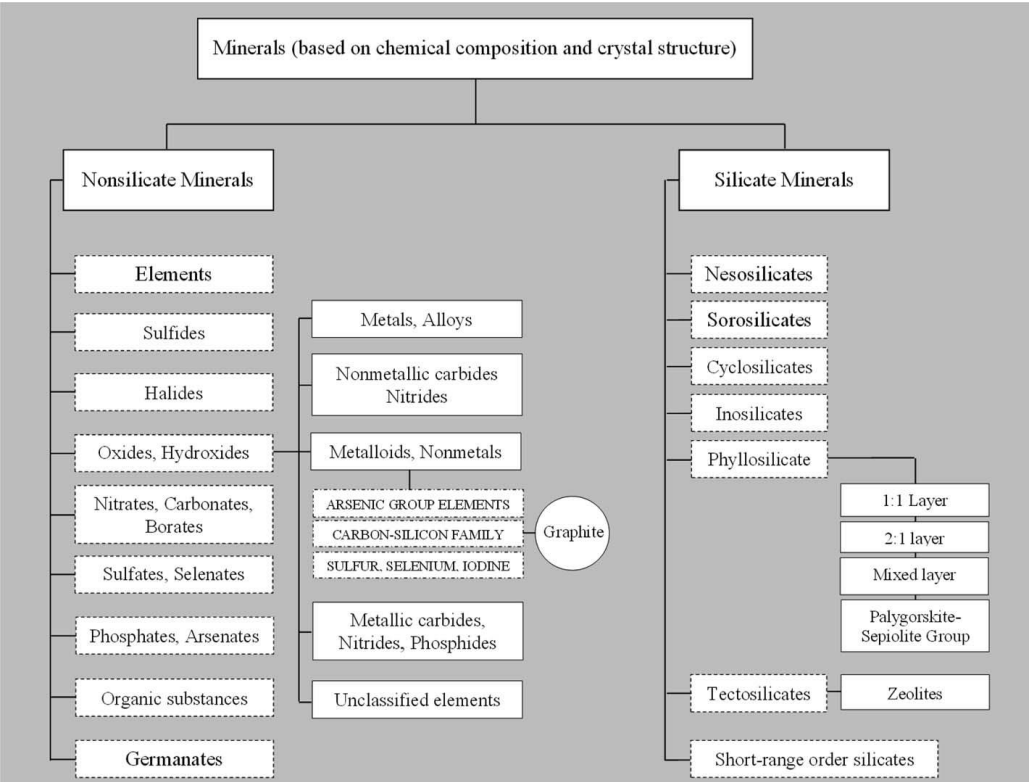


Chart 1.1. Classification of inorganic fillers based on chemical composition and crystal structure (Source: Uysal Unalan et al., 2014).

1.1.2. Graphene

1.1.2.1 Graphene: structure and properties

Graphene is the building unit of graphite, a three-dimensional layered mineral allotrope of carbon composed of several stacked layers of graphene (Terrones et al., 2010) (Figure 1.2). More specifically, graphene is a two-dimensional material composed of a single planar sheet of sp^2 -bonded carbon atoms packed in a honeycomb crystal lattice with large specific surface area although the first reported method for production of graphene nanosheets dates back to 1970 (Eizenberg & Blakely, 1979), its individual layered form was first discovered in 2004 through a micromechanical cleavage method using flake graphite as a starting material (Novoselov et al., 2004). Graphene nanosheets have extremely high Young modulus values (~ 1000 GPa) (Lee et al., 2008) fracture strength (~ 125 GPa) (Lee et al., 2008), thermal conductivity (~ 5000 W m^{-1} K^{-1}) (Balandin et al., 2008), mobility of charge carriers ($\sim 200\,000$ cm^2 V^{-1} s^{-1}) (Bolotin et al., 2008), specific surface area (calculated value, ~ 2630 m^2 g^{-1}) (Stoller et al., 2008), fascinating transport phenomena (e.g., the quantum Hall effect) (Zhang et al., 2005), and gas impermeability (Bunch et al., 2008). These properties make graphene one of today's most exciting materials, as it represents the best candidate for the enhancement of electrical, mechanical, thermal and gas barrier properties for advantageous exploitation in many areas, such as photovoltaics, biosensors, supercapacitors, super adsorbents and fuel cells (Imperiali et al., 2014), just to provide some examples.

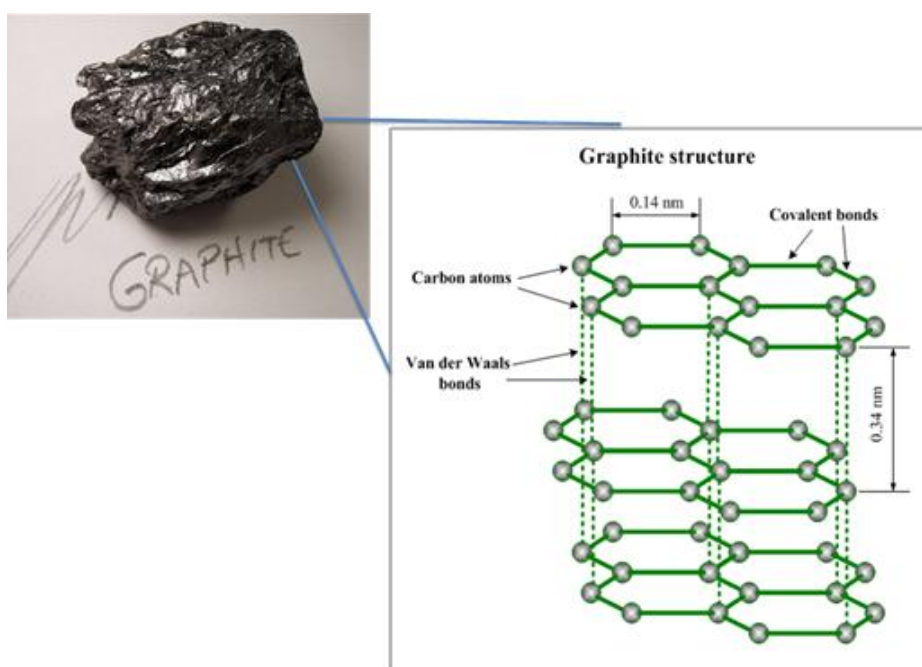


Figure 1.2. Graphite structure

More recently, graphene has been suggested as a potential filler for food packaging materials due to the expected enhancement of mechanical (Lee et al., 2012; Ashori, 2013; Lee et al., 2013; Pinto et al., 2013; Yang et al., 2013), thermal (Al-Jabareen et al., 2013; Ashori, 2013; Lee et al., 2013; Yang et al., 2013;), and barrier properties against O₂ (Al-Jabareen et al., 2013; Lee et al., 2012; Lee et al., 2013; Pinto et al., 2013; Yang et al., 2013), N₂ (Pinto et al., 2013) and water vapour (Ashori, 2013) of the final materials (e.g., films and coatings). However, there are still many challenges for graphene to reach its full potential. Among others, production costs represent the main limitation to large scale utilization, mainly due to the highly expensive and low yielding methods and procedures to obtain graphene monolayers from graphite (Uysal Unalan et al., 2014).

1.1.2.2. Graphene: production methods

Several approaches have been pursued so far to address this issue. Besides bottom-up strategies based on the organic synthesis of graphene starting from small precursors (e.g. atoms, molecules, and so on), more affordable procedures fall within top-down strategies, which are based on the progressive reduction of macro-sized graphite (e.g., powder or flakes) into nano-sized sheets of graphene. With this regard, micromechanical cleavage of graphite, also known as ‘Scotch tape method’, was the first method to provide large and high-quality graphene sheets, but it enables only limited production, which makes this method suitable exclusively for fundamental studies (Novoselov et al., 2004). Chemical modification of graphene oxide, which is generated from graphite, has been a promising route to achieve mass production (Dreyer et al., 2010). Graphene oxide (GO) derived from graphene are a quasi-two-dimensional honeycomb lattice material with oxygen containing functional groups attached on the it basal planes and edges, such as hydroxyl, epoxide, carbonyl and carboxyl, significantly alter the van der Waals interactions between the layers of graphene and impart the desired solubility in water and some organic solvents (Rozada et al., 2013). Meanwhile, these polar functional groups modify surface of graphene to promote interfacial interaction between GO and a hydrophilic polymer, which provides a convenient access to fabrication of graphene-based materials by solution casting. In addition, some concerns point to the excessive use of harsh and aggressive reagents (e.g. H₂SO₄/KMnO₄), and organic solvents (e.g. dimethylformamide or tetrahydrofuran), which make these top-down routes not environmentally benign (Park & Ruoff, 2009). Of late, great attention has been paid to ultrasonication methods for the production of graphene layers starting from graphite flakes or particles based on its reported high quality and environmentally friendly process.

1.1.2.2.1. Ultrasonication process

Sonication is increasingly used in the top-down generation of nanoparticles. This is achieved through deagglomeration and reduction of microsized particles by means of sound waves (more frequently, ultrasound waves) as a result of the mechanical effects of the phenomenon called cavitation, which refers to the formation, growth, and implosive collapse of bubbles in a liquid (Hielscher, 2005) (Figure 1.3). After bubbles collapse, a number of major local events prompt the deagglomeration of microsized particles dispersed in the medium: heating (~5000 K), high pressure (~1000 atm), huge heating-cooling rates ($>10^9 \text{ K} \cdot \text{s}^{-1}$), and abrupt liquid jet streams (~400 km·h⁻¹) (Suslick, 1990; Suslick, 1998; Suslick & Flannigan, 2008) The speed of sound in a typical liquid is 1000 to 1500 m s⁻¹, and ultrasonic wavelengths will vary from roughly 10 cm down to 100 mm over a frequency range of 20 kHz to 15 MHz, much larger than the molecular size scale. The chemical and physical effects of ultrasound therefore arise not from a direct interaction between chemical species and sound waves, but rather from the physical phenomenon of acoustic cavitation:

the formation, growth, and implosive collapse of bubbles (Suslick, 1989; Leighton, 1994; Brenner, 1995)

Exfoliation of defect-free graphene in a liquid phase was first demonstrated using non-aqueous conditions in dimethylformamide (DMF) (Blake et al., 2008) and in a number of organic solvents (Hernandez et., 2008). Due to the significant advantages of aqueous systems over non-aqueous systems (e.g., lower costs and fewer potential health risks and environmental issues), the use of water-based systems has been attracting much attention over the recent years. Lotya et al. (2009) reported the first sonication-based exfoliation of graphite in an aqueous system using the cationic surfactant, sodium dodecyl benzene sulfonate (SDBS). The results arising from these few works make the ultrasonication an extremely promising technique for large-scale production of good quality and cheap graphene.

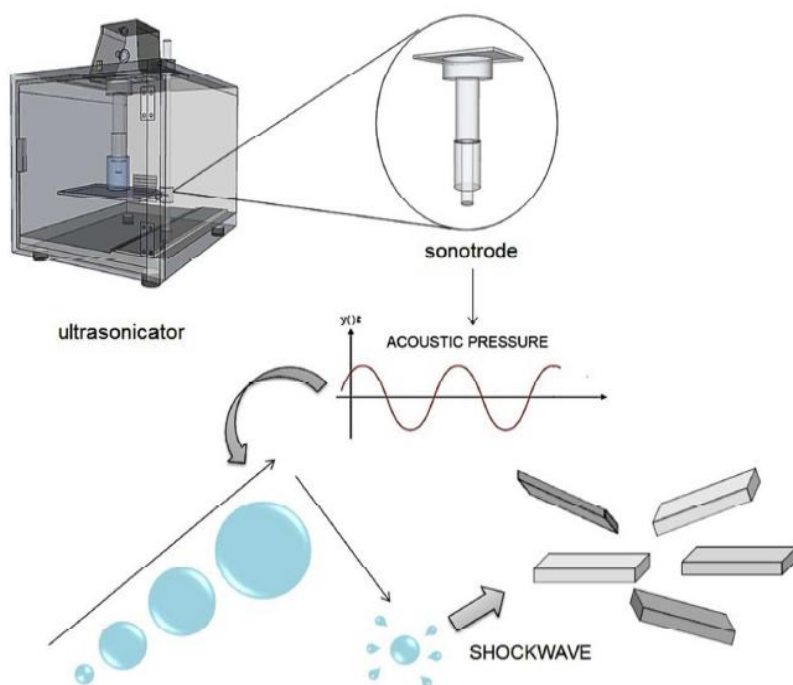


Figure 1.3. Schematic illustration of the ultrasonication method based on the acoustic cavitation. (Source: Uysal Unalan et al., 2014).

1.1.2.3. Graphene based nanocomposites

The use of graphene even at low loading makes obtainable nanocomposite polymer systems with highly improved properties, such as tensile strength and elastic modulus, electrical and thermal conductivity, thermal stability, gas barrier, and flame retardance. Due to this broad multifunctionality, graphene/polymer nanocomposites can find application in various fields, including: advanced biochemical and electrochemical applications, thermal interface applications,

electric and electronic engineering materials, automotive engineering, biomedical applications piezoelectric applications, aerospace and radar evasion applications (Uysal Unalan et al., 2014). However, only few works have clearly addressed the potential impact of graphene/polymer nanocomposites in the food packaging area (Compton et al., 2010; Gao et al., 2011; Lee et al., 2012; Al-Jabareen et al., 2013; Pinto et al., 2013).

However, most examples concern the incorporation of the inorganic phase directly into the bulky biopolymer. Only very recently it has been proposed the use of fillers within coatings made of biopolymers to produce bionanocomposite coatings (i.e., thin layers of a biopolymer matrix loaded with a nanoparticle filler) to improve the properties of a plastic substrate without jeopardizing its original attributes and optimize cost efficiency (Farris et al., 2012; Introzzi et al., 2012).

1.1.3. Bionanocomposite coatings in food packaging

The success of (bio)nanocomposite materials strongly depends on some important factors during the design and development steps. Besides significant costs, technological aspects may act as the “go-no go” gate before market applications. These aspects concern the coating system both before and after the deposition on the selected substrate.

From an industrial perspective, the development of (bio)nanocomposite coatings has aimed at improving three main properties of the base resin: mechanical (stiffness, impact, and wear resistance), flame-retardance (anti-flammable materials), and barrier properties (against gases, vapors, and radiation). In the food and beverage packaging sector, however, considerable industrial and research developments of nanocomposite coatings have focused on improving the barrier properties, which has led to several applications in recent years. Several nanocomposite coatings intended for food packaging applications are available in the market. InMat Inc. developed Nanolok™, a high barrier, water-based, environmentally friendly nanocomposite oxygen barrier coating for transparent packaging applications (In Mat, 2009). Recently, NanoPack Inc. has developed a water-based coating made of poly vinyl alcohol (PVOH) and vermiculite. This coating, sold under the NanoSeal™ trade name, is specifically intended for food packaging applications where protection of food against oxygen and aromas is required (NanoPack, 2013).

Besides advantages directly linked to their functional properties, the use of (bio)nanocomposite coatings may indirectly provide additional benefits, often underestimated or neglected. For example, the weight advantage could present a significant impact on environmental concerns. According to the “packaging optimization” principle (Farris et al., 2009), the use of high-performance thin layers may be a valuable approach to down-gauging current packaging structures, e.g. laminates and/or co-extruded materials (Figure 1.4).

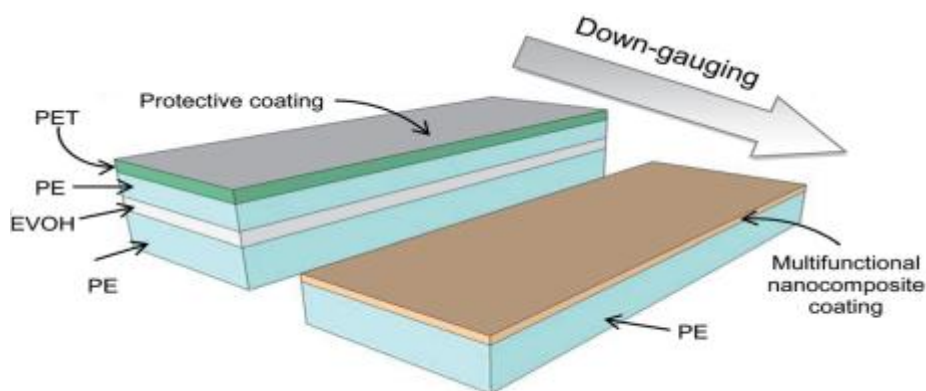


Figure 1.4. Schematic illustration of the ‘packaging lightweighting’ concept: the use of multifunctional nanocomposite coatings makes possible avoiding multiple layers packages (Source: Uysal Unalan et al., 2014).

1.1.4. Fabrication of (bio)nanocomposites

To take full advantage of the great potential of (bio)nanocomposites for real applications, the integration of the selected nano building blocks in the polymer matrices is of primary importance. Many factors, including the exfoliation degree of the fillers, their spatial arrangement (wrinkling or stretched), the morphology of the composite, and the dispersion state in the polymer matrix (stacked or agglomerated)—hence the extent of the interfacial interactions between filler and polymer—may dictate the final performance of the nanocomposite packaging material (Prolongo et al., 2014). Accordingly, for example, the ultimate barrier properties of nanocomposite polymers will be affected by nanosized fillers in two specific ways: (i) a more tortuous path for diffusion of the permeant and (ii) local changes in the polymer matrix properties (e.g., molecular mobility) at the interfacial (polymer nanoparticle) regions (Duncan, 2011). Historically, the nanofiller incorporation into the polymer matrix takes place through three main methods, i.e. (i) the in situ polymerization, (ii) the solution casting or (iii) the melt processing (Chivrac et al., 2009; Li et al., 2010) (Figure 1.5).

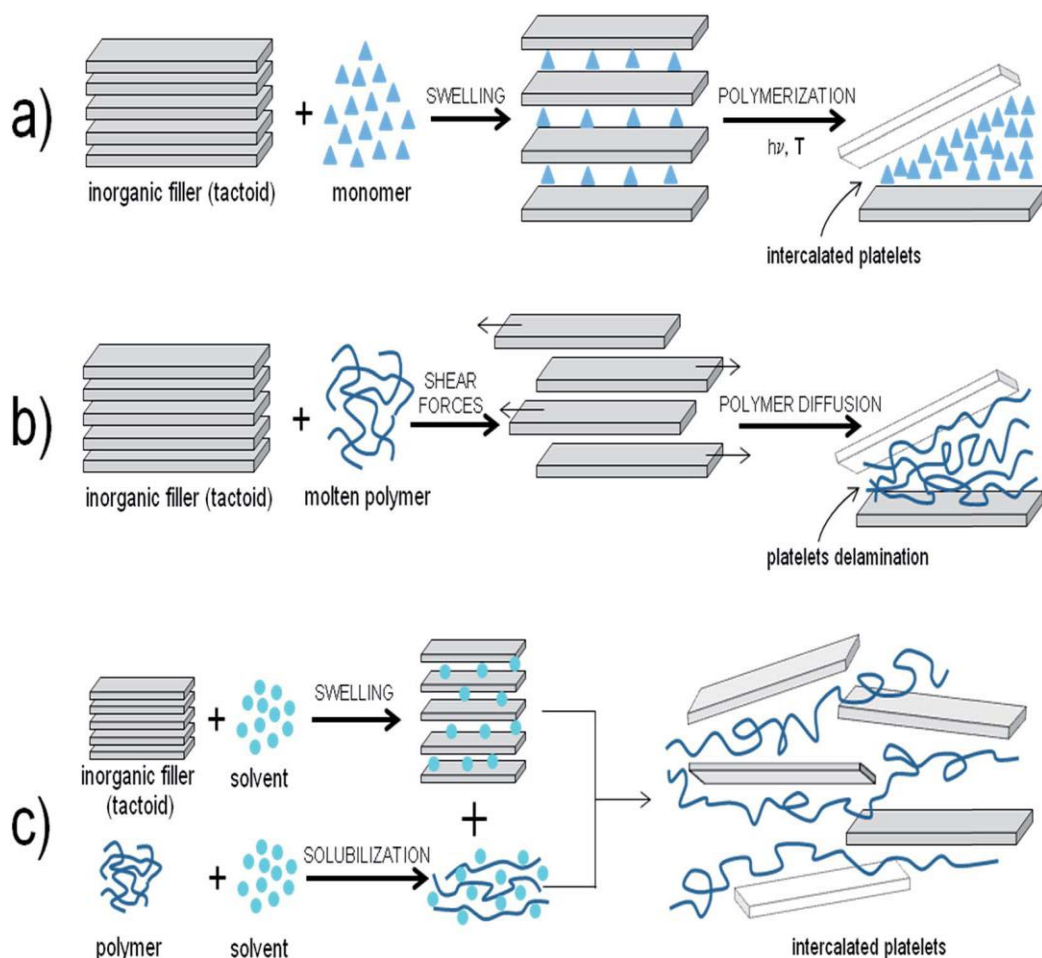


Figure 1.5. Schematic representation of (a) in situ polymerization, (b) melt processing, and (c) solution casting (Source: Uysal Unalan et al., 2014).

Among these three methods, the solution casting method has been adopted for the generation of bionanocomposites, for which both in situ polymerization and melt intercalation are often unsuitable due to the inherent characteristics of most biopolymers.

1.1.4.1. Solution casting method

The solution casting method is based on a solvent system in which the polymer (or pre-polymer, in case of insoluble polymers) and any other component of the mixture (e.g., surfactants) is soluble. The polymer is usually dissolved in a suitable solvent while the nano-fillers are dispersed in the same or a different solvent before the two are mixed together to generate a homogeneous dispersion (Figure 1.5c). The main advantage of this method is the relatively rapid exfoliation of the stacked layers by the use of an appropriate solvent (Sinha Ray & Okamoto, 2003). The successive addition of polymer solution to the dispersion of the complete delaminated nanoparticles (e.g., platelets) leads to the strong interaction between macromolecules and individual layers. The driving force for

the intercalation of the biopolymer into the clay galleries from solution is the entropy gained from desorption of solvent molecules, which compensates for the decreased entropy of the confined, intercalated chains. When the solvent is evaporated, the intercalated structure remains which results in the final nanocomposites (Ojijo & Sinha Raya, 2013). Due to the large amount of the solvent required, this method is perceived as un safe and non-environmentally benign when organic solvents are required (e.g., for non-polar or highly hydrophobic polymers) (Reddy et al., 2013). Conversely, this method has gained increasing attention for water-soluble polymers such as PVOH especially in the form of thin coatings, which reduces the amount of water used throughout the process.

1.2. References

- Al-Jabareen A et al., 2013, Improving the oxygen barrier properties of polyethylene terephthalate by graphite nanoplatelets. *J Appl Polym Sci* 128:1534-1539.
- Ashori A, 2013, Effects of graphene on the behavior of chitosan and starch nanocomposite films. *Polym Eng Sci* 54: 2258–2263.
- Balandin A et al., 2008, Superior thermal conductivity of single-layer graphene. *Nano Lett* 8:902-907.
- Bauer R, 1938, Physiology of *Dematium pullulans* de Bary. *Zentralbl Bacteriol Parasitenkd Infektionskr Hyg Abt 2* 98:133-167.
- Bender H et al., 1959, Pullulan, ein extracelluläres Glucan von *Pullularia pullulans*. *Biochim Biophys Acta* 36: 309-315.
- Bernier B, 1958, The production of polysaccharides by fungi active in the decomposition of wood and forest litter. *Can J Microbiol* 4:195-204.
- Blake P et al., 2008, Graphene-based liquid crystal device. *Nano Letters* 8:1704-1708.
- Bolotin K et al., 2008, Ultrahigh electron mobility in suspended graphene. *Solid State Commun* 146:351-355.
- Brenner CR, Cavitation and bubble dynamics, Oxford University Press, Oxford, 1995.
- Bunch JS et al., 2008, Impermeable atomic membranes from graphene sheets. *Nano Lett* 8:2458-2462.
- Chaudhry Q et al., 2008, Applications and implications of nanotechnologies for the food sector. *Food Addit Contam Part A* 25:241-258.
- Chaudhry Q et al. in *Nanotechnologies in food*, Chaudhry Q, Watkins R and Castle L, eds., RSC Publishing, Cambridge, 2010, pp. 1.
- Chivrac F et al., 2009, Progress in nano-biocomposites based on polysaccharides and nanoclays. *Mater Sci Eng R* 67:1-17.
- Cientifica, 2006, Nanotechnologies in the food industry, <http://www.cientifica.com/www/details.php?id=47> (accessed: 10/06/ 2014).
- Compton OC et al., 2010, Crumpled graphene nanosheets as highly effective barrier property enhancers. *Adv Mater* 22: 4759-4763.
- Cozzolino CA et al., 2014, Microfibrillated cellulose (MFC): pullulan bionanocomposite films. *Cellulose* 21:4323-4335.
- Dreyer DR et al, 2010, The chemistry of graphene oxide. *Chem. Soc Rev* 39:228–240.

Duncan TV, 2011, Applications of nanotechnology in food packaging and food safety: barrier materials, antimicrobials and sensors. *J Colloid Interface Sci* 363:1-24.

Eizenberg M, Blakely JM, 1979, Carbon monolayer phase condensation on Ni(111). *Surf Sci* 82:228-236.

Farris S et al., 2009, Effects of different sealing conditions on the seal strength of polypropylene films coated with a bio-based thin layer. *Packag Technol Sci* 22:359-369.

Farris S et al., 2012, Self-assembled pullulan-silica oxygen barrier hybrid coatings for food packaging applications. *J Agric Food Chem* 60:782-790.

Farris S et al., 2014, Pullulan-based films and coatings for food packaging: Present applications, emerging opportunities, and future challenges. *J Appl Polym Sci* 131: 40539.

Feynman RP, There's plenty of room at the bottom. In *Miniaturization*, Gilbert HD, ed., Reinhold, New York, 1961.

Fuentes-Alventosa JM et al., 2013, Self-assembled nanostructured biohybrid coatings by an integrated 'sol-gel/intercalation' approach. *RSC Adv* 3:25086-25096.

Gao J et al., 2011, A promising alternative to conventional polyethylene with poly(propylene carbonate) reinforced by graphene oxide nanosheets. *J Mater Chem* 21:17627-17630.

Gibbs PA, Seviour RJ. *Polysaccharides in medicinal applications*. Dimitriu S, Ed, Marcel Dekker: New York, NY, USA, 1996, p. 59.

Hernandez Y et al., 2008, High-yield production of graphene by liquid-phase exfoliation of graphite. *Nat Nanotechnol* 3:563-568.

Hielscher T, 2005, Ultrasonic production of nano-size dispersions and emulsions. *Proceedings of European Nanosystems Conference ENS '05*, Paris, France.

Imperiali L et al., 2014, A simple route towards graphene oxide frameworks. *Mater Horiz* 1:139-145.

Introzzi L et al., 2012, Ultrasound-assisted pullulan/montmorillonite bionanocomposite coating with high oxygen barrier properties. *Langmuir* 28:11206-11214.

InMat, 2009, Ultrahigh barrier coating breakthrough from InMat® reduces food packaging costs and environmental impact, http://www.inmat.com/upload/files/inmat_press_release_05072009.pdf, (accessed: 25/12/2013).

IRAP, 2009, Nano-enabled packaging for food and beverage industry, http://www.innoresearch.net/report_summary.aspx?id=68&pg=107&rcd=FT_102&pd=7/1/2009 (accessed: 21/05/2014).

Kristo E, Biliaderis CG, 2007, Physical properties of starch nanocrystal-reinforced pullulan films. *Carbohydr Polym* 68:146-158.

Labell F, 1991, Frozen fresh chopped herbs. *Food Process* 52: 106-108.

Lagaron JM et al., 2005, Improving packaged food quality and safety. Part 2: nanocomposites. *Food Addit Contam* 22:994-998.

Leathers TD in *Polysaccharides II: Polysaccharides from Eukaryotes*, Vandamme EJ, De Baets S, Steinblichel A., Eds, Wiley-VCH: Weinheim, Germany, 2002, Vol. 6, p 1.

Leathers TD, 2003, Biotechnological production and applications of pullulan. *Appl Microbiol Biotechnol* 62:468-473.

Lee C et al., 2008, Measurement of the elastic properties and intrinsic strength of monolayer graphene. *Science* 321: 385-388.

Lee D et al., 2012, Polynorbornene dicarboximide/amine functionalized graphene hybrids for potential oxygen barrier films. *J Polym Sci Part A* 50:1611-1621.

Lee Y et al., 2013, Preparation and characterization of poly(propylene carbonate)/exfoliated graphite nanocomposite films with improved thermal stability, mechanical properties and barrier properties. *Polym Int* 62: 1386-1394.

Leighton TG, *The Acoustic Bubble*, Academic Press, London, 1994.

Li S et al., 2010, Nanocomposites of polymer and inorganic nanoparticles for optical and magnetic applications. *Nano Rev* 1:5214.

Lotya M et al., 2009, Liquid phase production of graphene by exfoliation of graphite in surfactant/water solutions. *J Am Chem Soc* 131:3611-3620.

NanoPack, 2013, NanoSeal™ - Barrier coating, OPP barrier coated film, polypropylene film, liquid coating, <http://www.nanopackinc.com/products.asp>, (accessed: 25/02/2014).

Novoselov KS et al., 2004, Electric field effect in atomically thin carbon films. *Science* 306:666-669.

Ojijo V, Sinha Raya S, 2013, Processing strategies in bionanocomposites. *Prog Polym Sci* 38:1543-1589.

Park S, Ruoff RS, 2009, Chemical methods for the production of graphenes. *Nat Nano* 4:217-224.

Pinto AM et al., 2013, Effect of incorporation of graphene oxide and graphene nanoplatelets on mechanical and gas permeability properties of poly(lactic acid) films. *Polym Int* 62:33-40.

Prolongo SG et al., 2014, Graphene nanoplatelets thickness and lateral size influence on the morphology and behavior of epoxy composites. *Eur Polym J* 53:292-301.

Reddy MM et al., 2013, Biobased plastics and bionanocomposites: Current status and future opportunities. *Prog Polym Sci* 38:1653-1689.

Rozada R et al., 2013, Towards full repair of defects in reduced graphene oxide films by two-step graphitization. *Nano Research* 6: 216-233.

Sanguansri P, Augustin MA, 2006, Nanoscale materials development – a food industry perspective. *Trends Food Sci Technol* 17:547-556.

Siegrist M et al., 2007, Public acceptance of nanotechnology foods and food packaging: the influence of affect and trust. *Appetite* 49:459-466.

Siegrist M et al., 2008, Perceived risks and perceived benefits of different nanotechnology foods and nanotechnology food packaging. *Appetite* 51:283-290.

Singh RS, Saini GK, 2008, Pullulan: Microbial sources, production and applications. *Carbohydr Polym* 73:515-531.

Sinha Ray S and Okamoto M, 2003, Polymer/layered silicate nanocomposites: a review from preparation to processing. , *Prog Polym Sci* 28:1539-1641

Sorrentino A et al., 2007, Potential perspectives of bio-nanocomposites for food packaging applications. *Trends Food Sci Technol* 18:84-95.

Stoller MD et al., 2008, Graphene-based ultracapacitors. *Nano Lett* 8:3498-3502.

Suslick KS, 1989, The chemical effects of ultrasound. *Sci Am* 260:80-86.

Suslick KS, 1990, Sonochemistry. *Science* 247:1439-1445.

Suslick KS, Kirk-Othmer Encyclopedia of Chemical Technology, 4th edn, Wiley & Sons, New York, 1998.

Suslick KS, Flannigan DJ, 2008, Inside a collapsing bubble: sonoluminescence and the conditions during cavitation. *Annu Rev Phys Chem* 59:659-683.

Terrones M et al., 2010, Graphene and graphite nanoribbons: Morphology, properties, synthesis, defects and applications. *Nano Today* 5:351-372.

Trovatti E et al., 2012, Pullulan–nanofibrillated cellulose composite films with improved thermal and mechanical properties. *Composites Sci Technol* 72:1556–1561.

Tsujisaka Y, Mitsuhashi M. In Industrial gums, polysaccharides and their derivatives. Whistler RL, BeMiller JN, Eds., Academic Press, San Diego, 1993, p 447.

Uysal Unalan I et al., 2014. Nanocomposite films and coatings using inorganic nanobuilding blocks (NBB): current applications and future opportunities in the food packaging sector. *RSC Adv* 4:29393–29428.

Wallenfels K et al., 1961, Synthese von Cyananil und Cyananilsäure. *Angew Chem* 73:142-143.

Yang J et al., 2013, Thermal reduced graphene based poly(ethylene vinyl alcohol) nanocomposites: enhanced mechanical properties, gas barrier, water resistance, and thermal stability. *Ind Eng Chem Res* 52:16745–16754.

Zhang Y et al., 2005, Experimental observation of the quantum Hall effect and Berry's phase in graphene. *Nature* 438:201-204.

2. AIMS OF THE THESIS

The general aim of this PhD project was the development of a novel high oxygen barrier graphene based pullulan bionanocomposite materials with better mechanical and thermal properties owing to graphene's promising and attractive properties for the next generation of materials for packaging applications. Keeping suitable optical appearance of the final films for most applications in the food packaging sector was also included in this goal. In other words, the aim was to develop multifunctional "green" alternatives to the synthetic polymer solutions in food packaging sector.

In the final section, special attention has been paid to the production of graphene layers starting from graphite flakes by using one of recent top-down strategies so-called ultrasonication method. The target of this final part was to assess the capability of three different biopolymers (the positively charged polyelectrolyte chitosan, the uncharged pullulan, and the anionic polyelectrolyte alginate) to promote the direct exfoliation of graphite into graphene sheets in an aqueous medium by means of high-intensity ultrasound waves as a result of the mechanical effects of cavitation. We paid special attention to key parameters of the obtained graphene sheets, such as the yield of the overall process and the quality of the graphene dispersions.

3. TOPIC 1

Transparent pullulan/graphene oxide bionanocomposites with high oxygen barrier

This part investigated the potential of a novel bionanocomposite film based on graphene oxide and pullulan for food packaging applications is investigated in terms of oxygen barrier, tensile, thermal and optical properties. The excellent water solubility of graphene oxide imparts it feasibility as new filler for reinforcing hydrophilic biopolymer pullulan. The Nielsen and Cussler models, and the Halpin–Tsai model were built to predict the oxygen and mechanical properties of bionanocomposite films, respectively. Morphological characterization of the bionanocomposite films is also reported. To best our knowledge, it is the first work envisaging the use of pull as a bulk biopolymer to produce graphene oxide-bionanocomposites. This could pave the way for a new alternative to petrol-based films currently available on the market of food packaging.

3.1. Materials and Methods

3.1.1. Materials

Pullulan (PF-20 grade, Mw~200 000 DA) was obtained from Hayashibara Biochemical Laboratories Inc., Okayama, Japan. Graphene flakes were purchased from Sigma Aldrich, UK. Hydrogen peroxide aqueous solution (H_2O_2 , 20-35 wt%), hydrochloric acid (HCl), potassium permanganate ($\text{KMnO}_4 > 95 \text{ wt\%}$), sodium nitrate ($\text{NaNO}_3 > 95 \text{ wt\%}$), and sulfuric acid ($\text{H}_2\text{SO}_4 > 95 \text{ wt\%}$) were all analytical grade and purchased from Fisher Scientific, UK.

3.1.2. Methods

3.1.2.1. Chemical synthesis of graphene oxide

Graphite oxide was prepared following a modified Hummers method (Hummers & Offeman, 1958; Wan & Chen, 2012). Briefly, graphite (2.5 g), NaNO_3 (1.5 g) and concentrated H_2SO_4 (60 mL) were mixed and kept stirring in an ice-water bath for 30 min, and then KMnO_4 (7.5 g) was slowly added over 1 h to keep the temperature of the mixture below 5 °C. The mixture was kept stirring for 24 h at room temperature, and then H_2SO_4 aqueous solution (300 mL, 5 wt%) was gradually added to allow the temperature to increase up to 98 °C. The resultant mixture was further stirred for 2 h at 98 °C. After that the temperature was reduced to 60 °C, and H_2O_2 (25 mL, 30 wt%) was added to the mixture solution under continuous stirring for 2 h. The obtained graphite oxide solution was repeatedly washed with diluted HCl solution and distilled water several times, and vacuum-dried at 40 °C to obtain graphite oxide powder. The graphite oxide was dispersed in water (0.15 wt%) under continuous stirring and ultrasonicated for 10 min using an ultrasonic processor UP200S (maximum power = 200 W, frequency = 24 kHz, Hielscher, Teltow, Germany) equipped with a cone frustum titanium sonotrode (model micro tip S3, tip diameter = 3 mm, maximum amplitude = 210 μm , acoustic power density or surface intensity = 460 $\text{W}\cdot\text{cm}^{-2}$) under the following conditions: 0.5 cycle and 50% amplitude.

3.1.2.2. Preparation of pullulan/GO bionanocomposite films

Biopolymer solutions (5 wt%) were prepared by dissolving pullulan in water under gentle stirring for 1 h at ambient temperature. Pullulan solutions were then mixed with different amounts of the original GO/water dispersion (0.15 wt%) to obtain pullulan/GO water dispersions at different GO concentrations (0, 0.05, 0.1, 0.2, 0.3, 0.5 and 1 wt%). The resultant pullulan/GO solutions were cast onto Petri dishes and dried at ambient temperature for 3 days. The dried films were kept at sealed anhydrous desiccators for at least one week before analysis. Pullulan/graphene oxide films were indicated as pull/GO.

3.1.2.3. Atomic force microscopy

Atomic Force Microscopy (AFM) measurements were carried out in intermittent-contact mode with a Nanoscope V Multimode (Bruker, Germany) on diluted GO water dispersion (0.02 mg/ml). The images were collected with a resolution of 512 x 512 pixels with silicon tips (force constant 40 N/m, resonance frequency 300 kHz). The analyses performed on the acquired images were conducted with Nanoscope software (versions 5.12 and 7.30).

3.1.2.4. Transmission electron microscopy

Transmission electron microscope (TEM) (JEOL 2000FX) at an operating voltage of 200 kV was used for the analysis of graphene oxide structure. Digital images were captured with a GATAN ORIUS 11 megapixel digital camera. Samples for TEM analyses were prepared by drop-casting a few milliliters of dispersion onto holey carbon grids and letting the samples to rest for 24 hours at room temperature to allow water evaporation.

3.1.2.5. X-ray photoelectron spectroscopy

X-ray photoelectron spectroscopy (XPS) measurements were performed in an XM1000 instrument (Omicron NanoTechnology GmbH, Germany) equipped with a monochromatic Al K α source. Samples were first mounted on circular plates using electrically conducting carbon tape and then loaded in a vacuum chamber (base pressure 2×10^{-11} mbar). Data analysis was carried out using the CasaXPS package, using Shirley backgrounds, mixed Gaussian-Lorentzian (Voigt) line shapes and asymmetry parameters for the sp² graphitic components.

3.1.2.6. X-ray diffraction

X-ray diffraction (XRD) measurements of graphite and graphene oxide were performed in the form of powder on a Empyrean X-ray diffractometer (Panalytical Inc., Netherlands) equipped with a detector by use of a CoK α_1 (0.178901 nm) monochromatic X-ray beam. The following operating conditions were applied: 40 kV, 40 mA, 2 θ range 5–40°, step size 0.01, time per step 99 s.

3.1.2.7. Thermogravimetric analysis

Thermogravimetric analysis (TGA) of pristine pullulan and bionanocomposite films was carried by using a TGA/DSC 2 instrument (Mettler Toledo, Switzerland) in an inert environment (50 mL min⁻¹ N₂). Film samples (~ 5 mg) were placed in alumina pans (70 μ L) and heated from 25 °C to 600 °C at a linear heating rate of 10 °C min⁻¹.

3.1.2.8. Raman spectroscopy

Raman spectra were recorded at ambient temperature by a Renishaw inViaRaman spectrometer with an Ar-ion laser at an excitation wavelength of 514.5 nm.

3.1.2.9. Scanning electron microscopy

Field-emission scanning electron microscopy (FE-SEM) micrographs were obtained to acquire more detailed information on the morphology of GO loaded pullulan films. Cross sections were examined on a Hitachi S-4800 FE-SEM (Schaumburg, IL). Surface test specimens were mounted with carbon tape on stubs. Cross-sectioned samples were cut into thin pieces with a scalpel and mounted on a Hitachi thin specimen split mount holder, M4 (product 15335-4). Before insertion into the microscope, the samples were sputter-coated with gold to a thickness of approximately 10 nm (to avoid charging the samples) by use of an Agar high-resolution sputter coater (model 208RH) equipped with a gold target/Agar thickness monitor controller.

3.1.2.10. Oxygen barrier properties

The oxygen barrier properties of pullulan and pull/GO nanocomposite films were assessed on a 2 cm² surface sample using a Multiperm permeability analyzer (Extrasolution Srl, Capannori, Italy) equipped with an electrochemical sensor. Oxygen transmission rate (O_2TR) data were determined according to the standard method of ASTM F2622-08, with a carrier flow (N_2) of 10 ml min⁻¹ at 23 °C, 70% relative humidity (RH), 1 atm pressure difference on the two sides of specimen. Each O_2TR value was from three replicates. Final oxygen permeability coefficients ($P'O_2$) were calculated according to the following equation (Svagan et al., 2012):

$$P'O_2 = PO_2 \times t = \frac{O_2TR}{\Delta p} \times t \quad (3.1)$$

In eq. 3.1, $P'O_2$ is the oxygen permeability coefficient [ml μm m⁻² (24h)⁻¹ atm⁻¹], PO_2 is the permeance (defined as the ratio of O_2TR to the difference between partial pressure of the gas on the two sides of film, Δp), t is total thickness of the film.

3.1.2.11. Tensile properties

Tensile test of films (dimension 15 mm \times 3.2 mm with varying thickness) were performed on a Instron 5800R testing machine (Instron, UK) with a 500 N load cell and a crosshead speed of 2 mm min⁻¹ at room temperature and relative humidity was 45–50%. Young modulus, tensile strength and elongation at break were determined in accordance with the ASTM 638-10 standard. To ensure data accuracy and repeatability, at least 5 measurements were carried out for each film and the average values are reported

3.1.2.12. Optical properties

Total transmittance and haze were measured by Haze-Gard Dual-Transparency meter (BYK-Gardner GmbH, Germany) according to ASTM D 1003 standard. Three replicates were performed for each type of film.

3.1.2.13. Statistical analysis

When necessary, the statistical significance of differences was determined by one-way analysis of variance (ANOVA), using Minitab 17 software (Minitab Inc., State College, PA, USA). Where appropriate, the mean values were compared through a Fisher's least significant difference (LSD) test with a significance level of $P < 0.05$.

3.2. Results and discussion

3.2.1. Exfoliation and dispersion of graphene oxide

GO obtained by the Hummers method can be readily dispersed in water by ultrasonic treatment, which allows keeping full exfoliation of GO sheet and the formation of transparent and stable suspensions (no precipitation occurred after several months) (Figure 3.1).



Figure 3.1. GO water dispersion (0.15 wt%) after 6 months.

Information about the morphology of the as-prepared GO sheets was obtained by AFM and TEM (Figure 3.2a-c). A GO sheet is supposed to be thicker than an ideal atomically flat graphene sheet which has a well-known thickness of 0.34 nm, due to the oxygen-containing functional groups on the basal plane and their defects introduced by the oxidation process. In some cases, the thickness of a GO sheet is even larger than 0.8 nm as predicted by the theory (Schniepp et al., 2006). As shown in Figure 3.2a and b, the measured thickness of the GO sheets ranged uniformly around 1.0 nm (more specifically, 1.12 ± 0.18 nm), suggesting the complete exfoliation of GO sheets down to individual layers. GO sheets width ranged between 1.5 and 4.0 μm (mean of 2.5 $\mu\text{m} \pm 0.3$), although individual sheets as large as 12 μm were also observed.

The TEM results also verified the existence of fully exfoliated individual GO sheet in water with a wrinkled structure (Figure 3.2c) resulting from reaction sites involved in oxidation (Schniepp et al., 2006).

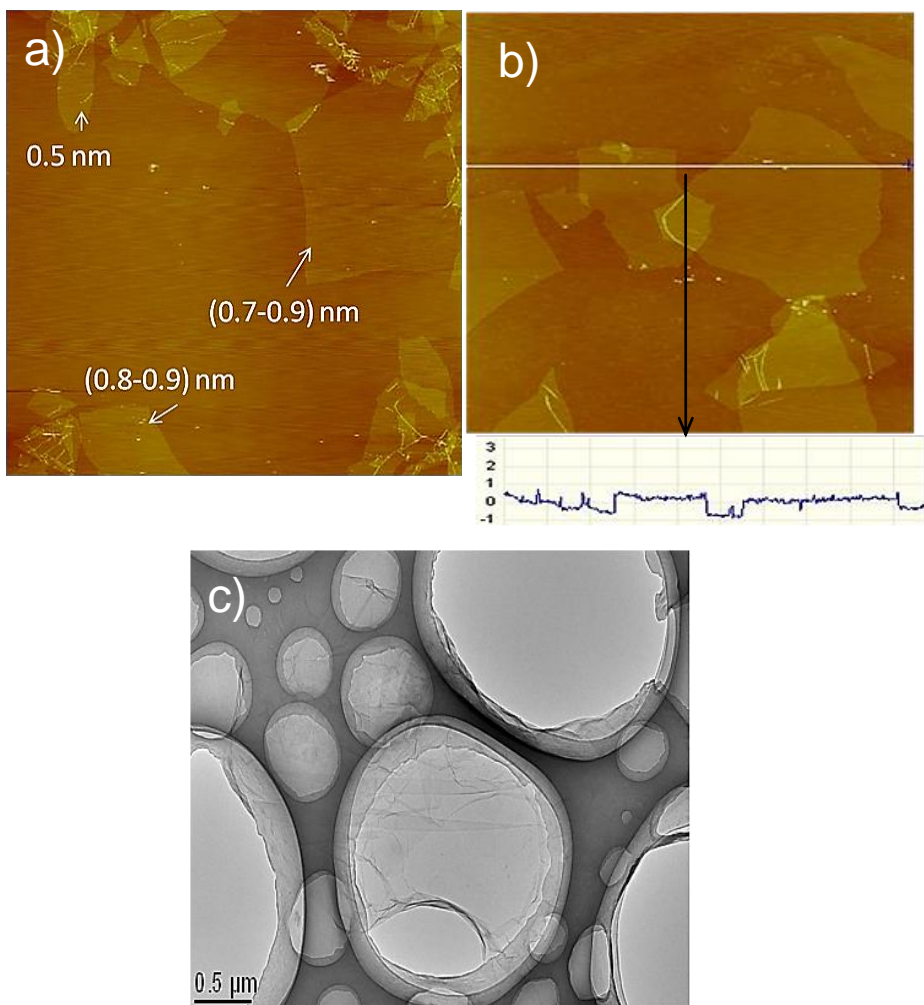


Figure 3.2. (a) $30 \times 30 \mu\text{m}^2$ AFM height image of GO nanosheets (both individual and overlapping sheets are clearly visible); (b) thickness determination of GO sheets by height profile of a $10 \times 10 \mu\text{m}^2$ AFM image; (c) TEM image of GO nanosheets.

The information on the functionalized groups on GO surface due to the oxidation process can be obtained from FTIR (Figure 3.3). In the GO spectrum, dominant peaks appear at 3318 cm^{-1} , 1714 cm^{-1} , 1623 cm^{-1} and 1164 cm^{-1} - 1045 cm^{-1} are assigned to OH stretching vibration, C=O stretching vibration of the carboxylic group, C=C stretching mode of the remaining sp^2 network, C-O stretching vibration of epoxy or alkoxy group, respectively (Li et al., 2012). This information unequivocally proved the successful oxidation of graphite.

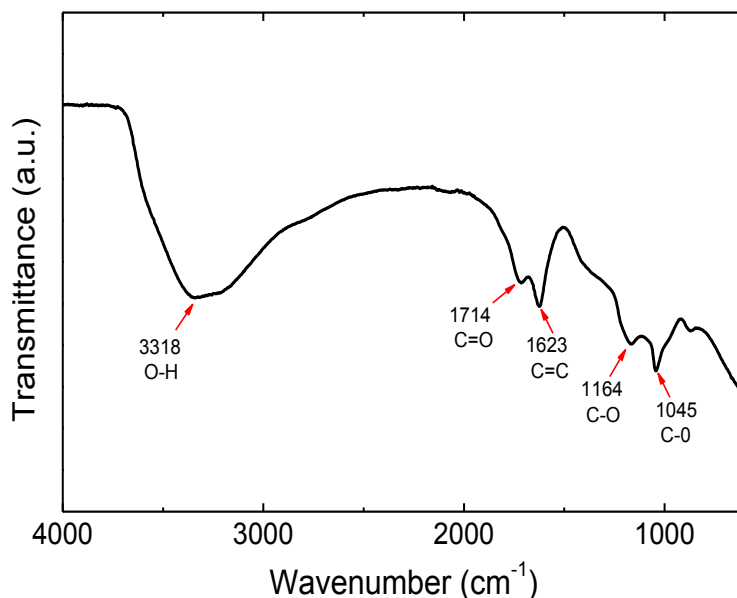
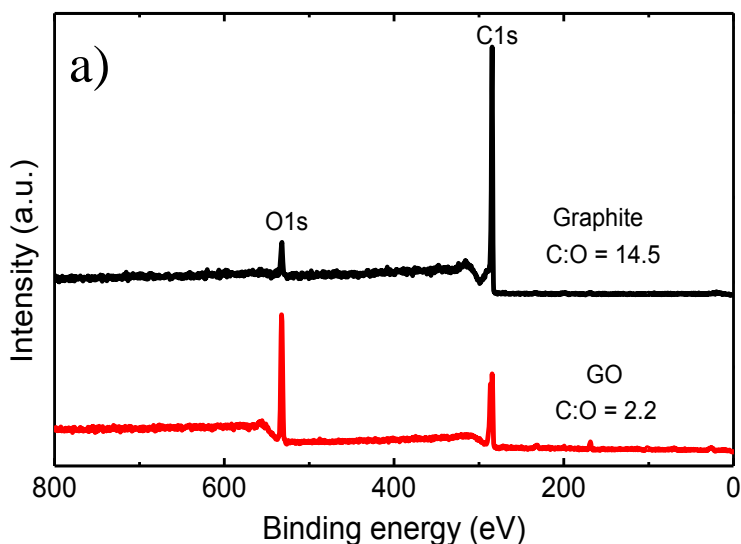


Figure 3.3. FT-IR spectra of GO.

The high degree of functionalization on GO was confirmed by XPS. The survey spectra of for graphite and GO (Figure 3.4a) yielded C/O atomic ratios of 14.5 and 2.2, respectively as a result of the oxidation process. As displayed in Figure 3.4b, the C 1s band can be fitted to three components corresponding of carbon atoms in different functional groups: C-C/C=C in aromatic rings, (284.4 eV) C-O (epoxy and alkoxy) (286.6 eV) and C=O (288.3 eV), (Stankovic et al., 2007; Gao et al., 2009) respectively. The ratios of C-C, C-O, and C=O were determined to be 55.33%, 34.07% and 9.46%, respectively.



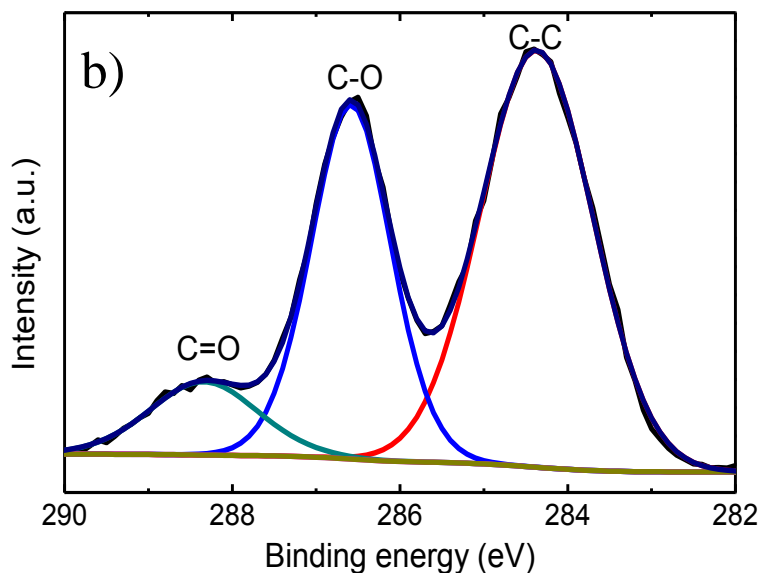
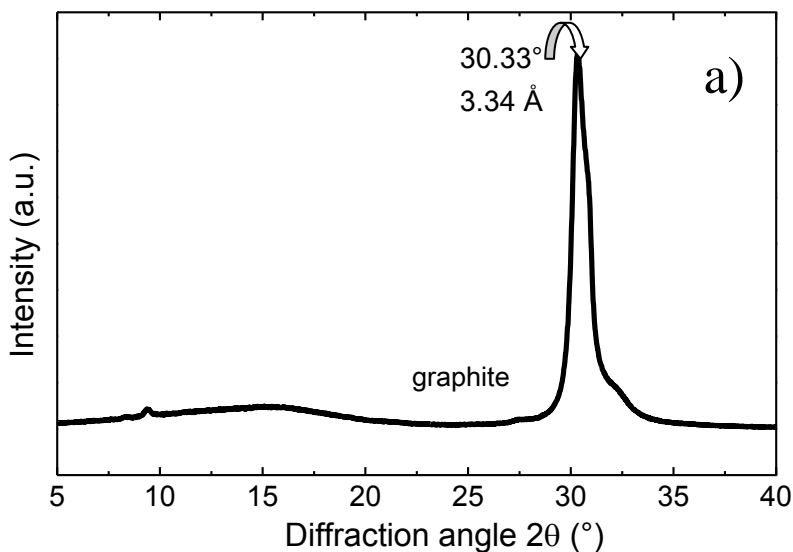


Figure 3.4. (a) XPS survey spectra of graphite and GO; (b) deconvolution of the C 1s peak of GO.

XRD patterns of graphite and GO powders are shown in Figure 3.5a and b. It can be seen that the crystallinity was sharply decreased after the oxidation. According to the Bragg equation, the interlayer distance of graphite oxide was expanded from 0.334 to 1.256 nm, giving the evidence of the presence of oxygen-containing functional groups. The diffraction peak observed at 30.33° of natural graphite was shifted to 8.17° , which was a clear indication of the complete transformation from graphite to GO.



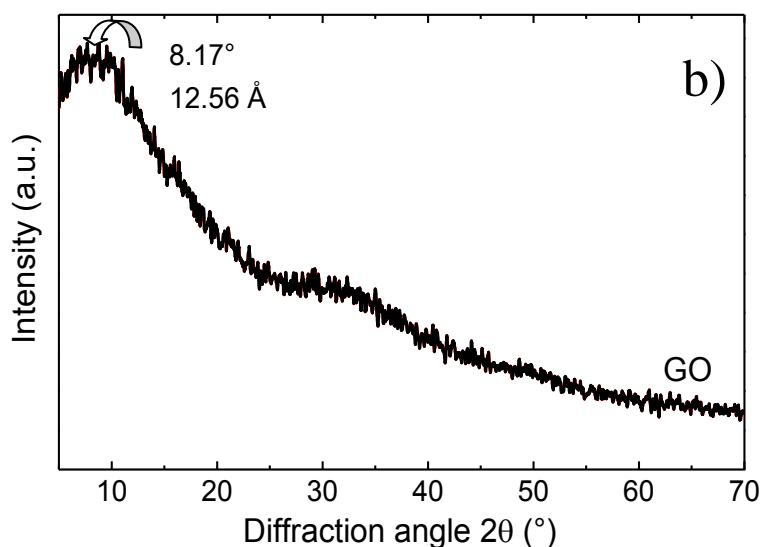


Figure 3.5. XRD diffractogram of (a) graphite; (b) GO powder.

Raman spectroscopy is widely used to characterize crystal structure, disorder and defects in graphene-based materials (Ferrari, 2007). As shown in Figure 3.6, GO showed two broad bands: the D band at 1355 cm^{-1} and G band at 1603 cm^{-1} . The prominent D band for GO clearly indicates the presence of structural defects induced by the attachment of hydroxyl and epoxide groups on the carbon basal plane. A weak and broad 2D peak was appeared at 2719 cm^{-1} indicating disorder as the result of an out-of-plane vibration mode after oxidation (Eda et al. 2008). These G, D, and 2D bands agree with previous characterizations of GO (Stankovich et al. 2007; Guo et al. 2010).

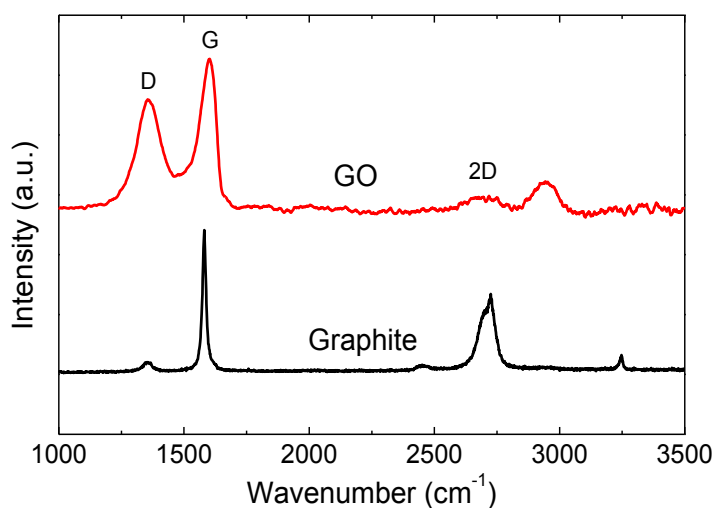


Figure 3.6. Raman spectra of graphite and GO.

TGA results confirmed that GO was less stable than graphite from a thermal point of view (Figure 3.7), undergoing degradation at ~ 170 °C with 50% mass loss due to the decomposition of labile oxygen functional groups (Chen et al., 2010).

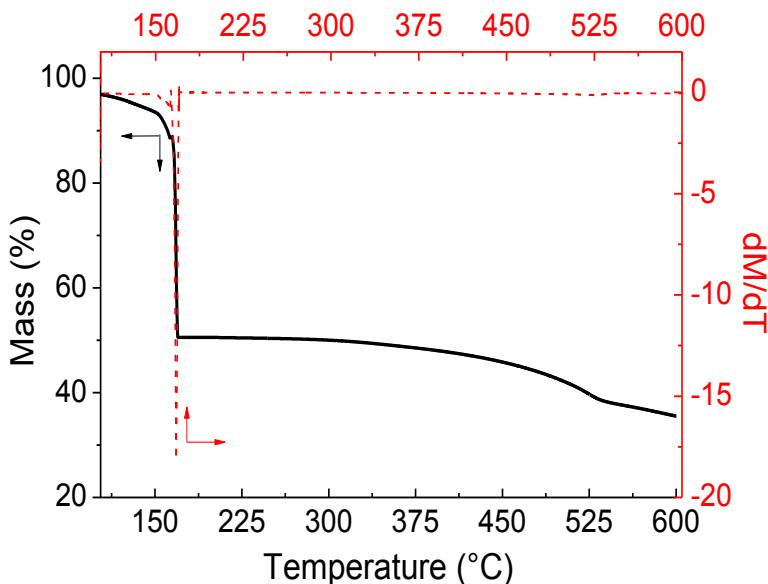


Figure 3.7. TGA and DTG curves of GO.

3.2.2. Characterization and pullulan/GO nanocomposite films

By employing casting technique well-dispersed pull/GO nanocomposite films were fabricated. Because of the abundant oxygen containing functional groups on the surface of the GO sheets that endow it with higher polarity, they were dispersed in pull water solutions at the level of individual sheets.

3.2.2.1. Thermal stability

The results arising from thermal gravimetric analysis are summarized in Table 3.1, in which only 4 representative samples are shown. Figure 3.8 depicts the traces obtained from the samples exposed to nitrogen atmosphere along with the first-order derivatives. The temperature at which the weight loss is 50% (T_{d50}) increased by about 16 °C in the case of the bionanocomposites with the highest amount of GO.

Accordingly, the residual weight of the bionanocomposites at 600 °C is higher than that of pristine pull, which can be attributed that most part of GO remained in the nanocomposites at high temperature and showed the good thermal stability over the process temperature. In Figure 3.8b, the different peak intensity reflects the increasing amount of the inorganic phase in samples 0.05, 0.2

and 1.0 wt%, respectively, which are degraded less upon heating. It can also be observed that the maximum decrease in mass occurred between 293.1 and 300.6 °C for all the four materials.

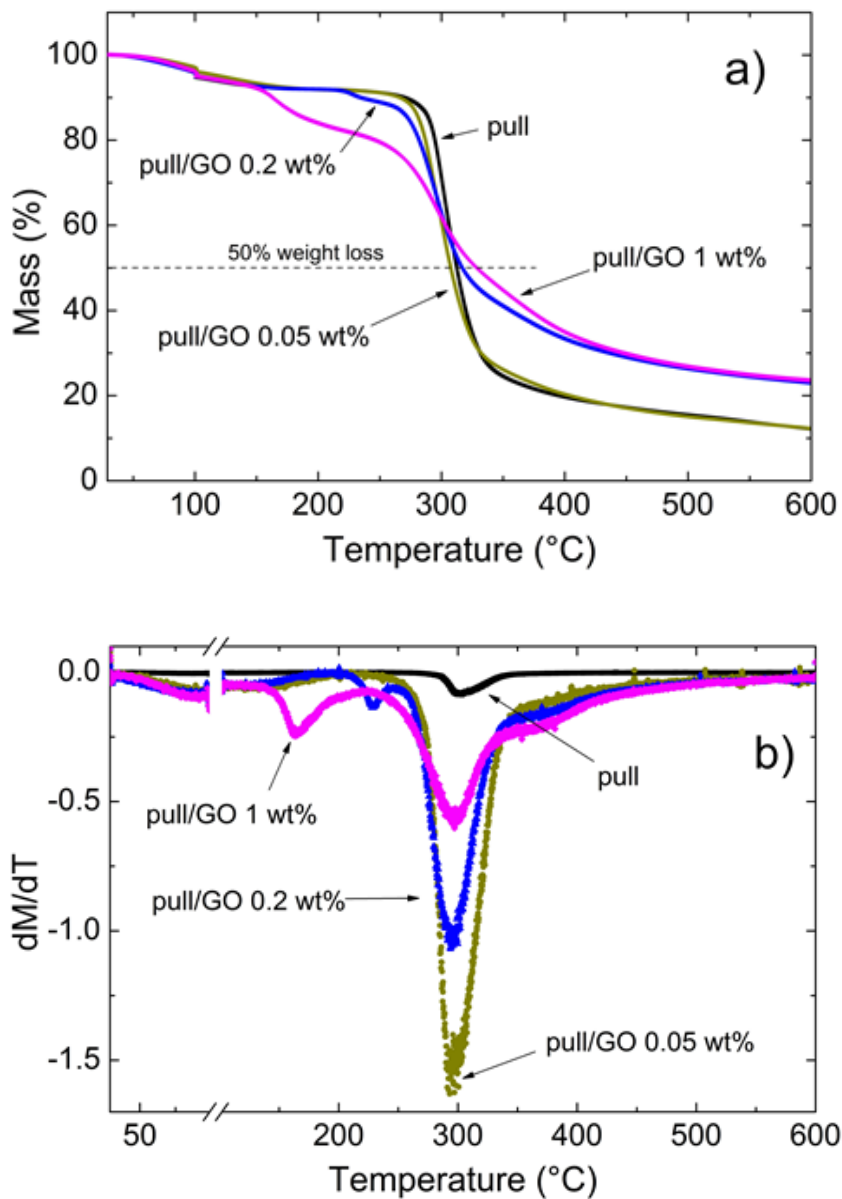


Figure 3.8. (a) TGA traces; b) their first-order derivatives of four representative bionanocomposite films exposed to N_2 atmosphere.

Table 3.1. Main parameters drawn from the TGA analysis of pull and pull/GO bionanocomposites.

Film type	Onset (°C)	T _{max} (°C)	T _{d50} (°C)	Char yield (%) at 600 °C
Pull	283.3	300.6	312.5	12.1
Pull/GO 0.05%	273.9	293.1	307.6	12.3
Pull/GO 0.2%	271.3	293.8	317.2	22.9
Pull/GO 1 %	270.4	297.2	328.6	23.6

More specifically, pull films was subjected one-step degradation with maximum degradation rate at 300.6 °C (T_{max}). T_{max} shifted to lower temperature (~ 293 °C) for the samples pull/GO 0.05 wt% and pull/GO 0.2 wt%, whereas a higher value (T_{max} ~ 297 °C) was recorded for the sample pull/GO 1.0 wt%, (Table 3.1). This observation (i.e., the higher T_{max} for the sample pull/GO 1.0 wt%) can be plausibly explained by the segregation of the polymer matrix and the filler at high GO concentrations (thus the ‘protective’ effect of the filler was partially lost).

This seems to be supported by the presence of two additional peaks for the pull films loaded with 0.2 wt% and 1.0 wt% GO at, respectively, 229.7 and 165.5 °C. The peak at 165.5 °C, in particular, can be associated with the decomposition temperature of GO, which is ~ 170 °C (Figure 3.7). Therefore, less interfacial effect between stacked GO at 1.0 wt% and pull most likely resulted in the clear detection of GO decomposition temperature. Further confirmation of this can be gathered by the SEM images (Figure 3.9). At low filler volume fraction (e.g., $\phi = 0.002$, 0.05 wt%) there is no evidence of GO aggregates throughout the scanned cross-sectional area of the films—the morphology in Figure 3.9b looks like that one of Figure 3.9a for pristine pull films. As the filler concentration increased (e.g., $\phi = 0.01$, 1 wt%), GO sheets stacking on top one of another were more often detected, indicating the tendency of exfoliated layers to re-aggregate (Figure 3.9c).

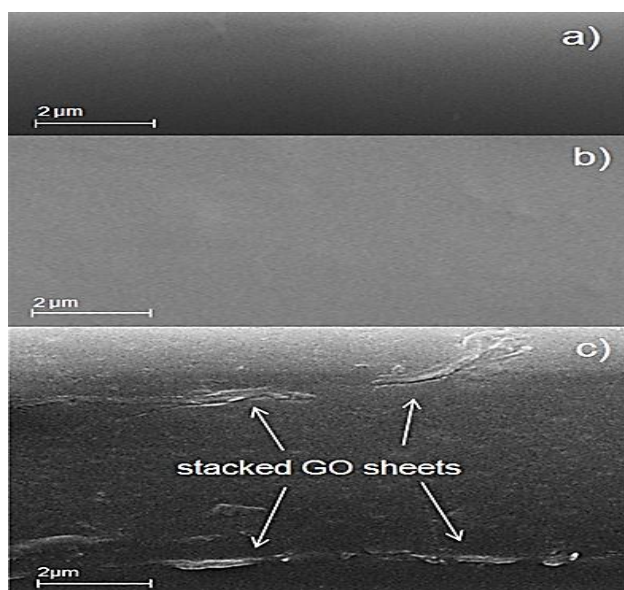


Figure 3.9. Cross-sectional SEM images of (a) pristine pull film; (b) pull/GO film (ϕ 0.002); (c) pull/GO film (ϕ 0.01).

3.2.2.2. Oxygen barrier performance

Experimental O_2TR values are reported in Table 3.2. However, to get a more realistic interpretation of the oxygen barrier performance, these values have been converted to oxygen permeability ($P'O_2$), which allows resetting any influence arising from a different thickness of final films.

Table 3.2. GO content, GO volume fraction (ϕ), thickness (l), oxygen transmission rate (O_2TR), and oxygen permeability coefficient ($P'O_2$) of bionanocomposite films at 70% RH and 23 °C.

GO content (wt%)	ϕ^*	l (μm)	O_2TR [mL m ⁻² (24h ⁻¹)]	$P'O_2$ [mL μm m ⁻² (24h ⁻¹) atm ⁻¹]
0	0	35±2.22 ^c	181.04±20.05 ^a	6337±285 ^a
0.05	0.00051	43±2.10 ^a	60.79±5.97 ^c	2614±180 ^b
0.1	0.00102	26±2.88 ^d	98.18±11.04 ^b	2553±191 ^b
0.2	0.00204	35±1.84 ^c	56.93±4.87 ^c	2277±251 ^c
0.3	0.00305	41±2.38 ^{ab}	33.09±2.94 ^d	1357±162 ^d
1.0	0.01009	40±2.26 ^{ab}	46.47±3.98 ^{cd}	1812±149 ^{cd}

* Calculated for a given GO density (ρ) = 0.981 g·cm⁻³.

Different superscripts within a group (i.e. within each parameter) denote a statistically significant difference ($P < 0.05$).

As shown in Figure 3.10, O₂ gas permeability of pristine pull film is sharply decreased with addition of very low concentration of GO (0.05 wt%), which yielded ~ 59% reduction in $P'O_2$ (from 6337 to 2614 mL $\mu\text{m m}^{-2} (24\text{h}^{-1}) \text{atm}^{-1}$).

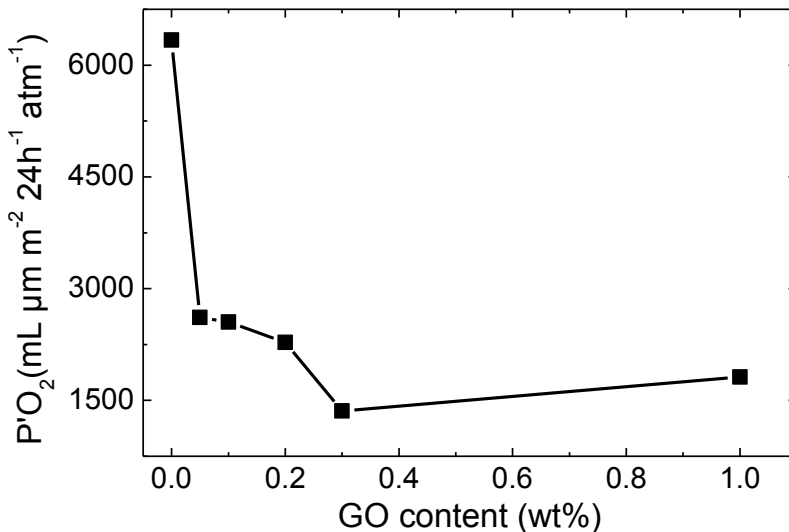


Figure 3.10. Oxygen permeability value at 70% RH as a function of GO concentration.

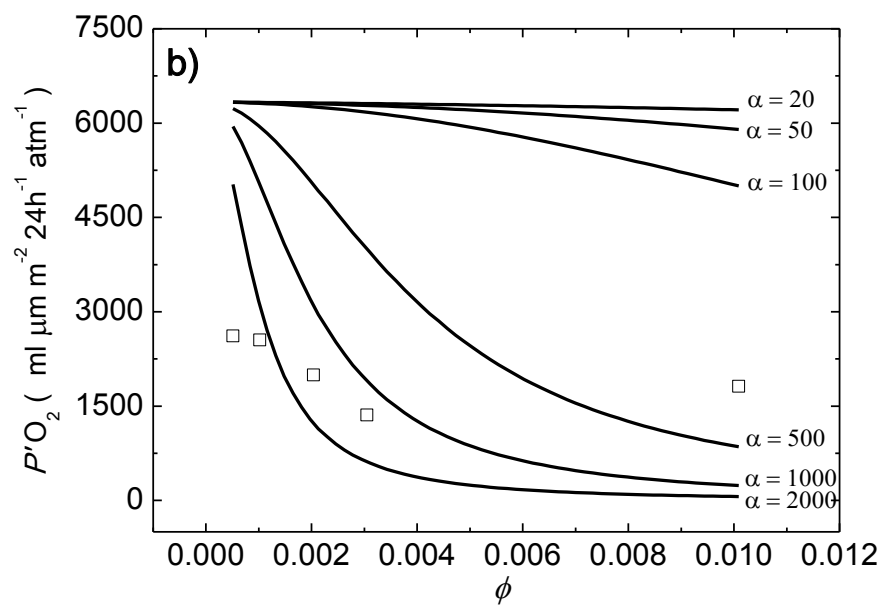
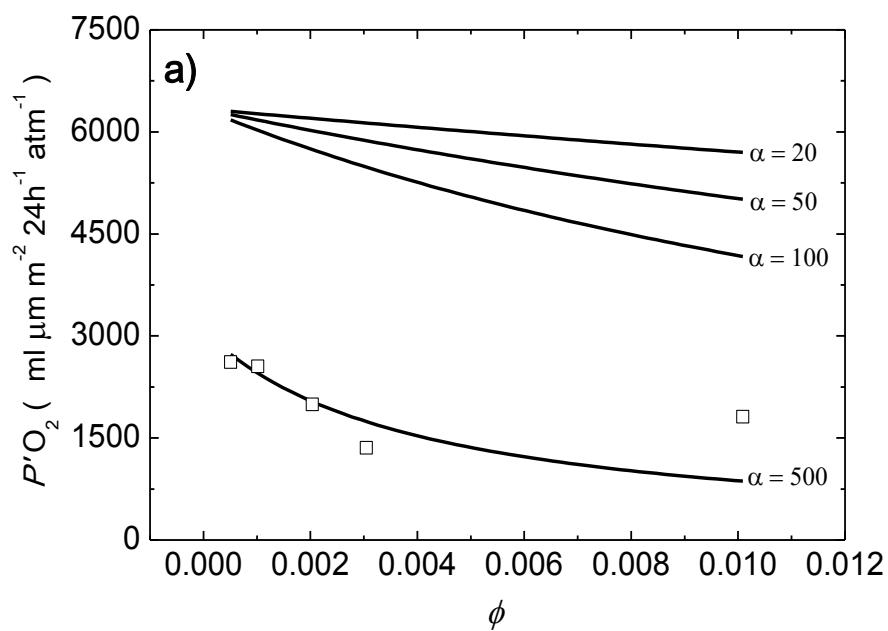
For GO content >0.05 wt% ($\phi > 0.0051$) a further increase in the barrier performance was obtained. For example, the addition of 0.3 wt% GO (i.e., $\phi = 0.00305$) led to 79% decrease in $P'O_2$ (1357 mL $\mu\text{m m}^{-2} (24\text{h}^{-1}) \text{atm}^{-1}$). Unexpectedly, a break in this trend was observed at 0.5 wt% loading ($P'O_2 = 4904$ mL $\mu\text{m m}^{-2} (24\text{h}^{-1}) \text{atm}^{-1}$) and, even though to a lesser extent, at 1.0 wt% loading ($P'O_2 = 1812$ mL $\mu\text{m m}^{-2} (24\text{h}^{-1}) \text{atm}^{-1}$), which can be attributed to poor dispersion and/or inefficient orientation of GO sheets in the pullulan matrix. Based on these results, the addition of GO even at low concentrations endows pullulan matrix with outstanding gas barrier capability, which in turn makes it more competitive than petroleum based polymers in the packaging industry. For example: $P'O_2$ values of PET [1560 mL $\mu\text{m m}^{-2} (24\text{h}^{-1}) \text{atm}^{-1}$] at 70% RH, 23 °C (Introzzi et al., 2012); $P'O_2$ values of PET, OPP, and LDPE (0% RH, 23 °C): 1381 mL $\mu\text{m m}^{-2} (24\text{h}^{-1}) \text{atm}^{-1}$, 33627 mL $\mu\text{m m}^{-2} (24\text{h}^{-1}) \text{atm}^{-1}$, and 124624 mL $\mu\text{m m}^{-2} (24\text{h}^{-1}) \text{atm}^{-1}$, respectively (Farris et al., 2009).

Modelling of $P'O_2$ data may provide information about the distribution of the inorganic platelets and the interphase organization in the final bionanocomposites, to the advantage of a more detailed interpretation of the ultimate O₂-barrier performance. Figure 3.11 displays the experimental $P'O_2$ data of the bionanocomposite films at 70% RH and 23 °C, together with theoretical predictions based on Nielsen's (eq. 3.2) and Cussler's permeation theoretical models (eq. 3.3a and 3.3b), which describe the permeation phenomenon for impermeable square platelets dispersed in a continuous matrix (Nielsen, 1967; Lape et al., 2004; Takashi et al., 2006):

$$P_0/P \cdot (1-\phi) = 1 + (\alpha\phi)/2 \quad (3.2)$$

$$P_0/P \cdot (1-\phi) = 1 + (\alpha\phi)^2/4 \quad (3.3a)$$

$$P_0/P \cdot (1-\phi) = 1 + (\alpha\phi/3)^2 \quad (3.3b)$$



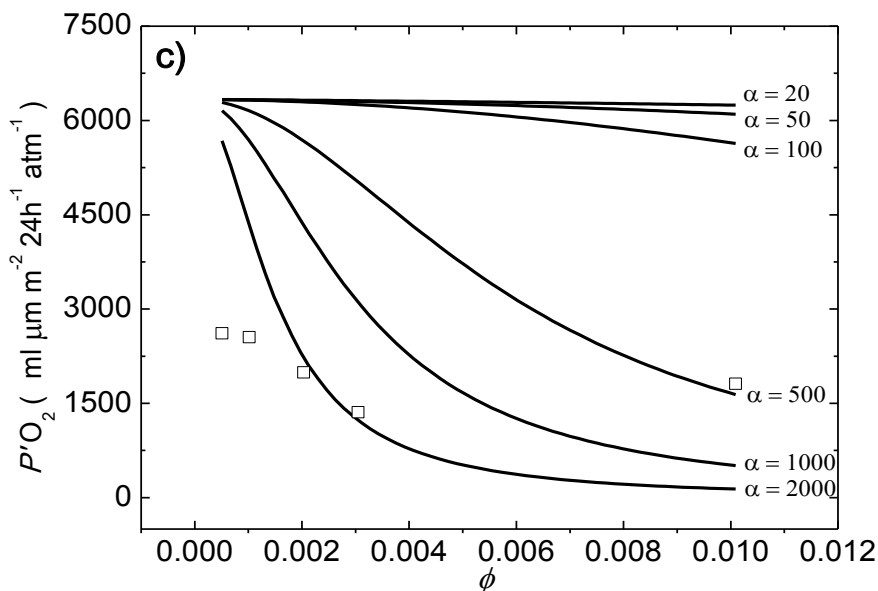


Figure 3.11. Oxygen permeability of bionanocomposite films. Experimental values (\square), and values predicted by Nielsen's model (panel a, eq. 3.2 in the text) and Cussler's models (panels b and c, eqs. 3.3a and 3.3b in the text) for different aspect ratios (\square) are depicted.

$P'O_2$ experimental data well fitted with Nielsen's prediction for $\alpha = 500$ (Figure 3.11a). However, a clear deviation was observed for the highest ϕ value, which can be reasonably due to the aggregation of GO at high loading, which reduces the effective aspect ratio of GO sheets. It should be here noted that the prediction by Nielsen's model applies for a regular array (also called "bricks-and-mortar", i.e. regularly spaced flake "bricks" held together by polymer "mortar") distribution of non-overlapping, fully intercalated platelets perpendicular to the gas diffusion direction (Lape et al., 2004; Choudalakis et al., 2009). In practice, Nielsen's model is accurate in the dilute regime, i.e. for low values of the volume fraction ($\phi \ll 1$) and the aspect ratio ($\alpha \ll 1$) of the nanoplatelets (thus when $\alpha\phi \ll 1$) (Picard et al., 2007). Because in our study $\alpha \sim 1500$ and $0.0005 < \phi < 0.01$, the product $\alpha\phi$ varies from 0.8-15.1, which locates our system between dilute and semi-dilute regimes, the latter being verified when the flake concentration is small but the flakes overlap. This means that ($\phi \ll 1$, $\alpha \gg 1$, and $\alpha\phi \gg 1$) (DeRocher et al., 2005).

Due to the inadequacy of the Nielsen's model in the semi-dilute regime, we also took into consideration Cussler's models (Lape et al., 2004) for regular (eq. 3.3a) and random (eq. 3.3b) arrays of ribbons in a semi-dilute regime, where permeability varies linearly with the square of the factor $\alpha\phi$ [i.e., $(\alpha\phi)^2$], contrary to the Nielsen's model.

The most relevant observation is that both Cussler's models approached the best fitting of experimental data for α between 1000 and 2000 (Figure 3.11b and c), in line with our experimental values gained by AFM. On one hand, this suggests an underestimation of the GO aspect ratio provided by the Nielsen's model compared to Cussler's models. On the other hand, the model simulation strongly support the higher aspect ratio of 2D GO compared to widely used inorganic clays, e.g. montmorillonite, which have been reported to have aspect ratios (α) between 10 and 100 for a similar pullulan-based system (Introzzi et al., 2012; Fuentes-Alventosa et al., 2013). This

aspect turns to be of great importance during the design of high performance barrier materials (e.g., films and coatings), as the performance provided by GO is in principle much more effective over clays due to the longer pathway offered to the permeant (eg., oxygen molecules).

3.2.2.3. Tensile properties

Figure 3.12 shows the typical stress–strain curves of pristine pullulan films and pullulan/GO nanocomposites, whereas tensile strength, Young modulus, and elongation at break for the different formulations are summarized in Table 3.3.

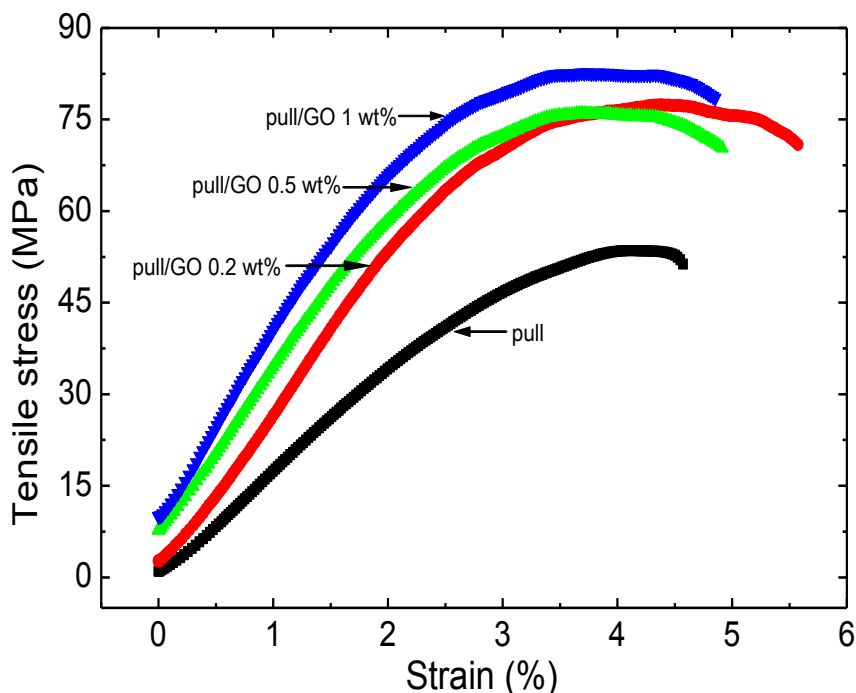


Figure 3.12. Typical stress–strain curves for pristine pull and pull nanocomposite films with various contents of GO.

Pristine pull film had tensile strength of ~ 57 MPa, Young modulus of ~ 1500 MPa, and an elongation at break of ~ 6.7%, in line with the values found in literature (Fernandes et al., 2014). However, the addition of GO led to a significant improvement of the tensile strength and Young modulus. The tensile strength and Young modulus increased sharply by 49% from 50 MPa to 74 MPa and by 104% from 1556 MPa to 3178 MPa, respectively, upon an increase of GO from 0 to 1.0 wt%, respectively. Interestingly, up to 0.2 wt% GO the elongation at break of the nanocomposite films gradually increases by 52% but unfortunately, more GO loading could not provide any further enhancement in elongation of biocomposites.

Table 3.3. Tensile properties of pristine pull and pull nanocomposite films with various contents of GO.

GO content (wt%)	Tensile Strength (MPa)	Young Modulus (MPa)	Elongation (%)
0	50.05±4.01 ^c	1556±92 ^c	4.36±0.76 ^b
0.05	57.49±4.55 ^{abc}	1819±164 ^c	5.65±1.54 ^{ab}
0.1	54.65±16.89 ^{bc}	1940±605 ^b ^c	5.85±2.77 ^{ab}
0.2	70.10±7.77 ^{ab}	2246±811 ^{bc}	6.62±1.69 ^a
0.3	59.48±10.09 ^{abc}	2184±552 ^b ^c	4.33±0.59 ^{ab}
0.5	69.57±18.92 ^{ab}	2647±717 ^{ab}	4.72±1.01 ^{ab}
1	74.30±13.89 ^a	3178±538 ^a	4.44±1.07 ^b

Different superscripts within a group (i.e. within each parameter) denote a statistically significant difference ($P < 0.05$).

Arising from these results, GO acted as a reinforcement of the main biopolymer phase, plausibly due to the enhanced interface effect resulting from the nano-scale dispersion of aligned GO sheets within the pull matrix. In particular, chemical affinity between GO and pull may contribute to extensive interactions (e.g., hydrogen bonding) at the polymer/filler interface, which in turn improve the interfacial adhesion, thus the stiffness of final films. Concurrently, the compatibility between phases greatly enhances the unidirectional dispersion of the large aspect ratio GO sheets on molecular scale. This leads to a more uniform stress distribution and minimizes the presence of stress concentration centers thus significantly increasing the mechanical properties of the nanocomposite films (Coleman et al., 2006; Yang et al., 2010).

Analogously to permeability data, Young modulus experimental values were compared to the prediction made by the well-established Halpin–Tsai’s models with the goal of acquiring more details about the distribution pattern of the filler within the main polymer matrix. In particular, the Halpin-Tsai’s models allow distinguishing between unidirectional and randomly distributed filler-reinforced nanocomposites (Gao et al., 2005; Schaefer & Justice, 2007; Zhao et al., 2010) according to eqs. 3.4a and 3.4b, respectively (Affdl et al., 1976):

$$E_r = E_m \left[\frac{3}{8} \frac{1 + \eta_L \xi V_g}{1 - \eta} + \frac{5}{8} \frac{1 + 2\eta_T V_g}{1 - \eta_T V_g} \right] \quad (3.4a)$$

$$E_u = E_m \frac{1 + \eta_L \xi V_g}{1 - \eta_L V_g} \quad (3.4b)$$

being:

$$\eta_L = E_m \frac{E_g / E_m - 1}{E_g / E_m + \xi}; \quad \eta_T = E_m \frac{E_g / E_m - 1}{E_g / E_m + 2}; \quad \xi = \frac{2l}{3d}$$

where E_r and E_u represent the Young modulus of the composites with randomly distributed GO sheets and aligned GO sheets parallel to the surface of the sample, respectively. E_g and E_m are the Young modulus of GO (207600 MPa) (Suk et al., 2010) and pullulan (1556 MPa) (Table 3.3), respectively. l and d refer to the average length and thickness of an individual GO sheet, which were 2.5 μm and 1.12 nm, respectively, as determined by AFM analysis. V_g is the volume fraction of GO in the composites (see Table 3.2). As shown in Figure 3.13, the experimental Young modulus values of the bionanocomposites fit very well with the theoretically calculated values for the ‘unidirectional orientation’ model. This finding further supports previous indications that the GO sheets are unidirectionally aligned and parallel within the main biopolymer matrix, which would also explain the impressive mechanical performance of final films.

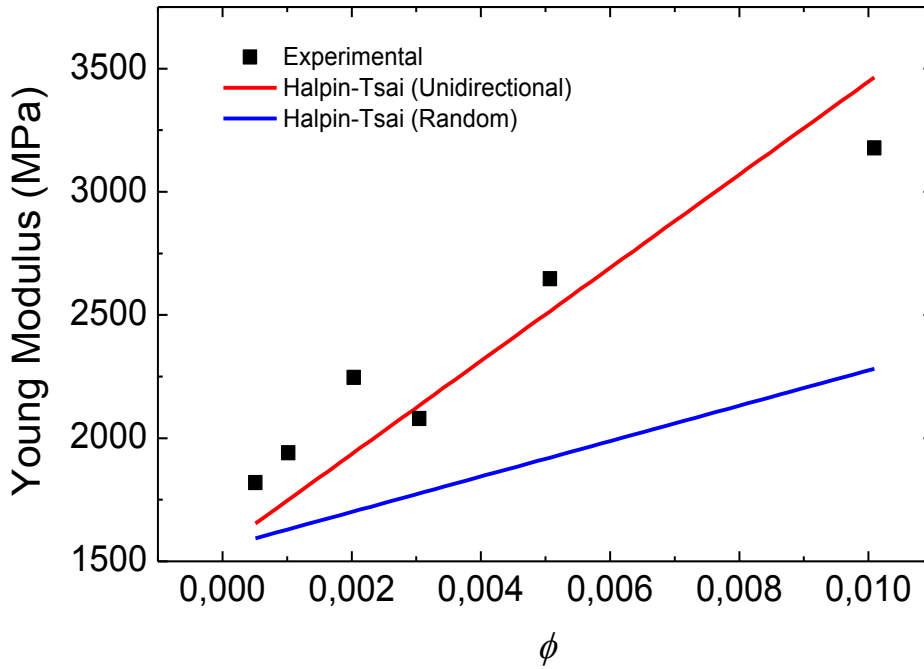


Figure 3.13. Experimental Young modulus values of bionanocomposite films and theoretical simulation for both random orientation and unidirectional distribution of GO sheets in the pullulan matrix according to Halpin–Tsai theoretical models (eqs. 3.4a and 3.4b in the text).

3.2.2.4. Optical properties

Optical properties of materials are particularly important in certain sectors, where they can impact either the performance of the final material or the consumer's choice. In the food packaging field, both aspects are relevant and worth high consideration when designing a new (bio)nanocomposite materials (Uysal Unalan et al., 2014). In particular, high transmittance of visible light (wavelengths between 340 nm and 800 nm) should be guaranteed, as it allows consumers to see through the package (visual inspection of the packaged food). Haze, defined as the percentage of transmitted light deviating by more than an angle of 2.5 from the direction of the incident beam, is an important optical property for packaging applications (Farris et al., 2009).

As confirmed by both the transmittance and haze values reported in Table 3.4, all the pull/GO binanocomposite films were fully comparable with pristine pullulan samples, with the exception of the transmittance value for the nanocomposite film at the highest GO concentration (1.0 wt%).

Table 3.4 Optical properties of pristine pull and pull nanocomposite films with various contents of GO.

GO content (wt%)	Transmittance (%)	Haze (%)
0	93.1±0.68 ^a	0.40±0.01 ^a
0.05	93.4±0.30 ^a	0.39±0.03 ^a
0.1	93.4±0.35 ^a	0.38±0.03 ^a
0.2	92.3±0.17 ^a	0.39±0.02 ^a
0.3	92.5±0.75 ^a	0.37±0.08 ^a
0.5	91.9±0.15 ^a	0.36±0.05 ^a
1	90.1±0.96 ^b	0.47±0.09 ^a

Different superscripts within a group (i.e. within each parameter) denote a statistically significant difference ($P < 0.05$).

For example, the light transmittance of pristine pullulan was found 93.1% and loading GO up to 0.5 wt% does not show any significant effect on the light transmittance, while the transmittance significantly decreases to 90% at the highest GO concentration (1.0 wt%). However, these bionanocomposite films still maintain favorable optical transparency.

Haze values, in particular, were below the 3% threshold, which is generally judged adequate in food packaging for a proper display of the products (Introzzi et al., 2012), although some plastics have haze values slightly higher (e.g., low-density polyethylene) (Cozzolino et al., 2014).

Overall, final films had smooth, uniform and transparent appearance, although the color of composite films gradually shifted from colorless to yellow-brown with increasing the GO content, as displayed in Figure 3.14. Based on these results, the pull/GO nanocomposite films exhibited acceptable optical properties for exploring new packaging applications.

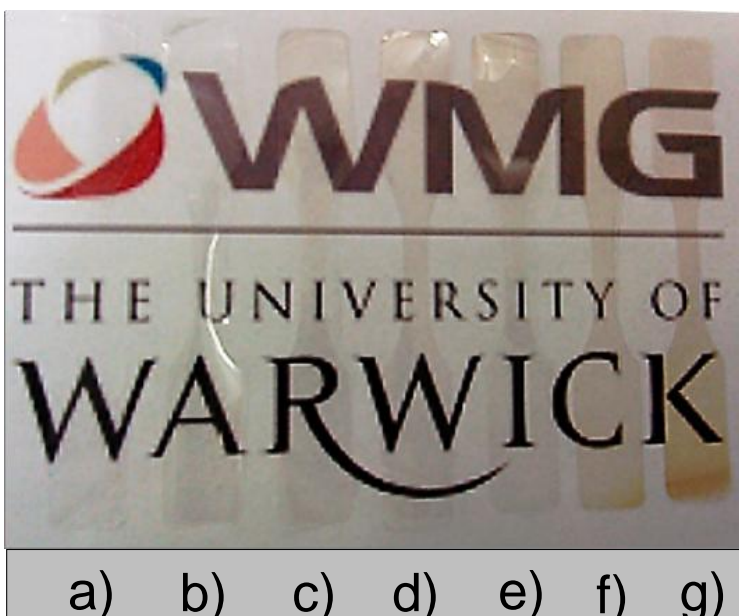


Figure 3.14. Image of a) pristine pullulan film and pull/GO films with different GO concentrations b) 0.05 wt%, c) 0.1 wt%, d) 0.2 wt%, e) 0.3 wt%, f) 0.5 wt% and g) 1 wt%.

3.3. Conclusions

Novel high-performance pull/GO nanocomposite films have been successfully prepared using a simple solution casting method. The high compatibility between GO sheets and pull allowed obtaining homogeneous and stable dispersions in water. Chemical affinity between GO and pull, which significantly enhanced the interfacial adhesion between the two phases was the main reason for the observed excellent oxygen, mechanical and thermal properties of the final nanocomposites. By comparing the experimental oxygen permeability and tensile modulus values with the values predicted by theoretical models it has been possible to understand that GO sheets are randomly arranged and aligned parallel to the surface of the main biopolymer matrix, as also suggested by the SEM images. Findings arising from this work reflect convincingly the fact that pull nanocomposite materials represent a promising alternative to the currently available synthetic polymer films, especially as far as their oxygen barrier and mechanical properties are concerned. Nonetheless, the optical transparency of all the nanocomposites was kept adequate for most packaging applications. It is thus expected that the pull/GO nanocomposite films and coatings may find important applications in the food packaging sector that increasingly requires largely improved barrier and tensile properties while trying to reduce the overall amount of plastics used.

3.4. References

- Affdl JCH, Kardos JL, 1976, The Halpin–Tsai equations: a review. *Polym Eng Sci* 16:344-352.
- Chen W et al., 2010, Chemical reduction of graphene oxide to graphene by sulfur-containing compounds. *J Phys Chem C* 114 :19885-19890.
- Choudalakis G, Gotsis AD, 2009, Permeability of polymer/clay nanocomposites: a review. *Eur Polym J* 45:967-984.
- Coleman JN et al., 2006, Mechanical reinforcement of polymers using carbon nanotubes. *Adv Mater* 18:689-706.
- Cozzolino et al., 2014, Microfibrillated cellulose (MFC): pullulan bionanocomposite films. *Cellulose* 21:4323-4335.
- DeRocher JP et al., 2005, Barrier membranes with different sizes of aligned flakes. *J membrane sci* 254:21-30.
- Eda et al., 2008, Large-area ultrathin films of reduced graphene oxide as a transparent and flexible electronic material. *Nat Nanotech* 3:270-274.
- Farris et al., 2009, Evaluation of a bio-coating as a solution to improve barrier, friction and optical properties of plastic films. *Packag Technol Sci* 22:69-83.
- Fernandes SC et al., 2014, Antimicrobial pullulan derivative prepared by grafting with 3-aminopropyltrimethoxysilane: Characterization and ability to form transparent films. *Food Hydrocolloids* 35:247-252.
- Ferrari AC, 2007, Raman spectroscopy of graphene and graphite: Disorder, electron–phonon coupling, doping and nonadiabatic effects. *Solid State Commun* 143:47-57.
- Fuentes-Alventosa JM et al., 2013, Self-assembled nanostructured biohybrid coatings by an integrated sol–gel/intercalation approach. *RSC Adv* 3:25086-25096.
- Gao W et al., 2009, New insights into the structure and reduction of graphite oxide. *Nat Chem* 1:403-408.
- Guo Y et al., 2014, Chitin/graphene oxide composite films with enhanced mechanical properties prepared in NaOH/urea aqueous solution. *Cellulose* 21:1781-1791.
- Hummers WS, Offeman RE, 1958, Preparation of graphitic oxide. *J Am Chem Soc* 80:1339.
- Introzzi L et al., 2012, Ultrasound-assisted pullulan/montmorillonite bionanocomposite coating with high oxygen barrier properties. *Langmuir* 28:11206-11214.
- Lape NK. et al., 2004, Polydisperse flakes in barrier films. *J membrane sci* 236:29-37.
- Li et al., 2012, Preparation and characterization of chitosan/graphene oxide composites for the adsorption of Au (III) and Pd(II). *Talanta* 93:350–357.

Nielsen LE, 1967, Models for the permeability of filled polymer systems.. J Macromol Sci A 1: 929-942.

Picard E et al., 2007, Barrier properties of nylon 6-montmorillonite nanocomposite membranes prepared by melt blending: influence of the clay content and dispersion state: consequences on modelling . J Membrane Sci 292:133–144.

Schaefer DW, Justice RS, 2007, How nano are nanocomposites? Macromolecules 40:8501-8517.

Schniepp HC et al., 2006, Functionalized single graphene sheets derived from splitting graphite oxide. J Phys Chem B 110:8535-8539.

Stankovich S et al., 2007, Synthesis of graphene-based nanosheets via chemical reduction of exfoliated graphite oxide. Carbon 45:1558-1565.

Suk JW et al., 2010, Mechanical properties of monolayer graphene oxide. ACS Nano 4: 6557–6564.

Svagan AJ et al., 2012, Transparent films based on PLA and montmorillonite with tunable oxygen barrier properties. Biomacromolecules 13:397–405.

Takahashi S et al., 2006, Gas barrier properties of butyl rubber/vermiculite nanocomposite coatings. Polymer 47:3083–3093.

Uysal Unalan I. et al., 2014, Nanocomposite films and coatings using inorganic nanobuilding blocks (NBB): current applications and future opportunities in the food packaging sector. RSC Adv 4:29393-29428.

Wan C, Chen B, 2012, Reinforcement and interphase of polymer/graphene oxide nanocomposites. J Mater Chem 22:3637-3646.

Yang X et al., 2010, Well-dispersed chitosan/graphene oxide nanocomposites. ACS Appl Mater Interfaces 2:1707-1713.

Zhao X et al., 2010, Enhanced mechanical properties of graphene-based poly(vinyl alcohol) composites. Macromolecules 43:2357–2363.

4. TOPIC 2

High performance pullulan/chitosan or pullulan/alginate blend systems with graphene oxide for food packaging applications

The results obtained in the first part allowed highlighting the great potential of graphene-based pullulan bionanocomposites as oxygen barrier even at high relative humidity (70% RH) values. Although pullulan/GO bionanocomposites showed highly desirable oxygen barrier performance, the use of pullulan is currently limited due to its high cost. One approach used to overcome this problem is blending pullulan with other relatively cheap compatible polysaccharides such as alginate and chitosan. Polymer blending continue to attract much attention both academically and industrially due to their potential for producing new polymeric material with tailored properties without having to synthesize totally new material. The advantages also include simplicity, versatility and cost efficiency.

Therefore, the present study was initiated to compare the thermal, mechanical and barrier properties of pullulan, GO enhanced pullulan/chitosan and pullulan/alginate blend systems prepared using the same technique used in part 1. Not less important, the optimized formulations may allow achieving a well-balanced performance/cost ratio.

4.1. Materials and methods

4.1.1. Materials

Pullulan (PF-20 grade, Mw~200 000 DA) was obtained from Hayashibara Biochemical Laboratories Inc., Okayama, Japan. Chitosan (viscosity < 200 mPa s, degree of deacetylation: 85–95%) was purchased from Shanglong Aokang Bio Ltd., China. Sodium alginate (medium viscosity; viscosity of 2% solution in water at 25°C \geq 2000 cps) and graphene flakes were purchased from Sigma Aldrich, UK. Hydrogen peroxide aqueous solution (H₂O₂, 20-35 wt%), hydrochloric acid (HCl), potassium permanganate (KMnO₄, > 95 wt%), sodium nitrate (NaNO₃, > 95 wt%), and sulfuric acid (H₂SO₄, > 95 wt%) were all analytical grade and purchased from Fisher Scientific, UK.

4.1.2 Methods

4.1.2.1. Chemical synthesis of graphene oxide

Please refer the section 3.1.2.1.

4.1.2.2. Preparation of blend systems

Pullulan and alginate film solutions (5 wt%) were prepared in water whereas chitosan film solution (2 wt%) was dissolved in water with 1 wt% acetic acid with a continuous 1 h stirring at ambient temperature. Then, the obtained polymer solutions were mixed to prepare pullulan:chitosan (80:20), pullulan:chitosan (60:40), pullulan:alginate (80:20) and pullulan:alginate (60:40) for 1 h. Resulting polymer blend film solutions were mixed GO/water dispersion with a continuous 1 h stirring at ambient temperature to prepare bionanocomposite solutions with GO concentrations of 0.2 wt%. The resultant blend polymer/GO solutions were cast onto Petri dishes and dried at ambient temperature for 3 days. The dried films were kept at sealed anhydrous desiccators for at least one week before analysis.

4.1.2.3. Thermogravimetric analysis

Please refer the section 3.1.2.7.

4.1.2.4. Oxygen barrier properties

Please refer the section 3.1.2.10.

4.1.2.5. Tensile properties

Please refer the section 3.1.2.11.

4.1.2.6. Optical properties

Please refer the section 3.1.2.12.

4.1.2.7. Statistical analysis

Please refer the section 3.1.2.13.

4.2. Results and discussions

4.2.1. Blend systems

Morphology of GO nanosheets were characterized by different characterization techniques in the first part of thesis. As characterized by AFM, thickness of the GO sheets ranged uniformly around 1.0 nm (more specifically, 1.12 ± 0.18 nm), suggesting the complete exfoliation of GO sheets down to individual layers. GO sheets width ranged between 1.5 and 4.0 μm (mean of $2.5 \mu\text{m} \pm 0.3$), although individual sheets as large as 12 μm were also observed.

Blend property and morphologies depend mainly on the degree of miscibility of individual components. A literature survey revealed that miscibility studies of pullulan/chitosan (Wu et al., 2013) and pullulan/sodium alginate (Prasad et al., 2012; Xiao et al., 2012) have been carried out by various techniques in different percentage of blend components and the finding of those studies have suggested that the blends are miscible and showed the enhanced film-forming properties. Therefore, in this part GO enhanced pullulan/chitosan and pullulan/alginate blend systems were prepared and investigated in terms of the thermal, mechanical and barrier properties.

4.2.2. Thermal stability

The results arising from thermal gravimetric analysis are summarized in Table 4.1.

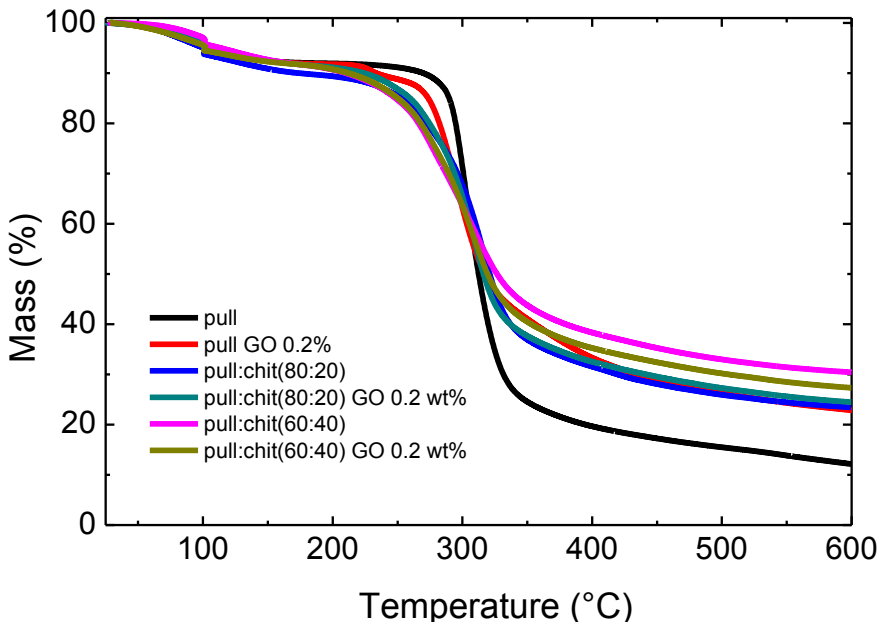
Table 4.1. Main parameters drawn from the TGA analysis of blend systems.

Film type	T_{max} ($^{\circ}\text{C}$)	T_{d50} ($^{\circ}\text{C}$)	Char yield (%) at 600 $^{\circ}\text{C}$
pull	300.6	312.5	12.1
pull GO 0.2 wt%	293.1	307.6	12.3
pull:chit (80:20)	318.2	321.1	23.4
pull:chit (80:20) GO 0.2 wt%	311.9	316.1	24.5
pull:chit (60:40)	305.5	326.4	30.4
pull:chit (60:40) GO 0.2 wt%	308.6	319.4	27.3
pull:alg (80:20)	299.9	302.4	22.3
pull:alg (80:20) GO 0.2 wt%	295.0	304.4	22.5
pull:alg (60:40)	282.6	292.1	25.2
pull:alg (60:40) GO 0.2 wt%	296.8	292.7	20.9

Figure 4.1 depicts the traces obtained from the samples exposed to nitrogen atmosphere along with the first-order derivatives. As shown in Figure 4.1b, the TGA tracings of pull:chit nanocomposites are quite similar to that of pristine pull matrice, however ~ 18 and ~ 5 °C increments on the maximum degradation temperatures (T_{max}) and ~ 8 and ~ 14 °C increments on the temperature at which the weight loss is 50% (T_{d50}) were observed for pull:chit (80:20) and pull:chit (60:40) blend films, respectively. On contrary, for pull:alg systems this behavior was not observed (Figure 4.2b). In particular, blending pull with alg led to two step degradation process and the reduction at T_{max} and T_{d50} . In other words, pull itself displayed a higher T_{max} and T_{d50} than the pull:alg blends as already referred.

Accordingly, the residual weight of the pull-chit blend films at 600 °C is considerably higher than that of pristine pull, which can be attributed that most part of GO remained in the nanocomposites at high temperature and showed the good thermal stability over the process temperature.

Contrary to the beneficial effect of chit addition, blending pull with alg didn't enhance thermal properties. Only the residual weights of the pull/alg blend films are higher than that of pristine pull and pull/GO 0.2 wt% films.



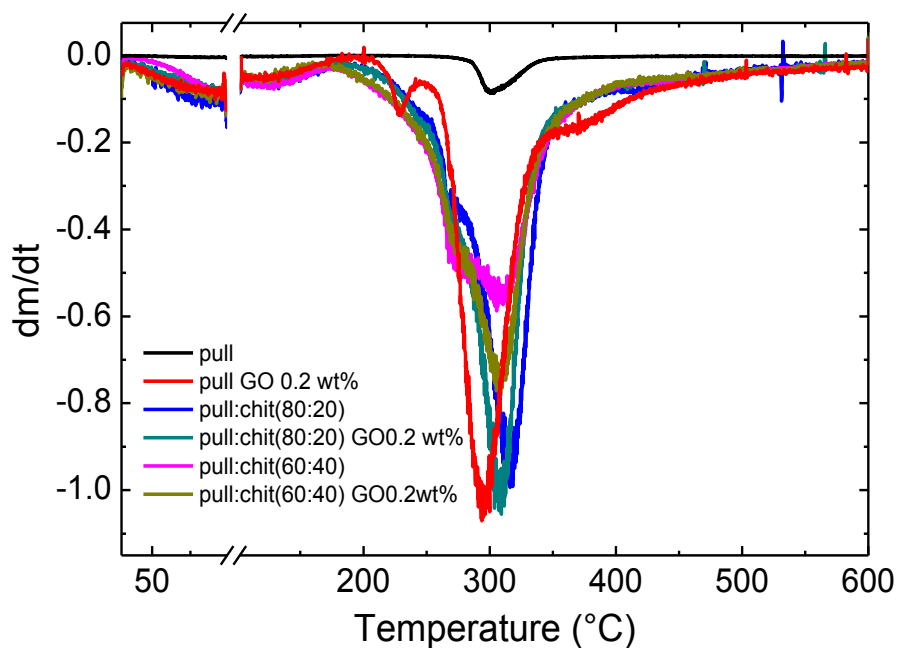
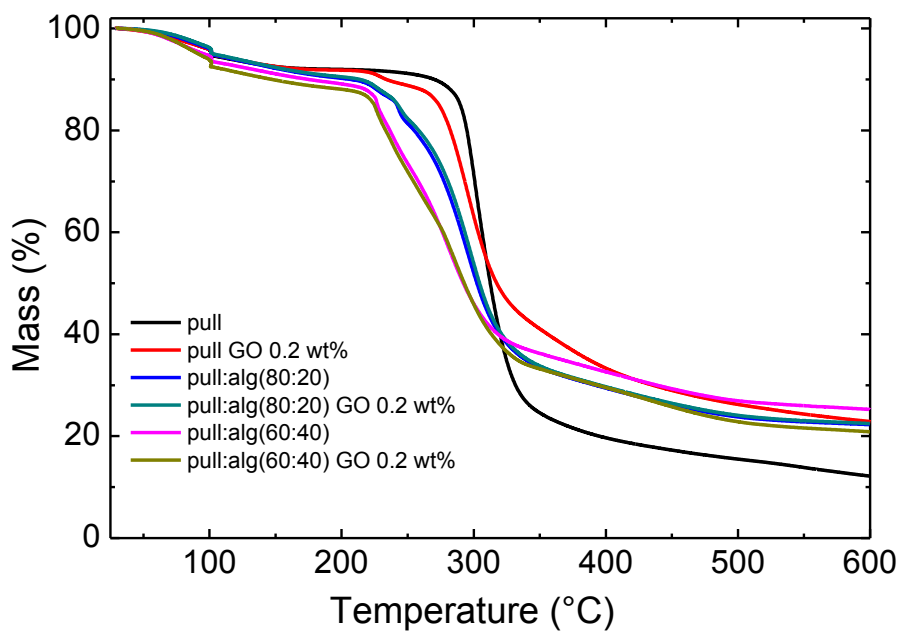


Figure 4.1. (a) TGA traces and (b) their first-order derivatives of pull and pull:chit blend systems exposed to an N_2 atmosphere.



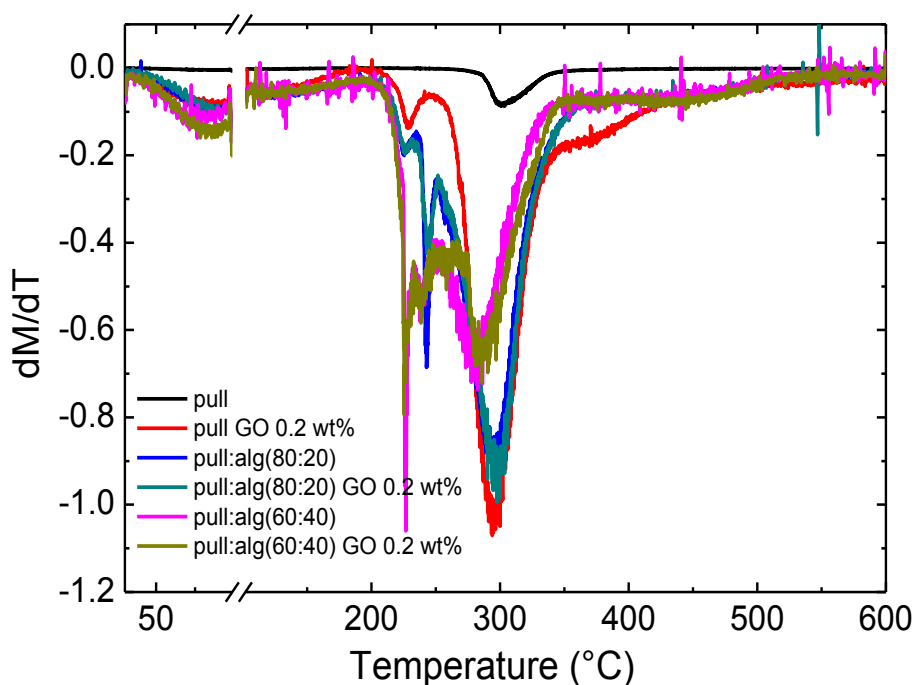


Figure 4.2. (a) TGA traces and (b) their first-order derivatives of pull and pull:alg blend systems exposed to an N_2 atmosphere.

4.2.3. Oxygen barrier performance

Experimental O_2TR values of pristine pull and pull blend systems are reported in Table 4.2. However, to get a more realistic interpretation of the oxygen barrier performance, these values have been converted to oxygen permeability ($P'O_2$), which allows resetting any influence arising from a different thickness of final films.

Table 4.2. GO content, GO volume fraction (ϕ), thickness (l), oxygen transmission rate (O_2TR), and oxygen permeability coefficient ($P'O_2$) of blend systems at 70% relative humidity and 23 °C.

GO content (wt%)	ϕ^*	l (μm)	O_2TR [$\text{mL m}^{-2} (24\text{h}^{-1})$]	$P'O_2$ [$\text{mL } \mu\text{m m}^{-2} (24\text{h}^{-1}) \text{ atm}^{-1}$]
pull	0	35 ± 2.22^c	181.04 ± 20.05^a	6337 ± 118.09^b
pull GO 0.2wt%	0.00204	35 ± 1.84^c	56.93 ± 4.87^c	1993 ± 88.10^d
pull:chit (80:20)	0	44 ± 2.22^b	96.08 ± 11.71^b	4227 ± 154.09^c
pull:chit (80:20) GO 0.2 wt%	0.00216	45 ± 1.20^b	60.24 ± 8.74^c	2711 ± 78.49^d
pull:chit (60:40)	0	49 ± 1.36^a	185.36 ± 18.09^a	9082 ± 124.09^a
pull:chit (60:40) GO 0.2 wt%	0.00231	47 ± 3.36^{ab}	59.367 ± 6.74^c	2790 ± 63.88^d
pull	0	35 ± 2.22^b	181.04 ± 20.05^a	6337 ± 118.09^a
pull GO 0.2wt%	0.00204	35 ± 1.84^b	56.93 ± 4.87^e	1993 ± 88.10^d
pull:alg (80:20)	0	44 ± 4.25^a	105.75 ± 16.7^c	4230 ± 115.25^b
pull:alg (80:20) GO 0.2 wt%	0.00204	35 ± 1.66^b	82.53 ± 10.77^d	2888 ± 44.16^c
pull:alg (60:40)	0	36 ± 1.49^b	157.21 ± 16.11^b	5660 ± 101.11^a
pull:alg (60:40) GO 0.2 wt%	0.00204	37 ± 1.47^b	114.70 ± 13.70^c	4244 ± 55.19^b

* Calculated for a given GO density (ρ) = $0.981 \text{ g} \cdot \text{cm}^{-3}$, pull (ρ) = $1 \text{ g} \cdot \text{cm}^{-3}$, chit (ρ) = $1.3 \text{ g} \cdot \text{cm}^{-3}$
alg (ρ) = $1 \text{ g} \cdot \text{cm}^{-3}$

Different superscripts within a group (i.e. within each parameter) denote a statistically significant difference ($P < 0.05$).

pull:chit and pull:alg blend systems was statistically analyzed within its own systems.

As given, $P'O_2$ of pristine pull film was $6337 \text{ mL } \mu\text{m m}^{-2} (24\text{h}^{-1}) \text{ atm}^{-1}$. Adding chit or alg to pull matrix resulted in a sharp decrease of $P'O_2$ at the blend ratio (80:20). However, upon the increase of alg and chit in the pull matrix caused to increase in $P'O_2$, probably due to the increased free-volume of the composite matrix caused by the bulkier anionic and cationic side groups of alg and chit (Tong et al., 2008). As shown in Table 4.2, O_2 gas permeabilities of GO/pull:chit and GO/pull:alg blend systems are sharply decreased with addition of very low concentration of GO

(0.2 wt%), however, this improvement was not enough to provide better performance than pull/GO (0.2 wt%) films.

4.2.4. Mechanical properties

Tensile strength, Young modulus and elongation at the break of the pull, pull blend systems with or without GO were measured and given in Table 4.3. Tensile strength, Young modulus and elongation of pristine pullulan films were found 50 MPa, 1556 MPa, and 4.7% at break, in line with the values found in literature (Fernandes et al., 2014). The tensile strength from 50 to 76 MPa, Young modulus from 1556 to 2967 MPa and elongation from 4.7 to 20% for pull:chit(80:20) blend films significantly increased when compared to pristine pullulan (Table 4.3).

Table 4.3. Tensile properties of pristine pull and blend systems with various contents of GO

Film Type	Tensile Strength (MPa)	Young Modulus (MPa)	Elongation (%)
pull	50.05±4.01 ^d	1556±92 ^d	4.36±0.76 ^c
Pull GO 0.2 wt%	70.10±7.77 ^c	2246±811 ^c	6.62±1.64 ^c
pull:chit(80:20)	76.36±7.19 ^c	2967±348 ^b	20.11±6.51 ^{ab}
pull:chit(80:20) GO 0.2 wt%	97.80±19.54 ^b	3722±340 ^a	15.76±2.39 ^b
pull:chit(60:40)	74.73±0.09 ^b	2713±83 ^{bc}	26.77±5.92 ^a
pull:chit(60:40) GO 0.2 wt%	91.13±9.03 ^b	3084±352 ^b	21.73±6.52 ^{ab}
pull	50.05±4.01 ^b	1556±92 ^c	4.36±0.76 ^b
Pull GO 0.2 wt%	70.10±7.77 ^{ab}	2246±811 ^b	6.62±1.64 ^a
pull:alg(80:20)	75.34±18.56 ^a	3213±284 ^a	5.37±0.54 ^{ab}
pull:alg(80:20) GO 0.2 wt%	77.14±14.63 ^a	3732±353 ^a	3.76±0.43 ^b
pull:alg(60:40)	83.50±15.66 ^a	3793±622 ^a	4.44±1.94 ^b
pull:alg(60:40) GO 0.2 wt%	78.47±16.68 ^a	3542±359 ^a	3.74±1.06 ^b

Different superscripts within a group (i.e. within each parameter) denote a statistically significant difference ($P < 0.05$).

pull:chit and pull:alg blend systems was statistically analyzed within its own systems.

The similar improvement was also observed for pull:chit(60:40) blend film. This may have been related to a raising level of the chitosan in the film would increase the number of amino groups, resulting into the strengthening of the inter-molecular hydrogen bonds and consequently, led to an improved tensile strength and modulus (Wu et al., 2013). As displayed in Figure 4.3, upon an addition of chit elongation dramatically increased by 360% for pull:chit(80:20) and by 500% for pull:chit(60:40) compared to pristine pull film. Strongly enhanced flexibility of pull films with addition of chit could be ascribed to the properties of the chit, which has good elongation at break (Pan et al., 2011).

Incorporation of GO into pull:chit blend films significantly enhanced the tensile and Young modulus. It is an indicator of homogeneous dispersion of GO sheets in the blend matrix and strong interfacial adhesion between them through the formation of amide linkages between GO's abundant carboxylic acid groups and chitosan's amine group in blend systems (Zuo et al., 2013).

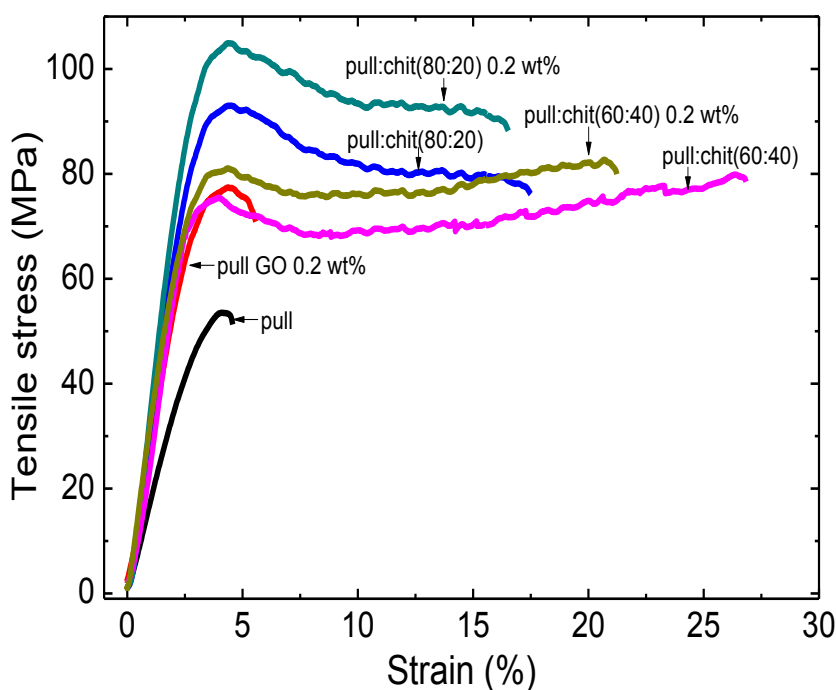


Figure 4.3. Typical stress–strain curves for pristine pull and pull:chit blend systems with various contents of GO

Incorporation of alg to pull matrix markedly increased tensile strength and Young modulus at both blend ratio. This strongly supports the idea that a hydrogen bonding can form between the hydroxyl groups of pullulan and carbonyl groups of NaAlg (Prasad et al., 2012). Interestingly, addition of GO did not provide any further beneficial in the tensile properties of pull:alg blend films (Figure 4.4), which can be attributed to poor dispersion and/or inefficient orientation of GO sheets in the pull:alg blend matrix. This needs further investigation.

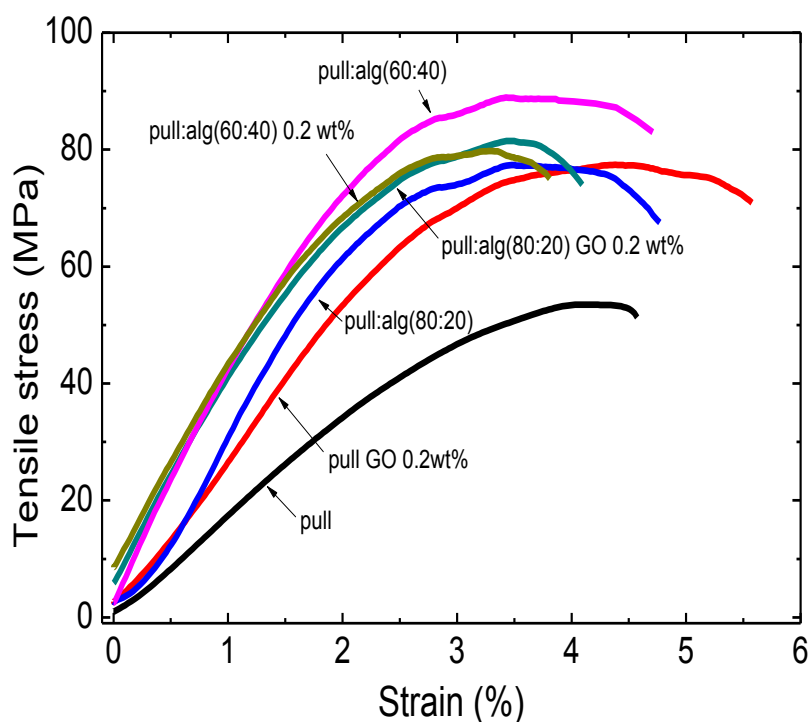


Figure 4.4. Typical stress–strain curves for pristine pull and pull:alg blend systems with various contents of GO.

4.2.5. Optical properties

As it is well explained in part 1, optical properties of materials (haze and transmittance) are considerably important in the food packaging field, both aspects are relevant and worth high consideration when designing a new (bio)nanocomposite materials (Uysal Unalan et al., 2014).

Table 4.4. Optical properties of pristine pull and blend systems with various contents of GO

Film Type	Transmittance (%)	Haze (%)
pull	93.1±0.68 ^{ab}	0.40±0.01 ^b
pull GO 0.2 wt%	92.3±0.17 ^b	0.39±0.02 ^b
pull:chit(80:20)	93.4±0.15 ^a	0.40±0.03 ^b
pull:chit(80:20) GO 0.2 wt%	89.9±0.90 ^c	2.69±0.41 ^a
pull:chit(60:40)	93.2±0.00 ^{ab}	0.69±0.13 ^b
pull:chit(60:40) GO 0.2 wt%	89.2±0.31 ^c	2.61±0.14 ^a
pull	93.1±0.68 ^a	0.40±0.01 ^d
pull GO 0.2 wt%	92.3±0.17 ^b	0.39±0.02 ^d
pull:alg(80:20)	93.7±0.17 ^a	0.56±0.13 ^c
pull:alg(80:20) GO 0.2 wt%	92.3±0.17 ^b	0.93±0.06 ^b
pull:alg(60:40)	93.5±0.23 ^a	0.65±0.06 ^c
pull:alg(60:40) GO 0.2 wt%	92.5±0.23 ^b	1.25±0.04 ^a

Different superscripts within a group (i.e. within each parameter) denote a statistically significant difference ($P < 0.05$).

pull:chit and pull:alg blend systems were statistically analyzed within their own systems.

As confirmed by both the transmittance and haze values reported in Table 4.4 pull-chit and pull-alg blending systems in absence of GO were fully comparable with pristine pull samples. Although the addition of GO led to a significant increase in transparency and haze, the values were maintained within the 90% and 3% threshold for transparency and haze, respectively (Introzzi et al. 2012).

The differences in film color were shown in Figure 4.5. The existing blended films were uniform, smooth and transparent but they became slightly yellowish following the incorporation of GO. This observation was in agreement with the findings of part 1.



Figure 4.5. Image of a) pristine pullulan film; b) pull:chit(80:20); c) pull:chit(60:40); d) pull:chit(80:20) GO 0.2 wt%; e) pull:chit(60:40) GO 0.2 wt%; f) pull:alg(80:20); g) pull:alg(60:40); h) pull:alg(80:20) GO 0.2 wt%; i) pull:alg(60:40) GO 0.2 wt%.

4.3. Conclusions

Findings arising from this work reflect that compared to pristine pullulan, GO enhanced pullulan-chitosan and pullulan-alginate blend systems have considerably provided improved mechanical properties and thermal stability, and comparable oxygen barrier performance. Nonetheless, the optical transparency of all the nanocomposites was kept adequate for most packaging applications in food sector. Considering that alginate and chitosan are less costly than pullulan, these biopolymers may be useful to reduce the cost of pullulan based bionanocomposites and enhance materials properties.

4.4. References

- Fernandes SC et al., 2014, Antimicrobial pullulan derivative prepared by grafting with 3-aminopropyltrimethoxysilane: Characterization and ability to form transparent films. *Food Hydrocolloids* 35:247-252.
- Introzzi L et al., 2012, Ultrasound-assisted pullulan/montmorillonite bionanocomposite coating with high oxygen barrier properties. *Langmuir* 28:11206-11214.
- Pan Y et al., 2011. Green fabrication of chitosan films reinforced with parallel aligned graphene oxide. *Carbohydr Polym* 83:1908–1915.
- Prasad P et al., 2012, Investigation on miscibility of sodium alginate/pullulan blends. *J Polym Environ* 20:887–893.
- Tong Q et al., 2008, Preparation and properties of pullulan–alginate–carboxymethylcellulose blend films. *Food Res Int* 41:1007–1014.
- Uysal Unalan I. et al., 2014, Nanocomposite films and coatings using inorganic nanobuilding blocks (NBB): current applications and future opportunities in the food packaging sector. *RSC Adv* 4:29393-29428.
- Wu J et al., 2013, Preparation and characterization of pullulan/chitosan and pullulan/carboxymethyl chitosan blended films. *Food Hydrocolloids* 30:82-91.
- Xiao Q et al., 2012, Properties of pullulan-based blend films as affected by alginate content and relative humidity. *Carbohydr Polym* 8:227–234.
- Zuo PP et al. Fabrication of biocompatible and mechanically reinforced graphene oxide-chitosan nanocomposite films. *Chem Cent J* 7:39.

5. TOPIC 3

Pullulan/graphene oxide bionanocomposite coatings with high oxygen barrier properties

The third part of the project was aimed to design bionanocoatings combining pullulan and GO to be applied on polyethylene terephthalate (PET). The rationale behind this approach lies in the fact that most examples on the use of nanosized fillers concern the incorporation of the inorganic phase directly into the bulky biopolymer. Only very recently it has been proposed the use of fillers within coatings made of biopolymers to produce bionanocomposite coatings (i.e., thin layers of a biopolymer matrix loaded with a nanoparticle filler) to improve the properties of a plastic substrate without jeopardizing its original attributes and optimize cost efficiency. Full exfoliation of GO platelets during preparation of the coating water dispersions was mediated by ultrasonic treatment, which turned out to be a pivotal factor in the oxygen barrier performance of the final material at 0 and 30% RH condition as well as in its low friction coefficient and better tensile properties.

5.1. Materials and Methods

5.1.1. Materials

Pullulan (PF-20 grade, Mw~200,000 DA) was obtained from Hayashibara Biochemical Laboratories Inc., Okayama, Japan. Poly(ethylene terephthalate) (PET) films ($12.0 \pm 0.5 \mu\text{m}$ thick) was provided by Toray (Saehan, Kyungbuk, South Korea).

PET is a thermoplastic polymer of the polyester family, commonly used in the food packaging field for different purposes, such as liquids container, thermoforming applications, as a layer for flexible packaging solutions. Figure 5.1 shows the molecular structure of this polymer.

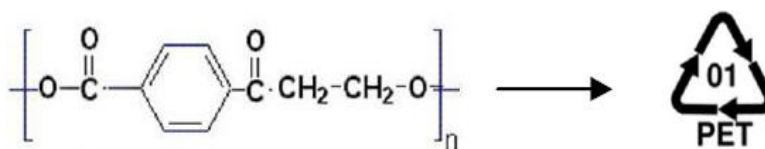


Figure 5.1. Molecular structure and plastic identification code of PET.

5.1.2. Methods

5.1.2.1. Chemical synthesis of graphene oxide

Please refer to section 3.1.2.1.

5.1.2.2. Preparation of bionanocomposite coatings

A fixed amount of pullulan (10 wt %, wet basis) was dissolved in distilled water at 25 °C for 1 h under gentle stirring (500 rpm). Afterward, 50 mL of the GO dispersion (0.2 wt % on wet basis) was ultrasonicated by means of an UP400S (powermax = 400 W; frequency = 24 kHz) ultrasonic device (Hielscher, Teltow, Germany) equipped with a cylindrical titanium sonotrode (mod. H14, tip Ø 14 mm, amplitude_{max} = 125 μm; surface intensity = 105 W·cm⁻²) under the following conditions: 0.5 cycle and 50% amplitude for 2 min. In parallel, the resulting GO were diluted in distilled water (18.3 MΩ·cm) under vigorous stirring (500 rpm) for 15 min. The organic pullulan solution and the inorganic dispersion were then mixed together under gentle stirring (300 rpm) for an additional 60 min. More specifically, the quantity of GO in pullulan-water solution was 0.002, 0.004, 0.006, 0.008, 0.01 and 0.02% (wet basis). After drying, the concentrations of GO corresponded to 0.2, 0.1, 0.08, 0.06, 0.04 and 0.02 wt% on dry basis. PET films were treated with high frequency corona treatment (Arcotec, Ülm, Germany). As it is shown in Figure 5.2 an aliquot of each bionanocomposite water dispersion was then placed on the corona treated side of rectangular (24 × 18 cm²). The deposition of the coating was carried out by using an automatic film applicator (ref 1137, Sheen Instruments, Kingston, UK) at a constant speed of 2.5 mm s⁻¹ was used, according to ASTM D823-07— Practice C. The deposition was performed using a horizontal steel rod with an engraved pattern, which yielded final coatings of comparable nominal thickness of 1 μm after water evaporation. Water evaporation was performed using a constant and perpendicular flux of mild air (25.0 ± 0.3 °C for 2 min) at a distance of 40 cm from the applicator. Coated films were then stored under controlled conditions (23.0 ± 0.5 °C in a desiccator) for 48 h before measurements.

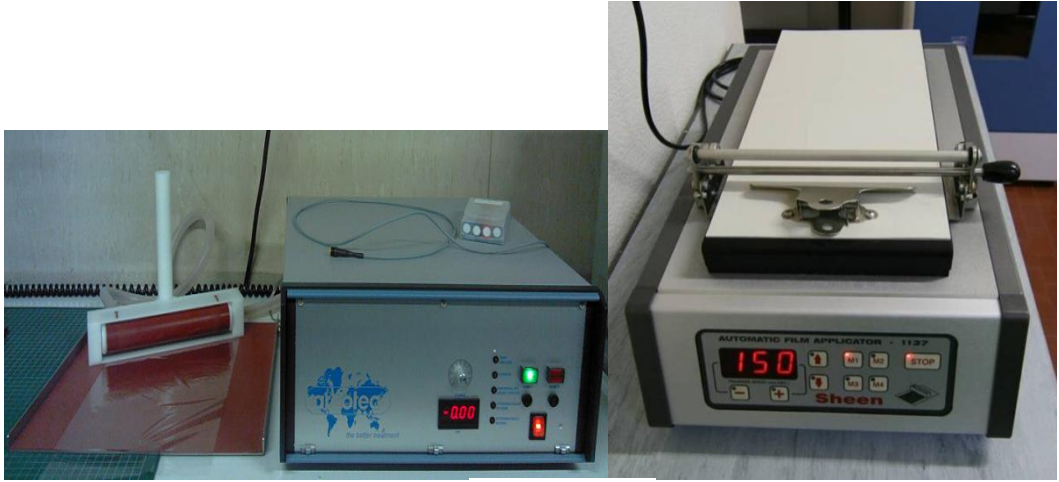


Figure 5.2. Coating preparation process (a) corona treatment; (b) automatic film applicator.

5.1.2.3. Thickness determination

A 10×10 cm sample (pristine pullulan coated PET) was cut and weighed (M_1 , grams). The coating was then mechanically removed by immersion in hot water (80°C) and the resulting PET film was weighed (M_2 , grams). The apparent thickness (micrometers) of the coating was obtained according to the following equation (Brown, 1992):

$$l = 100 \times \frac{M_1 - M_2}{\rho} \quad (5.1)$$

where ρ (g cm^{-3}) is the density of the aqueous dispersion. Three replicates were analyzed for each biopolymer composition.

5.1.2.4. Variable-angle spectroscopic ellipsometry

Variable-angle spectroscopic ellipsometry (VASE) measurements were performed in the spectral range from 400 nm to 800 nm (with steps of 2 nm) at different angles of incidence (from 40° to 70°) using the ellipsometer (J.A. Woollam Co. Inc.). The ratio between the elements of the Jones matrix (r_{pp} / r_{ss}) = $\tan(\Psi) e^{i\Delta}$ were acquired through Ψ and Δ , which depend on the wavelength λ of the incident polarized light.

The measured $\Psi(\lambda)$ and $\Delta(\lambda)$ data were analyzed with the software WVASE 32 by describing the sample using the following model. The fitting of the experimental data was performed by minimizing the mean-squared-error defined as

$$MSE = \sqrt{\frac{\sum_{i=1}^N \left[\left(\frac{\Psi_i^{\text{mod}} - \Psi_i^{\text{exp}}}{\sigma_{\Psi,i}^{\text{exp}}} \right)^2 + \left(\frac{\Delta_i^{\text{mod}} - \Delta_i^{\text{exp}}}{\sigma_{\Delta,i}^{\text{exp}}} \right)^2 \right]}{2N - M}} \quad (5.2)$$

where N is the number of measured Ψ and Δ pairs and M is the total number of model fit parameters.

5.1.2.5. Transmittance measurements

Transmittance measurements were performed at normal incidence with unpolarized light in the spectral range from 300 nm to 800 nm (with steps of 1 nm) using the spectrophotometer Perkin Elmer Lambda 900. Simulations of transmittance and reflectance spectra were performed with the software WVASE32.

5.1.2.6. Haze measurements

Haze was measured within the wavelength range 780–380 nm, in accordance with ASTM D 1003-00, by use of a UV–vis high performance spectrophotometer (Lambda 650, PerkinElmer, Waltham, MA) coupled with a 150 mm integrating sphere, which allows the trapping of the diffuse transmitted light. Three replicates were made for each uncoated and coated film sample.

5.1.2.7. Friction measurements

Both static (μ_s) and kinetic (μ_k) friction coefficients were measured. The former represents the friction opposing the onset on relative motion (impending motion), whereas the latter can be considered as the friction opposing the continuance of relative motion once that motion has started. In the case of solid-on-solid friction (with or without lubricants), these two types of friction coefficients are conventionally defined as follows:

$$\mu_s = F_s / P \quad (5.3a)$$

$$\mu_k = F_k / P \quad (5.3b)$$

where

F_s = force just sufficient to prevent the relative motion between two bodies;

F_k = force needed to maintain relative motion between two bodies;

P = force normal to the interface between the sliding bodies.

Both friction coefficients were measured using a dynamometer (model Z005, Zwick Roell, Ulm, Germany), in accordance with the standard method ASTM D 1894-87. The software TestXpert V10.11 (Zwick Roell, Ulm, Germany) Master was used for data analysis. Two types of analyses were carried out. In the first, friction opposing the motion of each type of film (coated and uncoated) against itself was evaluated. In the second, the motion of each type of film (coated and uncoated) on a metallic rigid surface (a polished stainless steel $150 \times 450 \times 3$ mm) was considered. This surface, other than acting as a supporting base to guarantee a firm position between the moving crosshead and the force-measuring device, served the purpose of simulating the friction between the plastic web and the metallic parts of the equipments used during the manufacturing process.

5.1.2.8. Tensile testing

Tensile properties of films were measured according to the ASTM D882-02 by means of a dynamometer (mod. Z005, Zwick Roell, Ulm, Germany) fitted with a 5 kN load cell and connected with two clamps placed at a distance of 125 mm apart. For each parameter, final results are the mean of at least five replicates.

5.1.2.9. Oxygen barrier measurements

The oxygen barrier properties of films were assessed on a 50 cm² surface sample using a Multiperm permeability analyzer (Extrasolution Srl, Capannori, Italy) equipped with an electrochemical sensor. Oxygen transmission rate (O₂TR) data were determined according to the standard method of ASTM F2622-08, with a carrier flow (N₂) of 10 ml min⁻¹ at 23 °C at 0, 30, 60 and 90% relative humidity (RH), 1 atm pressure difference on the two sides of specimen. Each O₂TR value was from three replicates.

5.1.2.10. Water vapor barrier measurements

The water vapor barrier properties of PET film and binanocomposites were assessed on a 50 cm² surface sample using a Multiperm permeability analyzer (Extrasolution Srl, Capannori, Italy) equipped with an electrochemical sensor. Water vapor transmission rate (WVTR) was assessed on a 50 cm² surface sample according to the standard method ASTM F1249-05, with a carrier flow (N₂) of 10 mL min⁻¹. Measurements were performed at 38 °C and 90 % relative humidity (RH), which is the humidity gradient between the two semi-chambers between which the sample was mounted. Final WVTR values were expressed as g m⁻² 24 h⁻¹.

5.1.2.11. Statistical analysis

Please refer to part 3.1.2.13.

5.2. Results and discussion

5.2.1. Ellipsometry

Morphology of GO nanosheets were characterized by different characterization techniques in the first part of thesis. As characterized by AFM, thickness of the GO sheets ranged uniformly around 1.0 nm (more specifically, 1.12 ± 0.18 nm), suggesting the complete exfoliation of GO sheets down to individual layers. GO sheets width ranged between 1.5 and 4.0 μm (mean of $2.5 \mu\text{m} \pm 0.3$), although individual sheets as large as 12 μm were also observed.

The first step has been the characterization of the PET substrate by ellipsometry measurements to deduce a proper model to simulate its optical properties. The ellipsometry results were fitted by assuming a semi-infinite bulk of a transparent material with refractive index described by the Cauchy model ($n(\lambda) = n_A + n_B / \lambda^2$), n_A and n_B being free parameters for the fitting. Experimental evidence of interference fringes due to a possible thin layer on top of the PET substrate was found. However, this layer was neglected in the model since its effects were not critical and a reliable fitting of the ellipsometry data were obtained with the simpler model of a semi-infinite bulk material. The fitting procedure provided $n_A = 1.8564$ and $n_B = 0.0019896$, corresponding to a mean refractive index of the PET substrate in the visible range (400-700 nm) equal to 1.864.

The obtained model of a PET semi-infinite substrate was used as substrate for the following characterizations. First of all, pristine pullulan coated PET sample was studied. The stack for the simulation was built by adding a transparent layer on top of the PET semi-infinite substrate. The PET optical properties were assumed known, as previously deduced from ellipsometry. The fitting of the ellipsometry data was performed with four free parameters, namely n_A and n_B , the thickness (l) of the added layer, and its thickness non-uniformity t_{n-u} . The results of the fitting are reported in Table 5.1, together with the corresponding MSE value of the fitting and the refractive index of the top layer. The mean refractive index is in reasonable agreement with data reported in the literature for pullulan (Gradwell, 2004).

The same procedure and model were adopted for other samples with different concentrations of GO in the pullulan layer (Table 5.1). We notice that the refractive index and the thickness non-uniformity of the top layer increase as a function of the GO concentration. The correlation factors (not shown) are found negligible due to not being large correlation values.

Table 5.1. Parameters n_A , n_B , t , and t_{n-u} of the top layer obtained by fitting the ellipsometry $\Psi(\lambda)$ and $\Delta(\lambda)$ experimental data, MSE of the fitting, and deduced refractive index of the top layer either at 589 nm (n_{589}) or averaged in the visible range from 400 to 700 nm (n_{mean}).

GO content (wt%)	n_A	n_B (μm^2)	l (nm)	t_{n-u} (%)	MSE	n_{589}	n_{mean}
0	1.5593	0.0020923	470.50	20.6	4.71	1.559	1.569 ± 0.002
0.04	1.6611	0.012045	472.29	49.0	1.91	1.696	1.704 ± 0.014
0.2	1.7174	0.027529	511.75	41.4	2.80	1.797	1.816 ± 0.033

5.2.2. Transmittance

Transmittance measurements were also performed at normal incidence on different GO samples (Figure 5.3). The PET substrate was found to show a relatively low transmittance, while a clear increase was detected for the sample pristine pullulan coated PET (0 wt% GO content), due to the anti-reflection behavior of the pullulan layer. Indeed, the refractive index of pullulan is intermediate between air and PET. When increasing the GO concentration, the refractive index of the top layer was found to increase approaching the PET refracting index value, thus reducing its anti-reflection behavior. For this reason, the transmittance of the GO samples is intermediate between the two extremes, towards the transmittance of the simple PET substrate for the highest GO concentration (0.2 wt%).

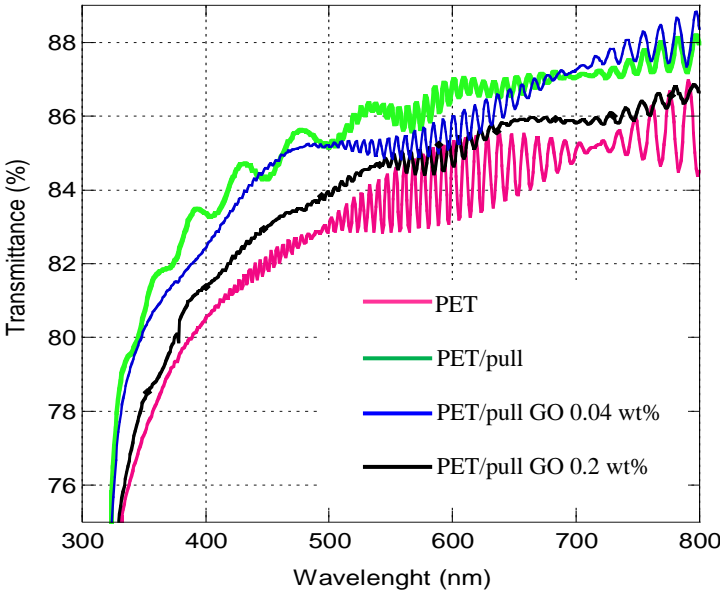


Figure 5.3. Measured transmittance spectra of PET, pristine pull coated PET and pull/GO coated PET films.

The mean value of the measured transmittance in the visible region is reported in Table 5.2. Transmittance was also simulated taking into consideration the model and parameters obtained by ellipsometry for each sample (Table 5.2). A good agreement was found between measured and simulated values. The lowest transmittance was found for the PET substrate, while the largest one was found for the pristine pullulan coated PET film. The presence of GO in the top layer determined a monotonous decrease of the transmittance, down to values close to the simple PET for the 0.2 wt% sample. Even if reflectance was not measured, the spectra were calculated for near-normal incidence (20° , polarization s), based on the ellipsometry models. The mean values in the visible range are also reported in Table 5.2. As expected, (i) the minimum reflectance was calculated for the pristine pullulan coated PET film due to the anti-reflection behavior of the pullulan layer and (ii) a monotonous increase was found when increasing the GO concentration, reaching a similar reflectance value as the PET substrate for GO concentration equal to 0.2 wt%.

Table 5.2. Measured transmittance ($T_{\text{mean}} \pm \text{std dev}$) and simulated transmittance and reflectance ($T_{\text{simul}} \pm \text{std dev}$, $R_{\text{simul}} \pm \text{std dev}$), averaged in the visible range from 400 to 700 nm.

GO content (wt%)	$T_{\text{mean}} \pm \text{std dev} (\%)$	$T_{\text{simul}} \pm \text{std dev} (\%)$	$R_{\text{simul}} \pm \text{std dev} (\%)$
uncoated PET	83.4 ± 1.3	83.3 ± 0.1	10.4 ± 0.1
0	85.9 ± 1.0	86.4 ± 1.2	6.4 ± 1.6
0.04	85.4 ± 1.1	85.1 ± 0.3	8.1 ± 0.3
0.1	84.1 ± 1.3	not available*	not available*
0.2	84.4 ± 1.3	83.9 ± 0.5	9.6 ± 0.5

* ellipsometry measurements were not performed.

5.2.3. Haze

Haze values were reported in Table 5.3. All GO based binanocomposite coatings were fully comparable with pristine PET film, with the exception of the value for the nanocomposite at the highest GO concentration (0.2 wt%).

Table 5.3. Haze value of uncoated PET and bionanocomposite coatings.

GO content (wt%)	Haze (%)
uncoated PET	2.72±0.08 ^{bc}
0	2.63±0.22 ^{cd}
0.02	2.49±0.10 ^d
0.04	2.74±0.02 ^{bc}
0.06	2.70±0.13 ^{bc}
0.08	2.61±0.04 ^{cd}
0.1	2.87±0.04 ^{ab}
0.2	3.03±0.11 ^a

Different superscripts within a group (i.e. within each parameter) denote a statistically significant difference ($P < 0.05$).

However, as we have discussed in previous parts since the haze values as high as 3 % are generally judged adequate for a proper display of the products in food packaging (Introzzi et al., 2012), haze value of pullulan coated PET film with 0.2 wt% GO content is still favorable. The increase in haze observed for film and coating samples can be explained in terms of surface roughness (Tilley, 2011) rather than presence of scattering centers (Introzzi et al., 2012). As highlighted by the AFM analysis on $10 \times 10 \mu\text{m}^2$ areas, the pristine pullulan coatings showed highly smooth topographies, with an average roughness of ~ 1.2 nm (Figure 5.4a). Addition of the GO with 0.06 wt% led to a slightly increase in roughness of the coating's surface (1.43 nm, Figure 5.4b). However, the highest GO content (0.2 wt%) yielded a relatively high roughness value (3.1 nm) which was in line with its significantly increased haze value. As observed in previous works, the addition of the other fillers, for example, micro-fibrillated cellulose and montmorillonite to pullulan coatings leads to an increase in surface roughness as measured by AFM (Introzzi et al., 2012; Cozzolino et al., 2014).

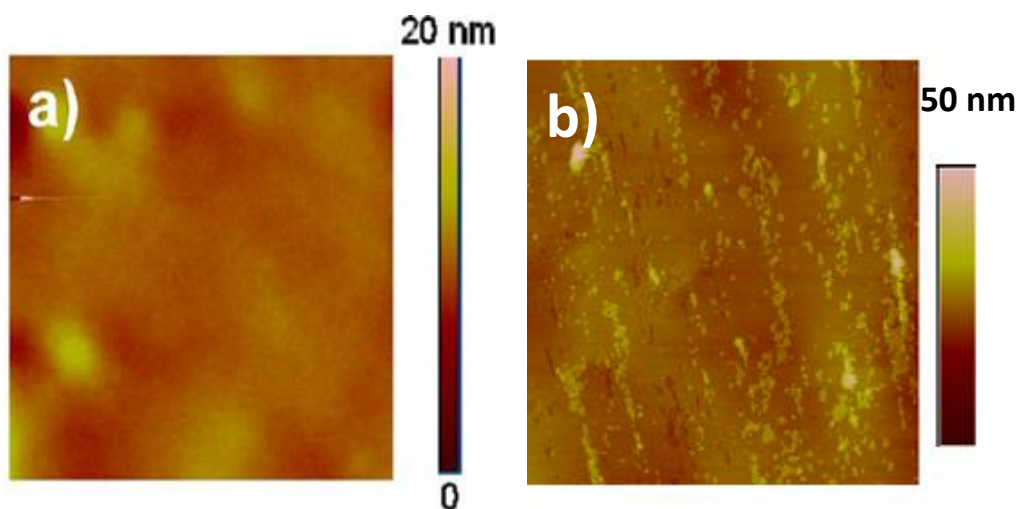


Figure 5.4. AFM height images ($10 \times 10 \mu\text{m}^2$) of (a) pristine pullulan coating and (b) pullulan/GO nanocomposite coating with 0.06 wt% GO content.

Color change with loading the highest amount of GO (0.2 wt%) was not clearly detectable as shown by the images inset in Figure 5.5.

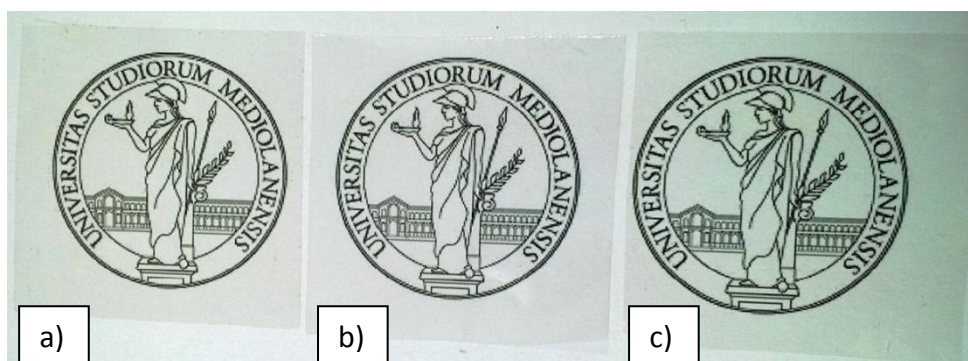


Figure 5.5. Image of (a) uncoated PET (b) pristine pullulan coated PET and (c) GO/pullulan coated PET with 0.2 wt% of GO content.

5.2.4. Mechanical properties

5.2.4.1. Friction behaviors

Graphitic carbon has previously been found to have outstanding tribological properties. Therefore, they were generally used as solid lubricant to improve the tribological properties for the matrix. Most of the researchers, have however, focused on the study of the frictional properties of pristine

graphene, whereas few studies have been devoted to the friction behaviors of the GO/polymer nanocomposites (Li et al., 2012; Liu et al., 2012).

In order to simulate the practical situation often occurring at industrial level, two different analyses of the same test were performed in this work: the sliding of parallel film surfaces over each other and the sliding of film surfaces over a metal substrate. Significant differences were observed after the deposition of the thin pullulan coating with different GO content on PET film (Table 5.4).

Table 5.4. Friction coefficients of uncoated PET and bionanocomposite coatings.

GO content (wt%)	Frictions coefficient			
	coating-to-coating		coating-to-metal	
	μ_s	μ_k	μ_s	μ_k
uncoated PET	0.67±0.08 ^d	0.46±0.05 ^b	0.35±0.01 ^d	0.26±0.02 ^{ab}
0	0.84±0.11 ^{cd}	0.50±0.03 ^b	0.42±0.02 ^{ab}	0.27±0.01 ^a
0.02	1.28±0.25 ^a	0.62±0.18 ^a	0.43±0.02 ^a	0.26±0.02 ^{ab}
0.04	1.23±0.18 ^a	0.57±0.03 ^{ab}	0.41±0.02 ^{ab}	0.25±0.01 ^{bc}
0.06	0.89±0.18 ^b	0.49±0.07 ^b	0.42±0.02 ^{ab}	0.26±0.01 ^{ab}
0.08	0.94±0.14 ^b	0.54±0.07 ^{ab}	0.39±0.01 ^c	0.25±0.01 ^{bc}
0.1	0.80±0.07 ^c	0.54±0.03 ^{ab}	0.40±0.05 ^{bc}	0.24±0.01 ^{cd}
0.2	1.11±0.11 ^{ab}	0.63±0.02 ^a	0.33±0.02 ^c	0.23±0.00 ^d

Different superscripts within a group (i.e. within each parameter) denote a statistically significant difference ($P < 0.05$).

The obtained results appear interesting from a practical point of view, especially considering the potential industrial application. Whether this change is positive or negative strongly depends on the final application. For example, low coefficient of friction values aid the unwinding operations of plastic films on industrial lines, to avoid the “blocking effect” on the reels and decreasing overall throughput. Conversely, lower coefficient of friction values are problematic if the final packages (e.g., plastic bags) have to be stacked on top one of another; high coefficients of friction can keep the stack from collapsing (Uysal Unalan et al., 2014).

Overall, the findings indicated that coefficient values of pull/GO coatings on PET at the highest GO content (0.2 wt%) for coating to metal measurements was found significantly different compared to uncoated PET and pristine pullulan coated PET because the fundamental graphite lattices of GO consisted of loosely bound layers which intrinsically possess low shear strength (Lee

et al., 2009). This may be explained due to the homogenous dispersion of GO and the excellent tribological properties of multilayered GO (Liu et al., 2012). When coefficient values are considered for coating to coating measurements it was shown that the friction coefficients of bionanocomposite coatings with the addition of the highest GO content increased significantly compared to uncoated PET and pristine pullulan coated PET. If the final packages (e.g., plastic bags) have to be stacked on top one of another; this higher coefficient of friction can keep the stack from collapsing.

Using such GO based coatings allows a layer of film to slide easily over another layer of film (e.g. on a roll), or over machine surfaces during film manufacture and packing, reducing the coefficient of friction. Therefore, the final result will be the increased line speed in the manufacturing process and the enhancement of the packaging machine operations, resulting in an increased output.

5.2.4.2. Tensile properties

Mechanical properties of uncoated PET, pristine pullulan coated PET and bionanocomposite films with different amounts of GO were studied by tensile experiments, and their main properties are summarized in Table 5.5. There was a considerable enhancement in the tensile properties for the 0.1 and 0.2 wt% GO loadings compared with plastic film. For instance, bionanocomposites with 0.2% showed a rise in tensile strength, Young modulus and elongation of ~17, 8.5 and 42%, respectively, compared to PET film.

Table 5.5. Tensile properties of uncoated PET and bionanocomposite coatings.

GO content (wt%)	Tensile Strength (MPa)	Young Modulus (MPa)	Elongation (%)
uncoated PET	112.05±4.10 ^b	3652±196 ^c	17.40±0.91 ^b
0	115.88±3.38 ^b	3793±98 ^{abcd}	17.08±3.87 ^b
0.02	97.10±6.96 ^c	3630±237 ^d	7.00±1.36 ^c
0.04	107.22±11.66 ^b	3726±199 ^{bcd}	13.55±3.84 ^b
0.06	106.37±10.28 ^{bc}	3750±147 ^{abcd}	13.77±2.48 ^b
0.08	110.58±2.23 ^b	3876±145 ^{ab}	15.52±3.50 ^b
0.1	129.03±5.47 ^a	3868±186 ^{abc}	23.70±3.92 ^a
0.2	131.05±7.13 ^a	3958±47 ^a	24.72±6.00 ^a

Different superscripts within a group (i.e. within each parameter) denote a statistically significant difference ($P < 0.05$).

In this study, the significant improvement of the mechanical properties of bionanocomposite films at the highest GO concentration (0.2 wt%) can be ascribed to the uniform dispersion of GO within the biopolymer matrix, good GO–pullulan interactions, and high aspect ratio of GO, which were discussed in the first part of the thesis. When the amount of filler reaches a critical content and the distance between two sheets is so small that they may be apt to stack together easily due to the van der Waals force, then it turns to the restacked form (Balandin et al., 2008), weakening the efficiency of the mechanical improvement. This phenomenon is called as mechanical percolation (Zhao et al., 2010). However, since the exfoliated graphene nanosheets at even at its highest concentration (0.2 wt%) is well-dispersed in the polymer matrix, further loading may possibly lead to further mechanical improvements.

5.2.5. Barrier performance

Results from permeability measurements are reported in Table 5.6.

Table 5.6. GO content (wt%, on dry basis), thickness (*l*), oxygen transmission rate (O_2TR) and water vapor transmission rate ($WVTR$) of uncoated PET and bionanocomposite coatings.

GO content (wt%)	<i>l</i> * (μm)	O_2TR [mL m ⁻² (24h ⁻¹)]				$WVTR$ [g m ⁻² 24 h ⁻¹]
		0% RH	30% RH	60% RH	90% RH	90% RH
uncoated PET	12.00±0.50 ^b	56.60±1.20 ^{a,A}	57.38±1.10 ^{a,A}	51.72±0.70 ^{a,B}	51.47±3.19 ^{b,B}	41.93±1.34 ^a
0	12.75±0.07 ^a	1.68±0.11 ^{b,D}	11.79±1.30 ^{bc,C}	22.15±0.07 ^{cd,B}	47.14±2.20 ^{b,A}	41.09±2.55 ^a
0.02	12.63±0.0 ^a	0.97±0.05 ^{c,D}	10.27±0.07 ^{d,C}	25.76±1.27 ^{b,B}	61.49±0.39 ^{a,A}	38.61±0.27 ^b
0.04	12.67±0.05 ^a	1.02±0.02 ^{c,D}	10.39±0.98 ^{cd,C}	23.90±0.54 ^{bc,B}	45.29±1.40 ^{bd,A}	33.88±0.21 ^d
0.06	12.72±0.00 ^a	0.93±0.21 ^{c,D}	12.43±0.14 ^{b,C}	23.73±0.22 ^{bcd,B}	43.13±1.29 ^{de,A}	41.15±0.28 ^a
0.08	12.83±0.16 ^a	0.91±0.13 ^{c,D}	4.52±0.21 ^{e,C}	21.07±2.62 ^{d,B}	43.80±1.14 ^{ef,A}	34.46±1.13 ^{cd}
0.1	12.77±0.05 ^a	1.17±0.31 ^{c,D}	4.03±1.27 ^{ef,C}	22.29±1.31 ^{cd,B}	44.51±0.17 ^{bd,A}	36.60±0.14 ^{bc}
0.2	12.78±0.05 ^a	0.23±0.01 ^{d,D}	2.80±0.21 ^{f,C}	22.97±0.21 ^{bcd,B}	38.80±0.85 ^{f,A}	34.49±0.22 ^{cd}

*Thickness of total material (PET + coating)

a-f: Different superscripts within each group (relative humidity or thickness) denote a statistically significant difference ($P < 0.05$), A-D: Different superscripts within each group (GO content) denote a statistically significant difference ($P < 0.05$)

The oxygen barrier performance of the tested samples improved after pullulan coating was deposited on PET under dry, and 30 and 60% relative humidity conditions (Table 5.6). The O_2 barrier performance further improved by increasing GO content and turned to excellent for bionanocomposites with 0.2 wt% GO at both 0 and 30% RH (Figure 5.6). The ultrasound assisted procedure for exfoliation of GO resulted in an effective and efficient tool for the final performance of the PET/bionanocomposite material, as it allowed full exfoliation of the platelets during preparation of the coating water dispersions. This was reflected in the final oxygen barrier

properties of the bionanocomposite coatings, due to both the “tortuosity path” and “organic/inorganic interface” effects. As the relative humidity increased to 60%, the overall performance was not enhanced upon the addition of GO into pullulan coatings but it still showed better performance than uncoated PET. However, further increase in relative humidity to 90% caused the loss of pullulan coating efficiency on PET. This effect of humidity on the barrier properties of hydrophilic polymers is well-known (Zhang et al., 2001; Hu et al., 2005). It is ascribed to the plasticizing effect of water molecules adsorbed by the polymer surface and bulk, especially in correspondence with the amorphous regions (Aulin et al., 2010; Kurek et al., 2014). Weakening of the hydrogen bonds at intramolecular and intermolecular level may occur in the long run. Eventually, both phenomena lead to an increase in chain mobility and free volume, which is reflected in a higher diffusion of the permeant (e.g., oxygen) across the polymer matrix. This observation is in line with the previous studies which were on pullulan coated PET (Farris et al., 2012; Cozzolino et al., 2014).

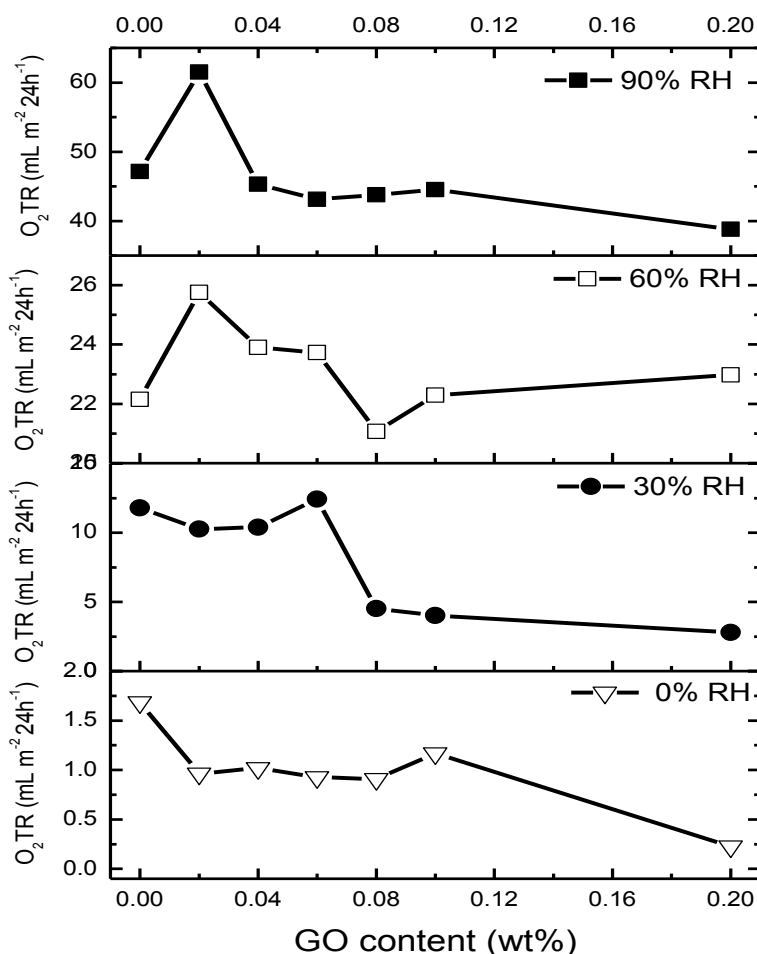


Figure 5.6. O_2TR evolutions at different relative humidities (%RH) as a function of GO content.

As summarized in Table 5.6, with respect to the WVTR values, it can be clearly seen that GO based pullulan coatings slightly enhanced water vapour barrier performance compared pristine pullulan coated PET due to the hydrophilic nature of these materials (thus the high affinity towards water molecules) (Cozzolino et al., 2014).

5.3. Conclusions

Novel “green” nanocomposite coatings based on pullulan and GO were prepared and characterized. This study has demonstrated that pullulan, in combination with GO, can be profitably used to generate oxygen barrier hybrid coatings in dry or low relative humidity conditions. The low degree of haze and high transmittance of bionanocomposite coatings even at the highest GO content as well as their low friction and better tensile properties demonstrated that they are suitable for packaging applications, especially when clear display of objects through the films is required. The findings arising from this work reflect convincingly the fact that pullulan nanocomposite coatings are a promising alternative to the currently available synthetic oxygen barrier polymer coatings. Although this new application may be beneficial with regard to expanding the market penetration of pullulan, its inefficiency in terms of oxygen barrier performance at high humidity conditions still represents an obstacle.

5.4. References

- Aulin C et al., 2010, Oxygen and oil barrier properties of microfibrillated cellulose films and coatings. *Cellulose* 17:559–574.
- Balandin A et al., 2008, Superior thermal conductivity of single-layer graphene. *Nano Lett* 8:902–907.
- Brown WE. *Plastics in food packaging – properties, design and fabrication*. Dekker, New York, 1992, 200–202.
- Cozzolino CA et al., 2014, Microfibrillated cellulose (MFC): pullulan bionanocomposite films. *Cellulose* 21:4323–4335.
- Farris S et al., 2012, Self-Assembled pullulan–silica oxygen barrier hybrid coatings for food packaging applications. *J Agric Food Chem* 60:782–790.
- Gradwell SE, *Self-assembly of pullulan abietate on cellulose surfaces*. Diss Virginia Polytechnic Institute and State University, 2004.
- Hu YS et al., 2005, Effect of water sorption on oxygen-barrier properties of aromatic polyamides. *J Polym Sci Pol Phys* 43:1365–1381.
- Introzzi L et al., 2012, Ultrasound-assisted pullulan/montmorillonite bionanocomposite coating with high oxygen barrier properties. *Langmuir* 28:11206–11214.
- Kurek M et al., 2014, Effect of relative humidity on carvacrol release and permeation properties of chitosan based films and coatings. *Food Chem* 144:9–17.
- Lee H et al., 2009, Comparison of frictional forces on graphene and graphite. *Nanotechnology* 20: 325701.
- Li Y et al., 2012, Preparation and tribological properties of graphene oxide/nitrile rubber nanocomposites. *J Mater Sci* 47:730–738.
- Liu H et al., 2012, In situ synthesis and thermal, tribological properties of thermosetting polyimide/graphene oxide nanocomposites. *Mater Sci* 47:1867–1874.
- Tilley RJD. *Colour and the optical properties of materials*, Wiley, Hoboken, 2nd edn., 2011, p 42.
- Uysal Unalan I et al., 2014. Nanocomposite films and coatings using inorganic nanobuilding blocks (NBB): current applications and future opportunities in the food packaging sector. *RSC Adv* 4:29393–29428.
- Zhang Z et al., 2001, Permeation of oxygen and water vapor through EVOH films as influenced by relative humidity. *J Appl Polym Sci* 82:1866–1872.
- Zhao X et al., 2010, Enhanced mechanical properties of graphene-based poly (vinyl alcohol) composites. *Macromolecules* 43:2357–2363.

6. TOPIC 4

High-concentration, stable, and water dispersible graphene through polysaccharide-assisted rapid ultrasonication

The aim of this work was to assess the capability of three different biopolymers (the positively charged polyelectrolyte chitosan, the uncharged pullulan, and the anionic polyelectrolyte alginate) to promote the direct exfoliation of graphite into graphene sheets in an aqueous medium by means of high intensity ultrasonication. To the best of our knowledge, this is the first time that the use of these biopolymers to exfoliate of graphite into graphene sheets by high intensity ultrasound waves is fully investigated. Special attention has specifically been paid to key parameters of the obtained graphene sheets, such as the yield of the overall process and the quality of the graphene dispersions.

6.1. Materials and Methods

6.1.1. Materials

Chitosan (viscosity < 200 mPa s, degree of deacetylation: 85–95%) was purchased from Shanglong Aokang Bio Ltd., China. Pullulan (PF-20 grade, Mw~200 000 DA) was obtained from Hayashibara Biochemical Laboratories Inc., Okayama, Japan. Sodium alginate (medium viscosity; viscosity of 2% solution in water at 25°C ≥ 2000 cps), graphite powder of purity of 99%, and acetic acid were supplied by Sigma-Aldrich, UK.

6.1.2. Methods

6.1.2.1. Direct exfoliation of graphite into graphene nanosheets

1.0 g of pullulan and alginate were separately dissolved in 20 ml of distilled water (DI), whereas chitosan (0.4 g) was dissolved in 20 ml of DI with 1 wt% acetic acid. Different amounts of graphite powder were then added to the aqueous biopolymer solutions contained in 50 ml glass vials and treated for 10, 20, 30, and 60 min using an ultrasonic processor UP200S (maximum power = 200 W, frequency = 24 kHz, Hielscher, Teltow, Germany) equipped with a cone frustum titanium sonotrode (model micro tip S3, tip diameter = 3 mm, maximum amplitude = 210 μm, acoustic power density or surface intensity = 460 W·cm⁻²) under the following conditions: 0.5 cycle and 50% amplitude. Subsequently, the mixtures were centrifuged at 1500 rpm for 60 min to separate the stable graphene dispersion from the unexfoliated graphite particles and macroscopic graphene flakes. Then, to remove the excess biopolymer, graphene sheets were washed with water and separated from top supernatants by centrifugation (5000 rpm for 20 min). This process was repeated five times. The resultant dark-gray solutions were dried at 40 °C in a vacuum oven for approximately 7 days until the mass no longer changed. The resulting polymer-graphene powders were redispersed in water (1 mg ml⁻¹ for pullulan and chitosan; 0.18 mg ml⁻¹ for alginate) for characterization. Graphene-pullulan, graphene-alginate, and graphene-chitosan sheets were indicated as pull-G, alg-G, and chit-G, respectively.

6.1.2.2. UV Spectroscopy

The yield of the overall process (i.e., the amount of exfoliated graphene sheets arising from the ultrasonication of graphite mediated by the polysaccharides) was determined gravimetrically, i.e. by weighing the dried graphene arising from the centrifugations and washing cycles. To this purpose, a Sartorius M-Power AZ214 (Göttingen, Germany) analytical balance was used. The final concentration was expressed in mg ml⁻¹ as a mean of three replicates. The same dried graphene-biopolymer samples were used to prepare a series of diluted dispersions, which allowed for the determination of the extinction coefficient using the Lambert-Beer law:

$$A = \varepsilon l c \quad (6.1)$$

where A is the absorbance of graphene water dispersions at 660 nm wavelength; ε is the extinction coefficient; l is the path length of the cuvette; and c is the concentration of graphene in water. Spectrophotometric measurements on five different diluted water dispersions were performed using a Varian Cary 50 UV-Vis spectrophotometer (Varian, Inc., Agilent Technology).

6.1.2.3. Transmission electron microscopy

Transmission electron microscope (TEM) (JEOL 2000FX) at an operating voltage of 200 kV was used for the analysis of graphene structure. Digital images were captured with a GATAN ORIUS 11 megapixel digital camera. Samples for TEM analyses were prepared by drop-casting a few millilitres of dispersion onto holey carbon grids (400 mesh), and letting the samples to rest for 24 hours at room temperature to allow water evaporation.

6.1.2.4. Atomic force microscopy

Atomic force microscopy (AFM) measurements were carried out in air in intermittent-contact mode with a Nanoscope V Multimode (Bruker, Germany) on diluted (1:100) pull-G, chit-G, and alg-G water dispersions 1 hour after their preparation. The images were collected with a resolution of 512 x 512 pixels with silicon tips (force constant 40 N/m, resonance frequency 300 kHz). The analyses performed on the acquired images were conducted with Nanoscope software (versions 5.12 and 7.30).

6.1.2.5. Thermogravimetric analysis

Thermogravimetric analysis (TGA) was carried out with the goal of quantifying the residual biopolymer on the exfoliated graphene sheets after the five washing cycles as described before. The analyses were run using a TGA/DSC 2 instrument (Mettler Toledo, Switzerland) in an inert environment (50 mL min⁻¹ N₂). Powder samples (~ 5 mg) were placed in alumina pans (70 µL) and heated from 25 °C to 1000 °C at a linear heating rate of 10 °C min⁻¹. At least three replicates were used for each sample.

6.1.2.6. Raman spectroscopy

Raman spectra were recorded at ambient temperature by a Renishaw inViaRaman spectrometer with an Ar-ion laser at an excitation wavelength of 514.5 nm.

6.1.2.7. X-ray photoelectron spectroscopy

X-ray photoelectron spectroscopy (XPS) measurements were performed in an XM1000 instrument (Omicron NanoTechnology GmbH, Germany) equipped with a monochromatic Al K α source. Samples were first mounted on circular plates using electrically conducting carbon tape and then loaded in a vacuum chamber (base pressure 2 x 10⁻¹¹ mbar). Data analysis was carried out using the CasaXPS package, using Shirley backgrounds, mixed Gaussian-Lorentzian (Voigt) line shapes and asymmetry parameters for the sp² graphitic components.

6.2. Results and discussion

6.2.1. Yield and quality of the exfoliated graphene

Graphene exfoliation was carried out by exposing a mixture of water-based pullulan solution and graphite flakes to ultrasonic waves. The efficiency of graphene exfoliation was investigated by varying the initial graphite concentration, polymer concentration in water, and ultrasonication time. The optimized protocol was then extended to exfoliate graphite by chitosan- and alginate-assisted ultrasonication. As shown in Figure 6.1, the final concentration of graphene increased linearly with the initial concentration of graphite. The initial concentration of the biopolymer played a role too. At a pullulan concentration of 10 mg ml^{-1} and at an initial concentration of graphite of 10 mg ml^{-1} , the amount of exfoliated graphene was 0.54 mg ml^{-1} (see the half square data point right downward in Figure 6.1). For the same graphite concentration (10 mg ml^{-1}) and increasing the concentration of pullulan to 50 mg ml^{-1} the amount of exfoliated graphene obtained was 2.3 mg ml^{-1} (see the half square data point left upward in Figure 6.1).

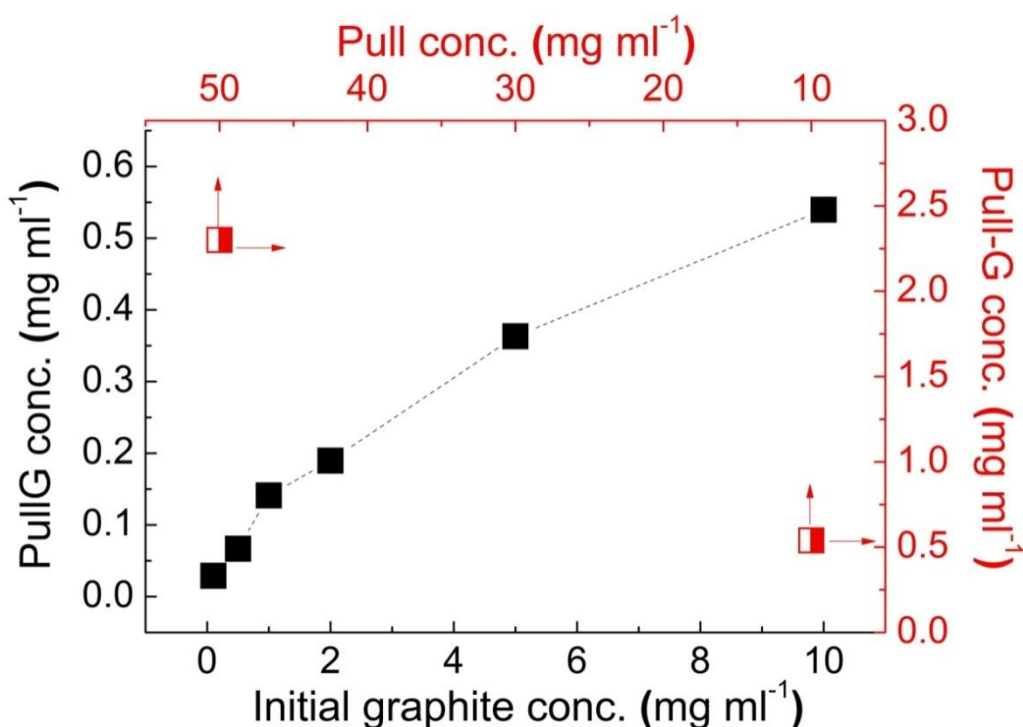


Figure 6.1. Effect of initial graphite concentration (full squared), and pullulan concentration (half squared) on the yield of graphene exfoliation.

The effect of sonication time on the quality of graphene flakes in pullulan solution was observed by TEM. As shown in Figure 6.2a-d, the polysaccharide-assisted ultrasonication process yielded thin and semi-transparent graphene flakes consisting of both individual and few stacked

layers. After the observation of a reasonable number of graphene flakes for each sonication time, it was possible to consider the 30 minutes treatment as a good compromise between number of layers, lateral dimensions, and surface area of the sheets (Figure 6.2a–d).

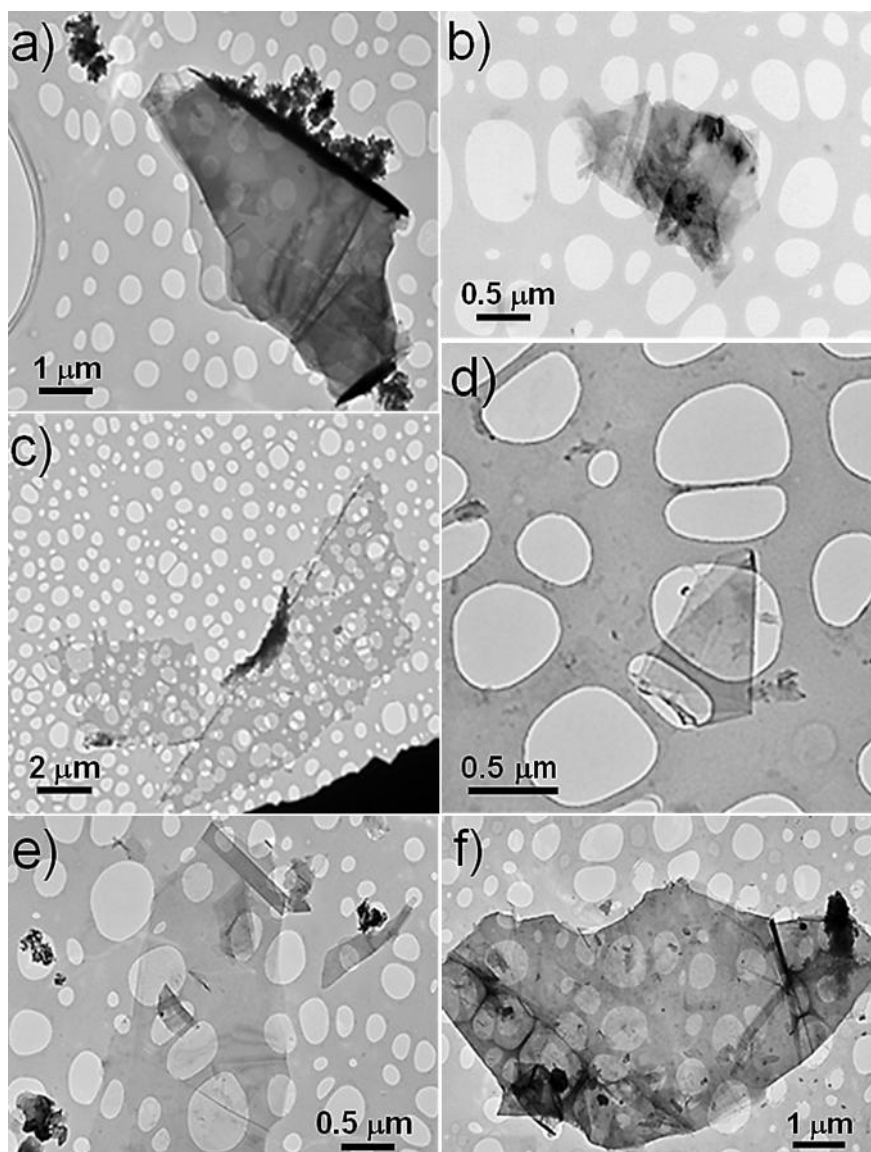


Figure 6.2. TEM images of pull-G for: (a) 10 min; (b) 20 min; (c) 30 min; (d) 60 min; (e) chit-G for 30 min; (f) alg-G for 30 min.

Chitosan- and alginate-assisted ultrasonicated graphene sheets were thus obtained according to the optimized conditions for pullulan-assisted graphite exfoliation (i.e.: initial graphite concentration = 10 mg ml⁻¹; polymer concentration = 50 mg ml⁻¹ for alginate and 20 mg ml⁻¹ for chitosan, the latter due to the high viscosity of the resulting water dispersion; sonication time = 30 min). It was possible to observe that 30 minutes sonication was more effective on chitosan rather than alginate, in terms of both number of stacked layers (visually detectable by the transparency of the flakes to electrons beam) and lateral dimensions (Figure 6.2e and 6.2f). The yield of the process was 0.18 mg ml⁻¹ for alg-G and 5.50 mg ml⁻¹ for chit-G.

6.2.2. Stability of the graphene-polysaccharides water dispersions

The exfoliation of graphite was further confirmed by visual inspection of the obtained water suspensions (Figure 6.3). The absence of both precipitation and macroscopic aggregates in the freshly-prepared samples confirmed the effect of acoustic cavitation of high frequency ultrasound in the formation, growth, and implosive collapse of bubbles in a liquid medium, which induces shock waves on the surface of the bulk material, causing the exfoliation (Hielscher, 2005; Vadukumpully et al., 2009). The exfoliated flakes in chitosan and pullulan solutions were stable for long periods (over 6 months), oppositely to the alginate-based water suspension that started to collapse after 24 h.

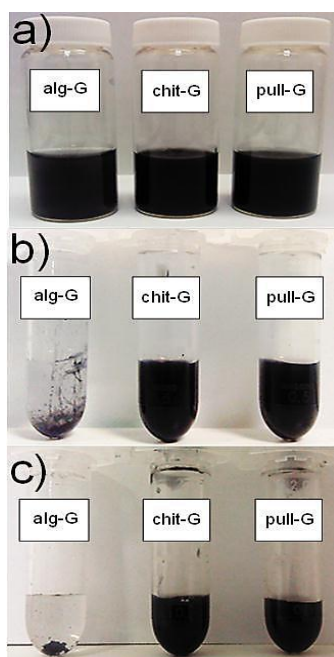


Figure 6.3. Digital images of freshly-prepared graphene in alginate, chitosan, and pullulan water dispersions after (a) 24 h; (b) 7 days; and (c) 6 months storage at room temperature.

The possible behavior of graphene into water based polymer solutions was displayed in Figure 6.4. Preferential interaction between graphene and the polycationic chitosan can be explained in terms of affinity between the non-polar chain segments of chitosan and the surface of graphene. This is corroborated by the high dispersive (apolar) component of the surface free energy measured for chitosan ($\sim 47 \text{ mJ m}^{-2}$) (Farris et al., 2011), very close to that of graphene (46.7 mJ m^{-2}) (Wang et al., 2009), which would give reason for the adsorption of chitosan molecules onto the surface of graphene through hydrophobic-hydrophobic interactions (Feng et al., 2014). The electrostatic repulsion between positively charged amino-groups exposed to the aqueous medium would instead prevent the re-stacking and agglomeration of the exfoliated flakes, thus leading to a stable dispersion.

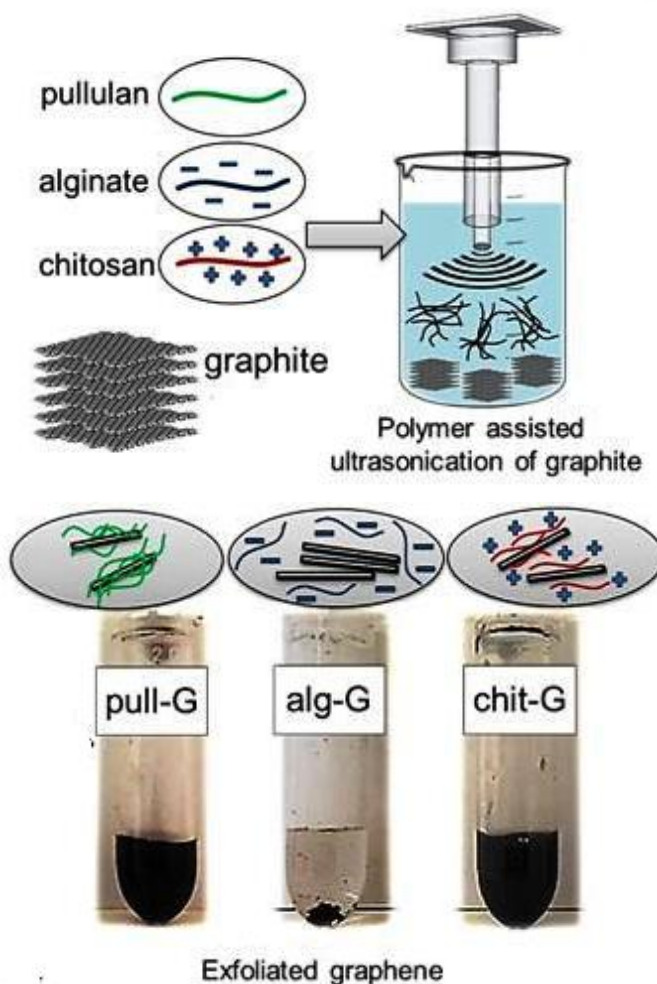


Figure 6.4. Representative image of graphene behavior in pullulan, alginate and chitosan water dispersions.

Analogously, pullulan-based dispersions were stable for a long time due to the affinity between the biopolymer and the surface of graphene. Although highly polar and yet largely hydrophilic in nature, this exopolysaccharide exhibits quite a high dispersive component ($\sim 44 \text{ mJ m}^{-2}$) (Farris et al., 2011), which would ensure the adsorption on the surface of the graphene sheets. The final colloidal stability in water is eventually achieved by the high affinity with the surrounding aqueous medium as well as by steric or/and depletion stabilization (Bourlinos et al., 2009), although the lack of charged functional group does not provide any electrostatic repulsion as seen for chitosan (indeed the pullulan-graphene dispersions started to precipitate earlier than those based on chitosan).

Finally, the completely different behavior observed for the alginate dispersions can be again explained in terms of affinity between the biopolymer and the graphene sheets. It is plausible that the compatibility at the interface between the two entities (alginate and graphene) is thermodynamically unfavorable, so that the adsorption of the biopolymer on the graphene surface is somehow hindered, with subsequent re-stacking and precipitation of the graphene layers. This hypothesis is supported by the dispersive component of the surface free energy measured for alginate ($\sim 20 \text{ mJ m}^{-2}$) (Çaykara et al., 2005), far lower compared to chitosan and pullulan. These considerations seem to confirm that good compatibility (e.g., solvents, surfactants, polymers) for graphite are characterized by surface tensions in the region of $40\text{--}50 \text{ mJ m}^{-2}$ (Hernandez et al., 2008).

6.2.3. Adsorption of polysaccharides on the graphene surface

The results arising from the TGA experiments are displayed in Figure 6.5. Graphite showed degradation starting after 700°C . Therefore, if we consider the trend of the curves at 700°C it is possible to get information about the residual biopolymer adsorbed on the graphene surfaces, as the contribution arising from the pristine graphene sheets would be excluded. The amount of pullulan, alginate, and chitosan polymers in graphene nanosheets was estimated to be approximately $\sim 2.5\%$, $\sim 1.5\%$, and $\sim 8.5 \text{ wt}\%$, respectively (see the insets of Figure 6.5). These values are much lower if compared to guar gum-graphene sheets, for which the residual biopolymer amount was 23% at 550° (Chabot et al., 2013), 48.7% at 750°C (Fan et al., 2013), and 56% at 800°C (Fan et al., 2012). Besides difference in the sample preparation procedures (e.g., centrifugation and washing steps), it is plausible an even stronger interaction between graphene and guar gum compared e.g. to chitosan. This is also supported by the work of Chabot et al. (2013) who adopted a strong acid hydrolysis procedure to completely remove the residual guar gum from the graphene surface. However, it should be noted here that the amount of biopolymer found on pull-G samples before the 5 washing steps ranged between 48% and 68% , in line with previous results on guar gum-graphene bionanocomposites.

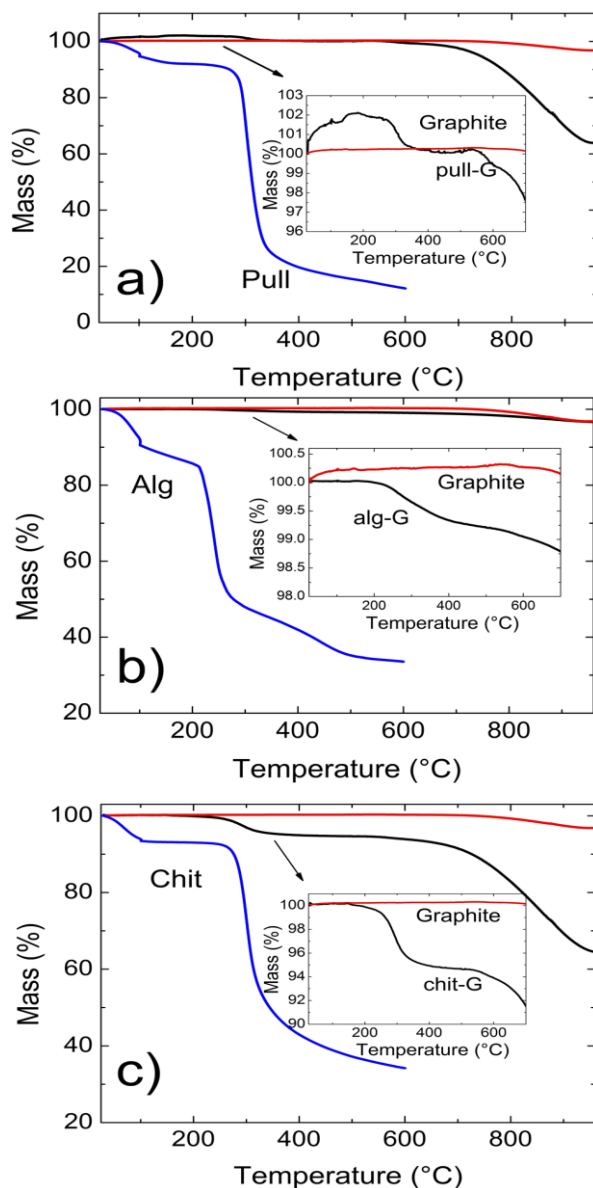


Figure 6.5. TGA traces of graphite, pullulan, alginate, chitosan and pull-G, alg-G and chit-G exposed to a N_2 atmosphere. The inset in each panel is a zoomed view of the traces within the 0–700 °C range.

These results confirm the preferential affinity of graphene for the three biopolymers according to the following decreasing order: chitosan > pullulan > alginate. The high amount of residual chitosan may have a practical impact because it would allow easy re-dispersibility of the particles in water. At the same time, the adsorbed chitosan would be of great advantage in the

preparation of chitosan-based graphene bionanocomposites according to the so-called ‘one-pot’ procedure (Ge et al., 2012; Zheng et al., 2012; Liu et al., 2013; Feng et al., 2014; Nuvoli et al., 2014), because the affinity between polymer and filler is inherently achieved. This would represent the simplest, most efficient, and environmentally friendly strategy for the preparation of graphene-based bionanocomposite materials (Nuvoli et al., 2014). On the other hand, the presence of the biopolymer on the surface of graphene can represent a problem if this will hamper the graphene properties. However, this aspect needs further investigation.

The same kind of information was acquired from the extinction coefficient values of a series of diluted water dispersions prepared for each graphene-biopolymer system after the 5-steps washing procedure. As can be seen from Figure 6.6, the absorbance unit values for the three systems increased monotonically with the concentration.

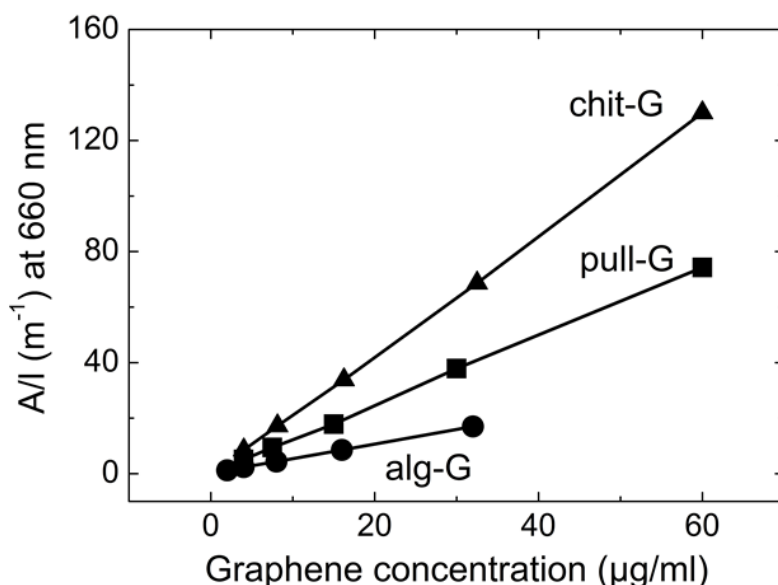


Figure 6.6. Absorbance unit values for different concentrations of pull-G (■), chit-G (▲), and alg-G (●) water dispersions.

The extrapolated extinction coefficient was $525 \text{ ml mg}^{-1} \text{ m}^{-1}$, $1240 \text{ ml mg}^{-1} \text{ m}^{-1}$, and $2287 \text{ ml mg}^{-1} \text{ m}^{-1}$ for alg-G, pull-G, and chit-G, respectively. As explained by Su et al. (2014), the different extinction coefficient calculated for the three systems can be explained considering the light absorption characteristics of mono- or multi-layers graphene, which depend on lateral size distribution, number of layers per flake, and number and type of functional groups. In particular, a higher content of small flakes and fewer layers per flake concurrently give smaller absorption coefficients (ϵ), which was ascribed to the shrinkage of the π -conjugated system at 660 nm. Contrary, high absorption coefficients are encountered for high content of functional groups because of the increase in the auxochromic effect. Therefore, the higher extinction coefficient calculated for the chitosan-coated graphene flakes compared to both pullulan- and alginate-

graphene systems can be attributed to both a ‘surface chemistry’ effect ($-\text{COOH}$, $-\text{OH}$, $-\text{C-O-C-}$, and NH groups along its backbone) and a ‘mass’ effect, being the amount of chitosan per unit area adsorbed on the graphene flakes thicker compared to pullulan and, especially, alginate.

6.2.4. Morphology and thickness of graphene sheets

Information on both morphology and thickness of pull-G, alg-G, and chit-G nanosheets was gathered by AFM analyses. Representative AFM images are shown in Figure 6.7. Individual graphene sheets can be clearly detected in the pull-G sample (Figure 6.7a), whereas the alg-G sample apparently showed macroscopic aggregates (Figure 6.7b). Chit-G AFM images exhibited a peculiar pattern, with graphene sheets masked presumably by the polymer matrix (Figure 6.7c). These morphologies are reflected in the measured size of the graphene layers.

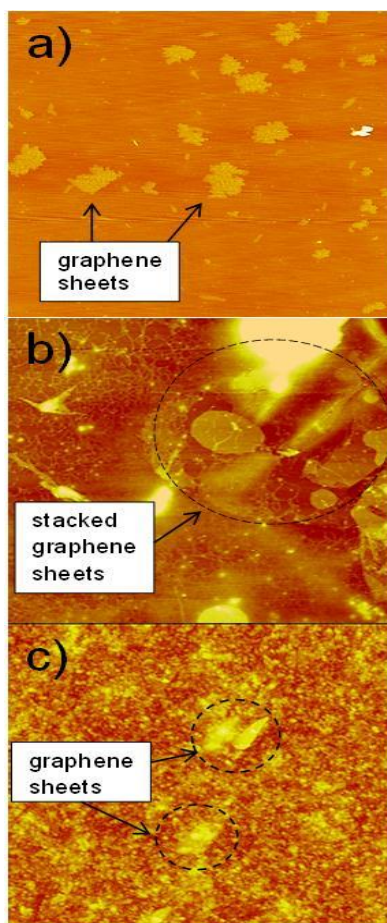


Figure 6.7. AFM height images ($5 \times 5 \mu\text{m}^2$) of (a) pull-G, (b) alg-G and (c) chit-G nanosheets deposited on mica substrates.

As a general trend, it has been observed that the ultrasonication process mediated by pullulan yielded graphene sheets with a surface area mostly centered between $2.5 \cdot 10^5$ and $5.0 \cdot 10^5$ nm², with a thickness between 0.7 nm and 1.5 nm. The surface area and the thickness of alg-G samples increased to approximately $5.7 \cdot 10^5$ nm² and 1.3 – 5.5 nm, respectively, confirming previous indication of the tendency of graphene sheets to re-stack. As for the chit-G samples, the surface area of the graphene sheets was of approximately $1.8 \cdot 10^5$ nm², while the thickness dramatically increased to 10 – 15 nm, which can be attributed to the large amount of polymer adsorbed on the graphene sheets.

Considering that the intrinsic limits of AFM in tapping mode generate a thickness of 0.6 – 0.9 nm for a single layer of graphene (the actual thickness of an individual graphene sheets is ~ 0.34 nm) (Nemes-Incze et al., 2008) and in light of the residual polysaccharides adsorbed on the graphene sheets (~2.5%, ~1.5%, and ~8.5% for pull-G, alg-G, and chit-G, respectively) it can be concluded that pull-G sheets are single or few layers (≤ 5 layers); alg-G are few layers or quite thick sheets; chit-G are single or few layers with a high amount of polymer adsorbed.

6.2.5. Raman spectroscopy

The exfoliation of graphite into graphene was further demonstrated by Raman spectroscopy, which is one of the most useful tools to assess the quality of exfoliated graphene (Ferrari, 2007; Graf et al., 2007). Indeed, Raman spectroscopy allows clear identification of a single layer, few layers (≤ 5), and multilayer (> 5) by taking into account some specific diagnostic parameters. Raman spectrum of pristine graphite is characterized by a dominant G band at 1582 cm^{-1} and two additional bands, D and 2D bands, located at 1350 cm^{-1} and 2700 cm^{-1} , respectively (Graf et al., 2007) (Figure 6.8a). After exfoliation, the D-band with a relatively strong intensity can be mainly ascribed to the increased fraction of graphene edges (Ferrari et al., 2006; Graf et al., 2007; Cassiraghi et al., 2009). Moreover, the intensity ratio of the D and G bands (I_D/I_G) reflects the structural defects and the indication of disorder (Ferrari, 2007). In this work, although the D-peak was present in all the three exfoliated graphene samples (Figure 6.8), the I_D/I_G ratio was reasonably low, as it increased from 0.08 for graphite to 0.18, 0.33, and 0.49 for alg-G, pull-G and chit-G, respectively (Figure 6.8a), in line with the values found for guar gum-assisted graphene sheets (0.29 and 0.25) (Fan et al., 2012; Chabot et al., 2013). This indicates that low-edge defects rather than basal plane defects arisen from the sonication process (Gayathri et al., 2014) supporting the unaltered graphitic character of the flake basal planes after ultrasonication (Chabot et al., 2013). Our results thus confirm that graphene sheets produced using polysaccharide-assisted ultrasound exfoliation are relatively defect-free (Fan et al., 2012; Chabot et al., 2013) compared to reduced GO, which is primarily due to the use of harsh oxidizing reagents used during the oxidation of graphene (the successive reducing process does not allow full recovery of the original graphitic structure) (Chabot et al., 2013).

The (I_{2D}/I_G) ratio and the full width at half maximum (FWHM) of the 2D band provide information of the average thickness of graphene sheets (Graf et al., 2007; Green & Hersam, 2009). In particular, the I_{2D}/I_G ratio decreased from ~ 2.1 for single-layer graphene to ~ 0.8 for quadruple-

layer samples (Green & Hersam, 2009). It was also found that FWHM is $\sim 30\text{--}35\text{ cm}^{-1}$ for individual graphene layers and this value increases with increasing the graphene thickness (Graf et al., 2007; Green & Hersam, 2009). FWHM nearly doubles in two layers (Graf et al., 2007) and quadruple-layer samples (Green & Hersam, 2009) and gets almost constant ($\sim 65\text{--}70\text{ cm}^{-1}$) for multiple layers (Graf et al., 2007). The shape of the 2D peak is another important parameter (Figure 6.8b). The 2D peak of graphite spectrum consists of two components, $2D_1$ and $2D_2$. These two peaks disappear in a single graphene layer, which exhibits a single, sharp and intense 2D peak at lower wavenumbers, roughly four times more intense than the G peak. Bi-layer graphene has much a wider peak compared to single layer graphene, whereas the peak of more than five layers graphene becomes hardly distinguishable from that of graphite due to similarity of the 2D-band in shape (Ferrari et al., 2006; Ferrari, 2007). In this work, the FWHM was found to be 53.34 cm^{-1} , 54.72 cm^{-1} , and 70.99 cm^{-1} for pull-G, alg-G, and chit-G, respectively, while the value of the I_{2D}/I_G parameter was ~ 0.8 for all the three systems. Significant changes also occurred in the shape of the 2D peak of the polysaccharides-graphene nanosheets compared to the pristine graphite powder, especially in terms of shifting toward lower wavenumbers (Figure 6.8b).

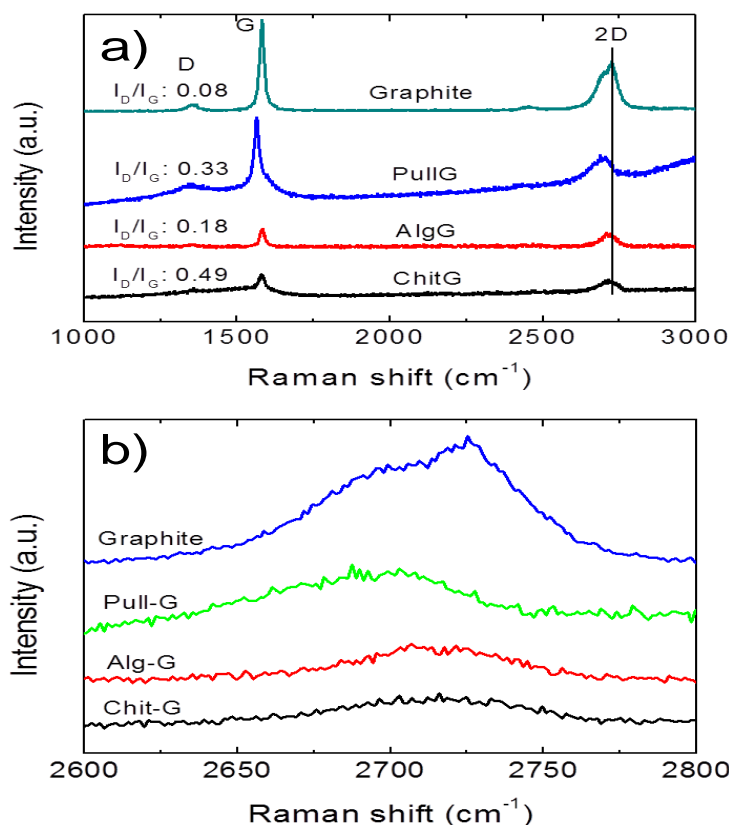


Figure 6.8. (a) Raman spectra of graphite, pull-G, alg-G, and chit-G; (b) detail of the 2D Raman band.

These results confirmed that the polysaccharide-assisted ultrasonication of graphite powder was able to provide exfoliated graphene, most likely consisting of a mixture of mono-layer, bi-layer, and few-layer sheets, in any case less than 5 layers, in particular for the pullulan-assisted ultrasonication, in agreement with the AFM results. The highest value of both I_D/I_G and FWHM for chitosan could be affected by the high amount of residual chitosan adsorbed on the surface of graphene as discussed before.

6.2.6. XPS analyses

To corroborate the presence of the polysaccharides on the surface of graphene we carried out XPS analyses on pristine graphite powder and exfoliated graphene samples. As shown by the XPS survey spectra in Figure 6.9., a dramatic increase in oxygen (peak at 531.9 eV) in pull-G, alg-G, and chit-G sheets and a new peak related to nitrogen (peak at 399.8 eV) in only alg-G and chit-G sheets were observed compared to pristine graphite, where a main peak at 284.4 eV (due to the presence of sp^2 C-C bonds) was present.

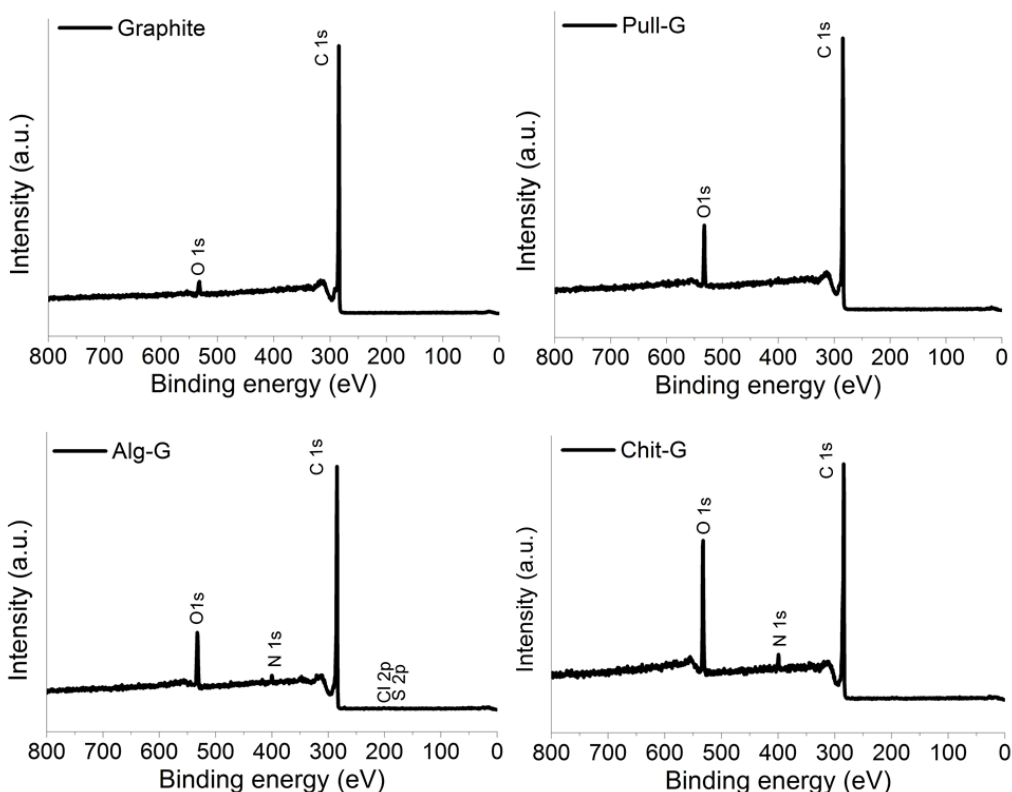


Figure 6.9. XPS survey spectra of pristine graphite powder, pull-G, alg-G, and chit-G.

Table 6.1. Elemental surface analysis of pristine graphite powder, pull-G, alg-G, and chit-G samples determined by XPS.

Material	Total Composition (%)					C:O Ratio
	C	O	N	S	Cl	
Graphite	97.14	2.86	-	-	-	33.97
Pullulan-G	91.78	8.22	-	-	-	11.17
Alginate-G	87.58	10.23	1.62	0.29	0.28	8.56
Chitosan-G	80.97	16.03	3.00	-	-	5.05

The atomic composition of the polysaccharide-graphene samples (Table 6.1) reveals that the highest amount of oxygen (16.03%) was measured on chit-G samples, which also had a significant presence of nitrogen (3%) due to -NH_2 and -OH containing units (Fang et al., 2010). This further supports our previous observations on the preferential interaction of graphene with chitosan. The higher amount of oxygen measured for alg-G sheets (10.23%) compared to pull-G sheets (8.22%) is somehow unexpected, as well as the slight amount of nitrogen (1.62%), which still is under investigation.

6.2.7. Efficiency of the ultrasonication process

It is important to comment on the efficacy and efficiency of the ultrasonication process, especially in light of previous studies where high intensity (interchangeably called ‘tip’ or ‘sonotrode’) or low intensity (e.g., ultrasound bath) ultrasonication methods were used.

Table 6.2. Direct exfoliated graphene by ultrasonication in different polymer systems.

Polymer type / Solvent type	C_{Gmax} (mg/ml)	Sonication type	Sonication time (h)	C_P (mg/ml)	C_{Gi} (mg/ml)	ε (ml/mg.m)	Ref.
Pullulan / Water	2.30	Tip sonicator	0.5	50	10	1240	present study
Alginate / Water	0.18	Tip sonicator	0.5	50	10	525	present study
Chitosan / Water	5.50	Tip sonicator	0.5	20	10	2287	present study
Gum Arabic / Water	0.69	Bath sonicator	8	140	10	1390	Fan et al., 2012
GMA-Gum Arabic / Water	1.12	Bath sonicator	5	30	80	1390	Fan et al., 2013
Gelatin / Water	0.60	Bath sonicator	8	20	200	1390	Ge et al., 2012
Pyrene-functionalised block copolymer / Water	0.39	Bath sonicator	6	20	0.5	-	Liu et al., 2013
Acrylate polymer / Ethanol	4.00	Bath sonicator	24	20	200	2607	Sun et al., 2013
Gum Arabic / Water	0.60	Bath sonicator	100	50	10	5422	Chabot et al., 2013
PVP / Water	0.42	Tip sonicator	1	20	40	1293	Wajid et al., 2012
PVP / Water	0.10	Bath sonicator	9	20	5	-	Bourlino s et al., 2009

C_{Gmax} : maximum achieved graphene concentration; C_P : polymer concentration; C_{Gi} : initial graphene concentration; ε = extinction coefficient; GMA-gum arabic: glycidyl methacrylate-functionalized gum arabic; PVP: polyvinylpyrrolidone.

Table 6.2 summarizes the most relevant results reported in the literature on the ultrasound-assisted exfoliation of graphite in polymer-water mixtures. At first glance, it can be seen that our procedure involving chitosan as the ultrasonication-assisting biopolymer led to the highest yield never reached so far (5.50 mg ml^{-1}). Of course, this cannot be taken as an absolute value, as many parameters differ from one study to another (for example the sonication time may vary from 30 minutes to 100 hours). However, this work has demonstrated that pinpointing the best factors combination is of utmost importance to optimize the final yield and to define a reproducible protocol for the liquid phase exfoliation process. As much important is the type of ultrasound wave used to promote the exfoliation. Indisputably, high intensity ultrasounds are by far more effective compared to the low intensity ultrasound waves, e.g. those generated by the ultrasound bath, basically because of the greatly higher energy input involved, especially at local level. This is the reason for the 430 h needed to disperse graphene by bath sonication in both non-aqueous N-methylpyrrolidone (NMP) (Khan et al., 2010) and sodium cholate water based solutions (Lotya et al., 2010), which yielded at most 1.2 mg/ml and 0.3 mg/ml graphene concentration, respectively. A higher yield value (4 mg ml^{-1}) by bath sonication was achieved after 24 hours sonication of graphite in ethanol assisted by an acrylate polymer (Sun et al., 2013). We found only one work where tip sonicator was used to exfoliate graphite in an aqueous medium containing PVP as a non-ionic polymer. However, after 1 h sonication, the yield was 0.42 mg ml^{-1} of single-to-few layers graphene (Wajid et al., 2012). Bourlinos et al. (2009) only obtained 0.10 mg/ml single layer graphene after 9 h bath sonication using the same polymer.

More recently, Guardia et al. (2014) pointed out that the power intensity of the ultrasonication process may have a great impact on the amount of exfoliated graphene analogues, MoS_2 and WS_2 , with a remarkable increase with increasing the power intensity. Within our work, we have used a power of 16.25 W for 30 minutes of sonication, with energy consumption (in terms of energy output per unit volume) of 731 Ws ml^{-1} . It should also be noted that while high energy inputs may provide higher exfoliation, smaller lateral dimensions of the graphene sheets can be a concomitant undesired side effect (Guardia et al., 2014). In addition, it has been reported that prolonged sonication times do not provide any additional benefit in terms of yields rather they can lead to a more intense damage of the graphene lattice (Hernandez et al., 2008) besides higher and worthless energy input, confirming what was already demonstrated for the ultrasound-assisted exfoliation of clays (Introzzi et al., 2012). Therefore, to make ultrasonication an effective and efficient approach for mass production of high quality graphene sheets, a thoughtful balance between yield, quality of the graphene sheets, and overall costs involved is necessary.

6.3. Conclusions

The capability of non-ionic pullulan, anionic alginate, and cationic chitosan to assist the ultrasonication-mediated exfoliation of graphite into graphene nanosheets in an aqueous medium was investigated in this work. Out of the three systems, pullulan and chitosan were demonstrated to be effective biopolymers for the preparation of stable water dispersions of graphene sheets after only 30 minutes ultrasonication. The long lasting stability (more than 6 months), in particular, was attributed to the biopolymer adsorbed onto the graphene surface, which prevented re-aggregation due to electrostatic repulsions and/or increased affinity to the surrounding medium. In addition, we demonstrated that this method yielded exfoliated mono-, bi-, and few-layer graphene sheets with only low lateral (edges) defects.

Besides allowing new potential uses of biomass resources (e.g., chitin and algae), the proposed protocol could represent a high-throughput, high-yield, economical, and scalable route for new applications of graphene that hitherto lagged behind the latest and more sophisticated technologies (e.g., photovoltaics, biosensors, supercapacitors, super adsorbents, and fuel cells). For example, the biopolymer-coated graphene sheets may be suitable for the fabrication of a range of new graphene-based (bio)nanocomposite materials for packaging applications (e.g., food packaging), where intrinsic properties of graphene such as high elastic modulus and gas barrier properties are sought-after for many different uses.

6.4. References

- Bourlinos AB et al., 2009, Aqueous-phase exfoliation of graphite in the presence of polyvinylpyrrolidone for the production of water-soluble graphenes. *Solid State Commun* 149:2172-2176.
- Casiraghi C et al., 2009, Raman spectroscopy of graphene edges. *Nano Letters* 9:1433-1441.
- Chabot V et al., 2013, High yield production and purification of few layer graphene by Gum Arabic assisted physical sonication. *Sci Rep* 3: 1378.
- Çaykara T et al., 2005, Poly(ethylene oxide) and its blends with sodium alginate. *Polymer* 46:10750–10757.
- Fan J et al., 2012, Gum arabic assisted exfoliation and fabrication of Ag-graphene-based hybrids. *J Mater Chem* 22:13764-13772.
- Fan J et al., 2013, Glycidyl methacrylate-modified gum arabic mediated graphene exfoliation and its use for enhancing mechanical performance of hydrogel. *Polymer* 54:3921-3930.
- Fang M et al., 2010, pH-responsive chitosan-mediated graphene dispersions. *Langmuir* 26:16771-16774.
- Farris S et al., 2011, Wetting of biopolymer coatings: contact angle kinetics and image analysis investigation. *Langmuir* 27:7563–7574.
- Feng X et al., 2014, Liquid-exfoliated MoS₂ by chitosan and enhanced mechanical and thermal properties of chitosan/MoS₂ composites. *Compos Sci Technol* 93:76-82.
- Ferrari AC et al., 2006, Raman spectrum of graphene and graphene layers. *Phys Reviews Letters* 97:187401.
- Ferrari AC, 2007, Raman spectroscopy of graphene and graphite: Disorder, electron–phonon coupling, doping and nonadiabatic effects. *Solid State Commun* 143:47-57.
- Gayathri I et al., 2014, Synthesis of few layer graphene by direct exfoliation of graphite and a Raman spectroscopic study. *AIP Adv* 4:027116.
- Ge Y et al., 2012, Gelatin-assisted fabrication of water-dispersible graphene and its inorganic analogues. *J Mater Chem* 22:17619-17624.
- Graf D et al., 2007, Spatially resolved Raman spectroscopy of single- and few-layer graphene. *Nano Letters* 7: 238-242.
- Green AA and Hersam MC, 2009, Solution phase production of graphene with controlled thickness via density differentiation. *Nano Letters* 9:4031-4036.
- Guardia L et al., 2014, Production of aqueous dispersions of inorganic graphene analogues by exfoliation and stabilization with non-ionic surfactants. *RSC Adv* 4:14115-14127.

Hernandez Y et al., 2008, High-yield production of graphene by liquid-phase exfoliation of graphite. *Nat Nanotechnol* 3:563-568.

Hielscher T, 2005, Ultrasonic production of nano-size dispersions and emulsions. *Proceedings of European Nanosystems Conference ENS '05*, Paris, France.

Introzzi L et al., 2012, Ultrasound-assisted pullulan/montmorillonite bionanocomposite coating with high oxygen barrier properties. *Langmuir* 28:11206-11214.

Khan U et al., 2010, High-concentration solvent exfoliation of graphene. *Small* 6:864-871.

Liu Z et al., 2013, Preparation of graphene/polymer composites by direct exfoliation of graphite in functionalised block copolymer matrix. *Carbon* 51:148-155.

Lotya M et al., 2010, High-concentration, surfactant-stabilized graphene dispersions. *ACS Nano* 4:3155-3162.

Nemes-Incze P et al., 2008, Anomalies in thickness measurements of graphene and few layer graphite crystals by tapping mode atomic force microscopy. *Carbon* 46:1435-1442.

Nuvoli D et al., 2014, Preparation and characterization of polymeric nanocomposites containing exfoliated tungstenite at high concentrations. *Compos Sci Technol* 96:97-102.

Su R et al., 2014, Study on the absorption coefficient of reduced graphene oxide dispersion. *J Phys Chem* 118:12520-12525.

Sun Z et al., 2013, High-yield exfoliation of graphite in acrylate polymers: A stable few-layer graphene nanofluid with enhanced thermal conductivity. *Carbon* 64:288-294.

Vadukumpully S et al., 2009, Cationic surfactant mediated exfoliation of graphite into graphene flakes. *Carbon* 47:3288-3294.

Wajid AS et al., 2012, Polymer-stabilized graphene dispersions at high concentrations in organic solvents for composite production. *Carbon* 50:526-534.

Wang S et al., 2009, Wettability and surface free energy of graphene films. *Langmuir* 25:11078-11081.

Zheng X et al., 2012, High-throughput, direct exfoliation of graphite to graphene via a cooperation of supercritical CO₂ and pyrene-polymers. *RSC Adv* 2:10632-10638.

7. GLOSSARY

(most used acronym – alphabetical order)

AFM:	Atomic force microscopy
DMF:	Dimethylformamide
EVOH:	Ethylene vinyl alcohol
FE-SEM:	Field-emission scanning electron microscopy
FWHM:	Full width at half maximum
GO:	Graphene oxide
NMP:	N-methyl-pyrrolidone
O ₂ TR:	Oxygen transmission rate
PET:	Poly(ethylene terephthalate)
PHAs:	Poly-hydroxyalkanoates
PLA:	Poly(lactic acid)
P'O ₂ :	Permeability coefficients
PVOH:	Poly vinyl alcohol
RH:	Relative humidity
SDBS:	Sodium dodecyl benzene sulfonate
TEM:	Transmission electron microscope
TGA:	Thermogravimetric analysis
VASE:	Variable-angle spectroscopic ellipsometry
WVTR:	Water vapor transmission rate
XPS:	X-ray photoelectron spectroscopy
XRD:	X-ray diffraction

APPENDIX 1

HONORS AND AWARDS



8th ECNP International Conference on Nanostructured Polymers and Nanocomposites

Dresden, Germany
September 16 to 19, 2014

Poster Award

awarded to

Ilke Uysal Unalan

for the poster presentation

**Polysaccharides-assisted direct exfoliation of graphite
into defect-free graphene sheets and fabrication of
bionanocomposite films thereof**

authors:

I. Uysal Unalan, C. Wan, L. Piergiovanni, S. Farris

Dresden, September 19, 2014

on behalf of the chairpersons

Prof. Dr. Brigitte Voit and Prof. Dr. José Kenny



10 April 2014

To whom it may concern

Ms Ilke Uysal Unalan - Visiting Researcher

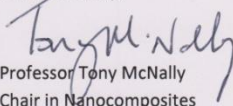
Ms Ilke Uysal Unalan has been a visiting researcher in the Nanocomposites Research Group within WMG, an academic department at the University of Warwick, between 1 July 2013 and 15 April 2014. She has worked closely with Dr Chaoying Wan, Assistant Professor of Nanocomposites.

Ilke is registered for a PhD in the Packaging Division of the Department of Food, Environmental and Nutritional Sciences (DeFENS) at the University of Milan in Italy. She joined WMG from 1 July 2013 until 30 November 2013 while on an ERASMUS Training Placement. Following completion of the ERASMUS work placement, Ilke returned to WMG as a visiting research student from 1 January 2014 to 15 April 2014. WMG agreed to pay her academic fees for this period.

During her visit, Ilke has been investigating methods for the preparation of graphene oxide and graphene nanosheets and has prepared a range of biopolymer/graphene nanocomposite materials on which she has carried out structural characterisation, mechanical, thermal, optical testing and gas permeability measurement. The resultant bio-nanocomposites are targeting to food packaging applications.

Ilke has been a highly committed member of the Nanocomposites team. We wish her success in the completion of her PhD and look forward to working with her again.

Yours sincerely,



Professor Tony McNally
Chair in Nanocomposites
Director of the International Institute for
Nanocomposites Manufacturing

International Manufacturing Centre
University of Warwick
Coventry CV4 7AL United Kingdom
Tel: +44 (0)24 7652 4871
Fax: +44 (0)24 7652 4307

Email: wmg@warwick.ac.uk
Web: www.wmg.warwick.ac.uk

APPENDIX 2

CONFERENCE ABSTRACTS

1. **Uysal Unalan, I.** (2012). Innovative Bionanocomposite Materials for Food Packaging Applications, *17th Workshop on the Developments in Italian PhD Research on Food Science Technology and Biotechnology*, 19-21 September, Bologna, Italy, *Proceeding*:357-358 (Poster Presentation).

17th Workshop on the Developments in the Italian PhD Research on Food Science Technology and Biotechnology
 Alma Mater Studiorum - University of Bologna, Cesena, 19-21 September, 2012

Innovative Bionanocomposite Materials for Food Packaging Applications

Ike Uysal Unalan (ike.uysal@unimi.it)

DeFENS, Dept. Food, Environmental and Nutritional Sciences, University of Milan, Milan, Italy

Tutor: Prof. Luciano Piergiovanni

This project aims to develop bionanocomposites for food packaging through the 'top-down' approach (Fig. 1). The specific goal is to generate new materials using inorganic fillers that have not yet been used in the food sector. Special attention will be paid on bionanocomposite coatings, according with the 'packaging optimization' principle. Solvent casting and extrusion methods will allow obtaining the final bionanocomposites. The effects of the fillers on the barrier, mechanical, optical, thermal and electrical properties of bionanocomposites will be investigated. The motivations behind this research lie in the potential of unexplored inorganic fillers as alternatives to the currently used nanofillers.

Materiali bionanocompositi innovativi per applicazioni nell'imballaggio alimentare

Il presente progetto di dottorato ambisce allo sviluppo di strutture bionanocomposite per l'imballaggio alimentare, mediante l'approccio cosiddetto 'top-down' (Fig. 1). L'obiettivo specifico è quello di generare materiali utilizzando cariche inorganiche ad oggi mai state utilizzate (o solo raramente) nel settore dell'imballaggio alimentare. Particolare attenzione verrà rivolta allo sviluppo di coatings bionanocompositi, secondo il principio dell'ottimizzazione dell'imballaggio, mediante deposizione/evaporazione del solvente ed estrusione. Verrà anche studiato l'effetto derivante dall'aggiunta delle cariche inorganiche sulle proprietà di barriera, meccaniche, ottiche termiche ed elettriche. Le motivazioni alla base di tale progetto risiedono nelle potenzialità delle cariche inorganiche come alternativa alle soluzioni attualmente in commercio.



Figure 1 Schematic representation of the well-known 'top-down' approach.

1. State-of-the-Art

There is a growing worldwide interest pushed by governments and societies to increment the responsible use of renewable resources in plastic commodity products in order to reduce the waste associated to their use, particularly in packaging applications (Petersen *et al.*, 2001). Biopolymers, mainly obtained from renewable resources and classified as agro-polymers (starch, protein, etc.) and polymers synthesized chemically from naturally derived monomers (polyhydroxyalkanoates, polylactic acid), represent an interesting alternative to common non-degradable oil-based polymers used in food packaging. However, biopolymers exhibit relatively poor mechanical and barrier properties, which currently limit their industrial use. In this respect, it has been suggested that inherent shortcomings of biopolymer-based packaging materials may be overcome by the nanocomposite technology (Sanchez-Garcia *et al.*, 2010).

Nanobiocomposites are novel materials with drastically improved mechanical, barrier and thermal properties, due to the incorporation of small amounts (less than 10 wt%) of nano-sized fillers into a biopolymer matrix. Nanofillers can be classified according to their morphology, such as particles that are (i) layered (e.g., clays), (ii) spherical (e.g., silica) or (iii) acicular (e.g., whiskers, carbon nanotubes) (Bordes *et al.*, 2009) (Fig. 2). So far, efforts have mainly concentrated on expandable layered silicate clays, with montmorillonite (MMT), a hydrated alumina-silicate layered clay consisting of an edge-shared octahedral sheet of aluminum hydroxide between two silica tetrahedral layers (Weiss *et al.*, 2006), among the most commonly used nanofillers for polymer nanocomposites. This PhD project is addressed to select new inorganic nanofillers, for biopolymer coatings and/or stand-alone films production, in an attempt of providing new

2. **Uysal Unalan I.**, Wan C., Piergiovanni L., Farris S. Pullulan/Graphene Oxide Bionanocomposites for Food Packaging Applications. *The 6th edition of the Shelf Life International Meeting (SLIM 2014)*, 11-13 June, New Brunswick, New Jersey, USA (Poster Presentation).

6th Shelf Life International Meeting - SLIM 2014
New Brunswick, New Jersey, USA
June 11-13, 2014

**PULLULAN/GRAPHENE OXIDE BIONANOCOMPOSITES FOR FOOD
PACKAGING APPLICATIONS**

Ilke Uysal Unalan^{1,2}, Chaoying Wan², Luciano Piergiovanni¹ and Stefano Farris¹

¹ DeFENS, Department of Food, Environmental and Nutritional Sciences—Packaging Division, University of Milan, Via Celoria 2 – 20133 Milan, Italy

² International Institute for Nanocomposites Manufacturing, WMG, University of Warwick, Coventry CV4 7AL, UK

ABSTRACT

As compared to petroleum-based plastics, such as polypropylene, polyethylene and polyethylene terephthalate, natural polymers or biodegradable polymers have demonstrated unique preference in food packaging applications due to their natural-abundance, biodegradability and environmentally friendly nature. Pullulan plays an important role in food packaging due to its high strength, good optical clarity, biodegradability and good oxygen barrier properties. However, its brittleness and high cost highly limit its applications. In this study, by incorporation of 2D lamellar graphene oxide nanoplatelets and natural biopolymer chitosan to pullulan, the mechanical and barrier properties of pullulan have been synergistically improved and the performance/cost ratio are well-balanced. As compared to pure pullulan films, the tensile strength (MPa), Young modulus (MPa) and elongation at break (%) of graphene based pullulan-chitosan films (60:40) are significantly improved by about 100, 130 and 500%, respectively, with incorporation of 0.2 wt% graphene oxide while keeping the haze formation within the 3% threshold & transmittance 91% at 550 nm which are adequate values for most applications in the food packaging sector. The simultaneous improvement of mechanical and oxygen barrier properties could be attributed to the homogeneous dispersion and alignment of graphene oxide sheets in the pullulan matrix as well as the high specific surface area and two dimensional geometry of graphene oxide. With regard to the gas-barrier properties, the optimized bionanocomposite exhibited lower oxygen barrier properties than pure pullulan films. This result can have a great impact from a practical point of view, because the interest of food packaging companies toward barrier solutions for O₂-sensitive beverages and foods (e.g., dairy products, meat products, RTD teas, tomato-based products, and wines) is still high. Our current work could provide an effective and promising method for preparing graphene oxide-based biopolymer composites for food packaging applications.

3. **Uysal Unalan, I.** (2014). Potential Use of Graphene For the Generation of Bionanocomposite Materials For Food Packaging Applications, 19th Workshop on the *Developments in the Italian PhD Research on Food Science Technology and Biotechnology*, University of Bari, Bari, 24-26 September 2014 *Proceeding*:381-385 (*Oral Presentation*).

19th Workshop on the *Developments in the Italian PhD Research on Food Science Technology and Biotechnology*, University of Bari, Bari, September 24th-26th, 2014

Potential Use of Graphene for the Generation of Bionanocomposite Materials for Food Packaging Applications

Ilke Uysal Unalan (ilke.uysal@unimi.it)

Dept. Food, Environmental and Nutritional Sciences (DeFENS), University of Milan, Milan, Italy

Tutor: Prof. Luciano Piergiovanni

This PhD thesis dealt with the synthesis of graphene oxide (GO) by a chemical method and graphene sheets (G) by a simple and environmentally friendly physical strategy. High-performance G-based pullulan (pull) bionanocomposite films for food packaging applications were also generated.

Potenziale impiego del grafene per lo sviluppo di materiali bionanocompositi per applicazioni nel settore dell'imballaggio alimentare

La presente tesi di dottorato ha riguardato la sintesi di grafene ossidato (GO) mediante metodo chimico e sottili foglietti di grafene (G) attraverso un approccio fisico a basso impatto ambientale. Inoltre sono stati sviluppati film bionanocompositi a base di grafene e pullulano (pull) altamente performanti per applicazioni nel settore dell'imballaggio alimentare.

Key words: graphene; ultrasonication; bionanocomposite materials; oxygen barrier function; food packaging.

1. Introduction

In accordance with the PhD thesis project, this oral communication reports the main results of the following activities directed to:

- A1) synthesis of GO by a modified Hummers method and fabrication of GO based pull bionanocomposite films
- A2) fabrication of GO based pull-chitosan (chit) or pull-alginate (alg) bionanocomposite films
- A3) polysaccharides-assisted exfoliation of graphite into defect-free G sheets and fabrication of bionanocomposite films thereof

New societal challenges will impact our lifestyle in the coming years. At the moment, we are in the middle of a "green" revolution, stemming from societal and industrial demands for a lower environmental impact, cost effectiveness, and high-performance goods and services. Like many other sectors, food packaging is moving to nanotechnology (Farris *et al.*, 2014). Recent advances in nanotechnology include the use of nanosized particles of both inorganic and organic origin for the improvement of specific properties of the polymer matrix, such as mechanical, thermal, and barrier properties. The use of biopolymers is one of the most promising strategies toward an optimized use of traditional packaging materials (e.g., plastics) (Farris *et al.*, 2014). Pull is one of the biopolymers that have attracted much attention over recent years due to its peculiar characteristics due to its high strength, excellent transparency, biodegradability, and good oxygen barrier properties. This non-ionic exopolysaccharide (EPS) is obtained from the fermentation medium of the fungus-like yeast *Aureobasidium pullulans* (originally called *Pullularia pullulans*) under limiting conditions (e.g., nitrogen). (Leathers, 2002). However, its brittleness and high cost, between 25 and 30 US\$/kg, which is much higher than most biopolymers of both polysaccharides and protein origin, limit its applications (Farris *et al.*, 2014). G is the building unit of graphite, a three-dimensional layered mineral allotrope of carbon composed of several stacked layers of G (Terrones *et al.*, 2010).

More specifically, G is a two-dimensional material composed of a single planar sheet of sp²-bonded carbon atoms packed in a honeycomb crystal lattice with large specific surface area. Although the first reported method for production of G nanosheets dates back to 1970, (Eizenberg and Blakely, 1979) its individual layered form was first discovered in 2004 through a micromechanical cleavage method using flake graphite as a starting material (Novoselov *et al.*, 2004). The tremendous interest in G lies in the unprecedented electrical, thermal, mechanical, and barrier properties (Yang *et al.*, 2013), which makes G one of today's most exciting materials for advantageous exploitation of nanocomposite polymers in the food packaging sector. Despite the broad spectrum of potential applications, there are still many challenges for G to reach its full potential. Among others, production costs represent the main limitation to large scale utilization, mainly due to the highly expensive and low-yielding methods and procedures to obtain graphite monolayers.

4. **Uysal Unalan I., Wan C., Piergiovanni L., Farris S.** Polysaccharides-assisted direct exfoliation of graphite into defect free graphene sheets and fabrication of bionanocomposite films thereof. *The 8th ECNP International Conference on Nanostructured Polymers and Nanocomposites (ECNP 2014)*, 16-19 September, Dresden, Germany (Poster Presentation).

P102

POLYSACCHARIDES-ASSISTED DIRECT EXFOLIATION OF GRAPHITE INTO DEFECT-FREE GRAPHENE SHEETS AND FABRICATION OF BIONANOCOMPOSITE FILMS THEREOF

Ilke Uysal Unalan^{1,2}, Chaoying Wan², Luciano Piergiovanni¹, Stefano Farris¹

¹ University of Milan, Packaging Division, Environmental and Nutritional Sciences, Department of Food, DeFENS, Via Celoria 2, 20133 Milan, Italy

² University of Warwick, WMG, International Institute for Nanocomposites Manufacturing, Coventry CV4 7AL, United Kingdom

ilke.uysal@unimi.it

Few layer of graphene was produced by direct exfoliation and functionalisation with polysaccharides with the assistance of ultrasonication. To this scope, we exploited the functional and intercalation properties of environmentally safe pullulan, chitosan and alginate. The graphene exfoliation was systemically studied by varying sonication time from 10 min to 60 min. Transmission electron microscopy, atomic force microscopy, Raman, UV-visible and wide-scanning X-ray photoelectron spectroscopy analyses were then carried out. Overall, large size and high quality graphene flakes with a very low defect ratio were obtained. According to transmission electron microscopy results, 30 min sonication yielded individual sheets with surface area of approximately 25 μm^2 . The resulting dispersions prepared by pullulan or chitosan were gray and stable over months while the alginate-graphene dispersion was only stable for one week, after which precipitation was observed. Pullulan films with the different concentrations of functionalized graphene sheets were also prepared. Graphene-loaded pullulan films (0.015 wt% - 0.5 wt%) showed an elastic modulus 4 times higher than the pristine pullulan films. The same composites exhibited enhanced oxygen barrier properties compared with pristine pullulan films. The ultrasonication-assisted processing of graphite with environmentally approved biopolymers such as pullulan and chitosan opens up a scalable and low-cost avenue for the production of nanoscale building blocks for practical applications, such as food packaging.

APPENDIX 3

PEER-REVIEWED PUBLICATIONS

1. Uysal Unalan I., Cerri G., Marcuzzo E., Cozzolino C. A., Farris S. (2014). Nanocomposite films and coatings using inorganic nanobuilding blocks (NBB): Current applications and future opportunities in the food packaging sector. *RSC Advances*, 4: 29393-29428.

Nanocomposite films and coatings using inorganic nanobuilding blocks (NBB): current applications and future opportunities in the food packaging sector

Cite this: *RSC Adv.*, 2014, 4, 29393

Ilke Uysal Unalan,^a Guido Cerri,^b Eva Marcuzzo,^c Carlo A. Cozzolino^a
and Stefano Farris^{*a}

The aim of this review is to provide an in-depth overview on the use of inorganic nano-sized entities for the generation of nanocomposite materials in the form of films and coatings for food packaging applications. According to recent trends toward "green" strategies, special focus has been dedicated to the development of nanocomposite coatings obtained using biopolymers as the main polymer matrix. After a first introductive part, the discussion has been addressed to the use of inorganic fillers, metals and metal-oxides, zeolites, and graphene. For each class of filler, a first 'in-depth' description of the most relevant physicochemical properties for the food packaging sector has been followed by case-by-case references to recent developments and envisaged implementations. The technical aspects that may be crucial in the design and end use of (bio)nanocomposite coatings have been covered in the last part of this work, which also includes an updated list of current applications on nano-sized inorganic fillers in the food packaging field.

Received 28th February 2014
Accepted 17th June 2014

DOI: 10.1039/c4ra01778a
www.rsc.org/advances

^aDeFENS, Department of Food, Environmental and Nutritional Sciences—Packaging Division, University of Milan, Via Celoria 2, 20133 Milan, Italy. E-mail: stefano.farris@unimi.it; Fax: +39 0250316672; Tel: +39 02 50316654

^bDepartment of Natural and Territorial Science, University of Sassari, via Piandanna 4, 07100 Sassari, Italy

^cDepartment of Food Science, University of Udine, via Sondrio 2/A, 33100 Udine, Italy



Ilke Uysal Unalan received her M.S. in Food Engineering from Izmir Institute of Technology, Turkey, in 2008 discussing a thesis on active food packaging by edible films. In March–June, 2010 she was a Federation of European Microbiological Societies (FEMS) research fellow at the National Food Institute, Technical University of Denmark (DTU), in the Prof. P. Dalgaard's group, where she worked on

shelf life studies based on modified atmosphere packaging strategies. She has been doing her PhD since January 2012 in the Food Packaging lab under the guidance of Dr S. Farris. Her research topic deals with the design and development of graphene-biopolymer nanocomposite films and coatings for food packaging applications. From July 2013 till May 2014 she has been a visiting research fellow at the University of Warwick, UK, in the Nanocomposite Research Group of WMG led by Prof. T. McNally, under the supervision of Dr Chaoying Wan.



Carlo Alessio Cozzolino received his M.S. in Agricultural Science & Technology in 2005 from the University of Sassari, Italy. In 2008 he joined the Food Packaging lab led by Prof. L. Piergiovanni at the University of Milan as a fellowship holder granted by the Government of Sardinia (September 2008–October 2009). In 2013 he earned his PhD in Food and Microbial Biotechnology at the University of Milan (granted by the University of Sassari), under the supervision of Dr S. Farris. His thesis defense focused on the development of an active packaging from biomacromolecules for the controlled release of natural antimicrobials. At present, he holds a research position at the Metahvoto Spa Company, while keeping ongoing collaborations with the Food Packaging lab.

2. Farris S., Uysal Unalan I., Introzzi L., Fuentes-Alventosa J.M., Cozzolino C. A. (2014). Pullulan-based films and coatings for food packaging: Present applications, emerging opportunities, and future challenges. *Journal of Applied Polymer Science*, **131**: 40539 (INVITED REVIEW).

Pullulan-Based Films and Coatings for Food Packaging: Present Applications, Emerging Opportunities, and Future Challenges

Stefano Farris,¹ Ilke Uysal Unalan,¹ Laura Introzzi,¹ José María Fuentes-Alventosa,² Carlo A. Cozzolino¹

¹Department of Food, Environmental and Nutritional Sciences (DeFENS), Packaging Division, University of Milan, Via Celoria 2, Milan I-20133, Italy

²Centro de Investigación y Formación Agraria "Alameda del Obispo," Instituto de Investigación y Formación Agraria y Pesquera (IFAPA), Avda. Menéndez Pidal s/n, Córdoba 14004, Spain

Correspondence to: S. Farris (E-mail: stefano.farris@unimi.it)

ABSTRACT: Societal and industrial demands for lower environmental impact, cost effectiveness, and high-performance goods and services are increasingly impacting the choice of technologies which are developed and deployed in consumer products. Like many other sectors, food packaging is moving to new technologies; the use of biopolymers is one of the most promising strategies toward an optimized use of traditional packaging materials (e.g., oil-based plastics) without impairing the goal of extending shelf life. Among other food packaging materials, pullulan is attracting much attention due to its unique features. The goal of this review is to provide an overview of current and emerging applications of pullulan within the food packaging sector. In particular, the functional properties of interest for the food packaging industry will be discussed in light of the physicochemical attributes of this exopolysaccharide. Future challenges that may dictate the successful penetration of pullulan in the food packaging market are also outlined. © 2014 Wiley Periodicals, Inc. *J. Appl. Polym. Sci.* **2014**, *131*, 40539.

KEYWORDS: coatings; biopolymers and renewable polymers; packaging; nanostructured polymers; surfaces and interfaces

Received 17 January 2014; accepted 3 February 2014

DOI: 10.1002/app.40539

INTRODUCTION

A number of biopolymers are currently used in many different areas, such as in the food, pharmaceutical, and biomedical fields, due to their unique physicochemical properties, especially when compared with their oil-derived counterparts (e.g., plastics). Applications include their use as emulsifiers, stabilizers, binders, gelling agents, coagulants, lubricants, film formers, thickening agents, and suspending agents, just to provide a few examples.¹

Pullulan is one of the biopolymers that have attracted much attention over recent years due to its peculiar characteristics. This non-ionic exopolysaccharide is obtained from the fermentation medium of the fungus-like yeast *Aureobasidium pullulans* (originally called *Pullularia pullulans*) under limiting conditions (e.g., nitrogen), with media composition and culture conditions highly affecting the final yield.² The production of pullulan by *A. pullulans* was first discovered by Bauer in 1938,³ although isolation and characterization of pullulan were described by Bernier 20 years later.⁴ The basic structure of pullulan was first provided by Wallenfels, Bender, Keilich, and Bechtler, who also

coined the name "pullulan."^{5,6} Large-scale production of pullulan was started in 1976 by Hayashibara Company Limited (Okayama, Japan); pullulan films from the same company appeared on the market in 1982.⁷ Hayashibara is still the leading commercial producer of pullulan worldwide, selling food grade (designated as PF) and deionized (PI) products with a mean molecular weight of 100,000 (PI-10 and PF-10) or 200,000 (PI-20 and PF-20).⁷

Pullulan is generally marketed as a white to off-white dry powder.¹ It is non-toxic, non-mutagenic, non-carcinogenic, and edible.⁸ It is tasteless, odorless, and highly soluble in both cold and hot water and in dilute alkali, though it is insoluble in alcohol and other organic solvents except dimethylsulfoxide and formamide.¹ It has a considerable mechanical strength and other functional properties such as adhesiveness, film and fiber formability, and enzymatically mediated degradability, though it is not attacked by the digestive enzymes of the human gut.⁹ Other properties of this exopolysaccharide concern the stability of its aqueous solutions over a broad range of pH, the low viscosity in comparison with other polysaccharides, the inability to form gels, and the good oxygen barrier properties of films and

© 2014 Wiley Periodicals, Inc.

Materials
Views

WWW.MATERIALSVIEWS.COM

40539 (1 of 12)

J. APPL. POLYM. SCI. 2014, DOI: 10.1002/APP.40539

3. **Uysal Unalan I.**, Wan C., Trabattoni S., Piergiovanni L., Farris S. Polysaccharides-assisted rapid exfoliation of graphite platelets into high quality water dispersible graphene sheets (submitted to Carbohydrate Polymers/under review).
4. **Uysal Unalan I.**, Wan C., Figiel F., Olsson R.T., Trabattoni S., Farris. S. Transparent pullulan/graphene oxide bionanocomposites with high oxygen barrier properties (to be submitted).
5. **Uysal Unalan I.**, Farris S. Ultrasound-assisted pullulan/graphene oxide bionanocomposite coatings with high oxygen barrier properties (in preparation).
6. **Uysal Unalan I.**, Wan C., Piergiovanni L., Farris S. Improved mechanical and thermal properties of pullulan blend systems with graphene oxide nanosheets (in preparation).